UNIVERZITA KARLOVA

Přírodovědecká fakulta

Katedra biochemie

Studijní program: Biochemie

Studijní obor: Biochemie

Bc. Martin Ivančík

Potenciace protinádorové aktivity HPMA kopolymerních konjugátů nesoucích gemcitabin pomocí IAP inhibitorů

Antitumor activity of HPMA copolymer-bound gemcitabine conjugate potentiation by IAP inhibitors

DIPLOMOVÁ PRÁCE

Školitel: RNDr. Marek Kovář, PhD

Praha 2024

I affirm that this thesis was elaborated independently under the supervision of RNDr. Marek Kovář, PhD, that all sources used were cited properly and that any part of the thesis has not been submitted for obtaining another degree.

Prohlašuji, že jsem tuto práci vypracoval samostatně pod vedením RNDr. Marka Kováře, PhD, že všechny použité informační zdroje byly řádně citovány a že žádná část práce nebyla předložena k získání jiného titulu.

February 8, 2024, Prague ……..

Abstrakt

Nádorová onemocnění představují významný celosvětový problém v oblasti zdraví. V nadcházejících dekádách se předpokládá výrazný nárůst nových případů a je tak nezbytně nutné zlepšit prevenci, včasnou detekci a léčebné postupy. Chemoterapie sice zůstává standardní léčbou mnoha druhů rakoviny, její efektivita je však často omezena cytotoxickými účinky na zdravé buňky a četnými vedlejšími účinky. V reakci na tato omezení se objevily nové léčebné strategie, jako je kombinovaná léčba a systémy dopravující léčiva. V tomto projektu jsme studovali cytostatické a cytotoxické účinky dvou inhibitorů IAP (z ang. inhibitor of apoptosis) proteinů, LCL-161 a AZD5582, a jejich potenciál zvýšit protinádorovou aktivitu konvenčního cytostatika gemcitabinu. Aktivita těchto látek byla studována na pěti lidských nádorových buněčných liniích: pankreatických (PANC1, BxPC-3, MiaPaca-2), prostatickém (PC-3) a mamárním (MDA-MB-231) karcinomu. Oba inhibitory IAP prokázaly protinádorouvou aktivitu jako samostatná léčiva, přičemž nejvyšší citlivost k působení IAP inhibitorů vykazovaly buněčné linie MiaPaca-2 a BxPC-3. Nebyla pozorována jasná korelace mezi hladinami exprese IAP genů (cIAP1, cIAP2, XIAP) a sensitivitou buněčných linií na IAP inhibitory. Poměr exprese těchto tří genů byl však u čtyř z pěti studovaných buněčných liniích srovnatelný. Inhibitory IAP byly schopny potencovat cytostatickou a cytotoxickou aktivitu gemcitabinu, přičemž nejvýznamnější synergie byla pozorována u buněčných linií MiaPaca-2 a MDA-MB-231. V další fázi projektu byly syntetizovány HPMA kopolymery nesoucí tato léčiva a byla testována jejich *in vivo* toxicita. Tyto výsledky naznačují potenciál systémů pro dopravu léčiv s kombinací gemcitabinu a IAP inhibitoru při léčbě nádorových onemocnění a poukazují na potřebu dalšího studia jejich protinádorové účinnosti.

Klíčová slova: gemcitabin, inhibitor IAP, HPMA kopolymery, kombinovaná terapie, doprava léčiv, řízené uvolňování léčiv, protinádorová aktivita

Abstract

Cancer represents a significant global health challenge, with a substantially increasing incidence. There is a critical need for enhanced prevention, early detection, and improved therapeutic approaches to treat malignant diseases. While chemotherapy remains a standard treatment for many cancers, its efficacy is often limited by cytotoxic effects on healthy cells and numerous side toxicities. In response to these challenges, novel strategies such as combination therapies and drug delivery systems have emerged. In this project, we investigated the cytostatic and cytotoxic effects of two inhibitors of IAP (inhibitor of apoptosis) proteins, LCL-161 and AZD5582, and their potential to boost the anticancer activity of gemcitabine. These compounds were evaluated in five human cancer cell lines: pancreatic (PANC1, BxPC-3, MiaPaca-2), prostatic (PC-3), and breast (MDA-MB-231) carcinomas. Both IAP inhibitors demonstrated anticancer activity as single agents, with the MiaPaca-2 and BxPC-3 cell lines showing the highest sensitivity. No correlation was observed between the expression levels of IAP genes (cIAP1, cIAP2, XIAP) and the sensitivity of cell lines to IAP inhibitors. However, four of five tested cell lines possessed a consistent pattern in the expression of these three genes. IAP inhibitors were able to potentiate the cytostatic and cytotoxic activities of gemcitabine, with the most significant synergy observed in the MiaPaca-2 and MDA-MB-231 cell lines. Furthermore, HPMA copolymers bearing these drugs were synthesized and tested for toxicity in mice. These findings suggest the potential of drug delivery systems with the combination of gemcitabine and IAP inhibitors in cancer treatment, indicating the need for further investigation for their antitumor efficacy.

Keywords: gemcitabine, IAP inhibitor, HPMA copolymers, combination therapy, drug delivery, controlled drug release, anticancer activity

[IN ENGLISH]

Acknowledgements

I want to express my sincere gratitude to my supervisor RNDr. Marek Kovář, PhD, for allowing me to join his team at the Institute of Microbiology of the Czech Academy of Sciences, and for his support and valuable guidance throughout my time here. Additionally, I am also grateful to RNDr. Petra Procházková, PhD, for the help with the gene expression studies, as well as to the colleagues from the Centre of Cytometry and the entire team of the Laboratory of Tumor Immunology for their assistance. Furthermore, I want to thank Bc. Kevin Kotalík and Ing. Robert Pola, PhD, from the Department of Biomedical Polymers of the Institute of Macromolecular Chemistry, led by RNDr. Tomáš Etrych, DSc., for synthesising and characterising the polymer systems, and my parents for their endless support. Last but not least, I want to thank for the support of the project National Institute for Cancer Research (Programme EXCELES, ID Project No. LX22NPO5102) – Funded by the European Union – Next Generation EU.

Table of Contents

List of abbreviations

% v/v	volume percentage
ABC	ATP-binding cassette
ADT	Androgen deprivation therapy
ATCC	American Type Culture Collection
ATP	Adenosine triphosphate
AVPI	Alanine-Valine-Proline-Isoleucine
BCRP	Breast cancer resistance protein
BIR	Baculovirus Inhibitor of the Apoptosis Protein Repeat
BRCA2	Breast cancer type 2 susceptibility protein
CARD	Caspase recruitment domain
CDKN2	Cyclin-dependent kinase inhibitor 2
c-FLIP	Cellular FLICE Inhibitory Protein
cIAP1	Cellular inhibitor of apoptosis protein 1
cIAP2	Cellular inhibitor of apoptosis protein 2
CTLA-4	Cytotoxic T-lymphocyte-associated protein-4
DC	Dendritic cells
DDS	Drug delivery system
DDR	DNA damage response
DISC	Death-inducing signaling complex
DNA	Deoxyribonucleic acid
ER	Estrogen receptor
FADD	Fas-associated protein death domain
FAS	FS-7-associated surface antigen
FasL	Fas ligand
GTP	Guanosine triphosphate
HER2	Human epidermal growth factor receptor 2
hNT	Human nucleoside transporter
HOIL1	Heme-oxidized IRP ubiquitin ligase 1
HOIP	HOIL-1-interacting protein
HPMA	N-(2-hydroxypropyl) methacrylamide
IBM	IAP-binding motif
IAP	Inhibitor of apoptosis

IKKα	Inhibitor of nuclear factor kappa-B kinase subunit alpha
IKKβ	Inhibitor of nuclear factor kappa-B kinase subunit beta
ILP-2	Inhibitor of apoptosis-like protein 2
IRP	Iron regulatory protein
KRAS	Kirsten rat sarcoma viral oncogene homolog
LUBAC	Linear ubiquitin chain assembly complex
MAPK	Mitogen-activated protein kinase
MDR	Multidrug resistance
ML-IAP	Melanoma IAP
MRP1	Multidrug resistance-associated protein 1
NAD^+	Nicotinamide adenine dinucleotide
NAIP	Neuronal apoptosis inhibitory protein
NEMO	NF-κB essential modulator
NET	Neoadjuvant endocrine therapy
NF-κB	Nuclear factor-κB
NK	Natural killer
PARP	Poly(ADP-ribose) polymerase
PD-1	Programmed Cell Death Protein-1
PD-L1	Programmed death-ligand 1
PEG	Polyethylene glycol
PET	Positron emission tomography
P-gp	P-glycoprotein
PgR	Progesterone receptor
PI3K	Phosphoinositide 3-kinase
PSA	Prostate-specific antigen
PSMA	Prostate-specific membrane antigen
RAFT	Reversible addition-fragmentation transfer
RING	Really interesting new gene
RIP1/RIP3	Receptor-interacting serine/threonine-protein kinase 1/3
RNA	Ribonucleic Acid
ROS	Reactive oxygen species
SHARPIN	SHANK-associated RH-domain interactor
SLC	Solute carrier
SMAC	Second mitochondria-derived activator of caspases
TAB1/2	TAK1-binding protein 1/2

TAK1	Transforming growth factor-β activated kinase 1
TLR-4	Toll-like receptor 4
TNBC	Triple-negative breast cancer
TNF	Tumor necrosis factor
TNFR	Tumor necrosis factor receptor
TRADD	TNF receptor-associated death domain
TRAF	TNFR-associated factor
TRAIL	TNF-related apoptosis-inducing ligand
Ub	Ubiquitin
UBA	Ubiquitin-associated domain
VEGF	Vascular endothelial growth factor
VPF	Vascular permeability factor
XIAP	X chromosome-linked IAP
ZIP	Zero interaction potency

1 Introduction

1.1 Cancer

Cancer represents a group of diseases characterised by the uncontrolled proliferation of cells and the migration from their primary site of origin to other body parts [1]. In 2020, an estimated 19.3 million new cancer cases and nearly 10 million cancer-related deaths were reported worldwide. Cancer is also recognised as the leading cause of death in every country, with the number of new cases and deaths rapidly increasing over the years. Additionally, a 47% rise from 2020 is expected in 2040 with an estimated 28.4 million new cases [2]. To overcome this increase, improved treatment, early cancer detection, and prevention are needed [3].

There are more than 200 types of cancer that are distinguished by the tissue of origin [1], [4]. The largest group are carcinomas, which are derived from epithelial cells and represent 85 % of all cancers and more than 80 % of cancer-related deaths in developed countries [1], [5]. Examples of carcinomas include cancers of the mouth, stomach, small and large intestines, skin, pancreas, mammary gland, liver, lung, gallbladder, and prostate. Carcinomas are divided into two groups: squamous cell carcinomas, tumors derived from epithelial cells forming protective layers, and adenocarcinomas, which arise from specialised epithelial cells that produce substances into the cavities or ducts [5].

The other types of tumors are derived from nonepithelial tissues. These include neuroectodermal tumors, which originate in the central and peripheral nervous system, leukemias and lymphomas, which arise from different hematopoietic cells, and sarcomas, derived from mesenchymal cell types. Leukemias and lymphomas can emerge from hematopoietic cell lineages (e.g. T and B lymphocytes) and constitute approximately 2.5 % of tumors [5], [6]. Less than 1 % of all tumors are sarcomas which can originate from fibroblasts, adipocytes, osteoblasts and myocytes [5].

Cancers originating from different cell types exhibit distinct characteristics. These include different molecular mechanisms responsible for carcinogenesis or the invasion of cells from the primary site. However, despite the differences in molecular and cellular routes, the underlying mechanism of the disease is comparable [1].

After thorough analysis, Hanahan and Weinberg defined six hallmarks of cancer in 2 000. Their theory suggested that acquiring the capability for evasion of growth inhibitory signals, autonomous growth signals, unlimited replicative potential, evasion of apoptotic cell death, angiogenesis, and invasion/metastasis are essential for carcinogenesis. A couple

of years later, they added two emerging hallmarks, i.e. avoiding immune destruction and reprogramming energy metabolism. They defined two enabling characteristics, tumor-promoting inflammation and genome instability, which are critical for acquiring the six hallmarks of cancer [5], [7], [8]. In 2022, they also proposed cellular plasticity as the next one to be added to the list [9].

The invasion of cells from the primary site of origin to distant tissues is the distinction between a benign and a malignant tumor [5]. A malignant tumor is invasive and metastasises to other parts of the body. On the other hand, benign tumors do not and are not defined as cancer [1]. These tumors arise from the same factors that cause malignant tumors (e.g. genetic disorders or stress) but typically do not require treatment or removal [3]. However, they can still be life-threatening because of their location or because of damaging other tissues [1]. For example, benign tumor formation and growth in the brain might affect the brain's normal functioning. In contrast, lung tumor growth can cause a blockage in the bronchus, leading to different respiratory disorders [3].

Maintaining the integrity of the genome is essential and alterations of the deoxyribonucleic acid (DNA) can be harmful [10]. Cancer can be caused by inherited gene alterations or by agents called carcinogens, with most of them defined as mutagens. This subgroup causes mutations or modifications to the DNA. Therefore, cancer belongs to genetic diseases and is caused by mutations ranging from point mutations (single base mutations) to large chromosomal aberrations. Carcinogenesis is a complex process involving the accumulation of cell mutations over time. This elucidates why cancer incidence has escalated over the centuries alongside a prolonged human lifespan and why the risk of cancer increases with age [1], [11].

Carcinogenesis is a process caused by the accumulation of genetic and epigenetic changes which lead to the disturbance of a cell. Plenty of factors are important for carcinogenesis, and the interaction between them has the biggest contribution to the development of the disease. 80 to 90 % of malignant tumors result from external environmental factors [12].

The most important ones are diet, excessive alcohol consumption, and smoking. Moreover, for women, giving birth has also been associated with reduced cancer development. Alteration of these lifestyle factors can prevent most cancers and approximately 35 % of cancer-related deaths [1], [12]. It was observed in 1775 that chronic exposure to soot led to a higher incidence of nasal cancer in chimney sweeps. Moreover, the formation of pyrimidine dimers due to unprotected exposure to the sun can increase the risk of melanoma. Another interesting observation is connected to having children, as it was

associated with a decreased risk of developing breast cancer in women [1]. Furthermore, chronic alcohol drinking has been connected with an increased risk of cancer of the breast, liver, throat and mouth, while smoking is the main cause of lung cancer [1], [12]. Lung cancer is the dominant type of cancer worldwide and is responsible for 40 % of all cancer deaths. The main reason for that is the identification of at least 81 carcinogens in cigarette smoke. In addition, the incidence of cancer has also been linked to different diets of various populations all around the world. For example, stomach cancer is a prevalent cancer in the Japanese population and a minor one in the USA. Notably, a decreased risk of developing this cancer has been observed in Japanese people who have migrated to the USA only if they switched to the American diet [1].

1.1.1 Pancreatic Cancer

Pancreatic cancer accounts for approximately 2 % of all cancers and is responsible for about 5 % of cancer-related deaths worldwide. Risk factors include obesity, smoking, advanced age, diabetes, alcohol consumption and family history (about 7-10 % of those affected). It is one of the deadliest malignant tumors. Its global burden has more than doubled in the last 25 years, with the highest incidence regions being Europe, North America and Australia [13], [14], [15].

Mutations in genes such as TP53, KRAS, BRCA2 and CDKN2 have been connected with an increased chance of developing this cancer. Moreover, epigenetic changes, like alterations in DNA methylation and histone modification, can also contribute to the development of the disease [13], [16]. Pancreatic cancer is categorized into two main categories: exocrine pancreatic cancer, which arises from exocrine cells and constitutes over 95 % of all pancreatic cancers (including adenocarcinoma, squamous cell carcinoma, and adenosquamous carcinoma), and neuroendocrine pancreatic cancer, which develops from cells in the endocrine gland [17].

One of the main challenges is, that the disease has no early signs, spreads rapidly and the majority of patients displaying symptoms associated with pancreatic cancer are in an advanced stage. Pancreatic cancer is a highly aggressive type of cancer, with a median survival of 9-15 months for patients with locally advanced disease and 3-6 months for those with metastatic disease. The standard treatment for patients with advanced disease involves FOLFIRINOX (a combination of folinic acid, fluorouracil, irinotecan and oxaliplatin), and a combination of gemcitabine and paclitaxel or gemcitabine and radiation therapy [13], [16], [18], [19].

1.1.2 Breast Cancer

Breast cancer belongs among the 3 top most common cancers worldwide and is the most common malignancy in women [20]. In 2020, there were over 2.3 million diagnosed breast cancer cases and approximately 685 000 deaths associated with the disease worldwide [21]. However, mortality in the European Union and North America has decreased in the last few years. This is mostly due to efficient systemic therapies and early detection [20].

There are 4 main types of breast cancer based on gene expression of estrogen receptor (ER), progesterone receptor (PgR) and human epidermal growth factor receptor 2 (HER2): luminal A and luminal B (hormone-positive), triple-negative and HER2 positive. These subtypes differ in their biological characteristics, prognoses, treatment strategies and responses [20]. The most common type of breast cancer is hormone-dependent (approximately 65 %). Therefore, hormone therapy is used as the primary therapeutic approach. Medications include tamoxifen, an estrogen blocker, or exemestane, which inhibits hormone production in the ovary [22].

Moreover, multiple anti-HER2 monoclonal antibodies, such as trastuzumab and pertuzumab, are used in the case of HER2-positive patients in combination therapies. The treatment of triple-negative breast carcinoma (TNBC) remains the biggest challenge, with the standard approach involving chemotherapy [22]. Standard treatments typically involve docetaxel, paclitaxel, doxorubicin, cyclophosphamide, carboplatin, cisplatin, and gemcitabine [20], [23].

1.1.3 Prostate Cancer

Prostate cancer is the second most common carcinoma in men, with over 1.4 million new cases and approximately 375 000 deaths in 2020 worldwide [24], [25]. While localised prostate cancer is characterised by high long-term survival, metastatic prostate cancer remains incurable [26]. Localised prostate cancer can often be characterised by morphological heterogeneity within individual patients. This can be observed as multiple tumor foci with genetic differences in the prostate, which can lead to treatment resistance and metastatic spread. Patients with distant metastases have a low 5-year overall survival rate of just 30 % [24].

Overall, mutations in various genes are a common factor in prostate cancer development. These include alterations in Ras, Raf, MYC, PTEN, and TP53 [27]. Additionally, genes associated with testosterone metabolism and the androgen signaling pathway are also implicated in the disease [28]. Nowadays, the detection of prostate-specific

antigen (PSA) levels is used as a screening test for prostate cancer detection. However, as the PSA levels can be increased in many other conditions, the testing suffers from a high rate of false positive findings [24]. Another marker of this disease, prostate-specific membrane antigen (PSMA), is used in clinical practice for imaging and detection of prostate cancer throughout the body. PSMA levels correlate with the more advanced stage of this disease and PSMA-positive lesions can be detected by positron emission tomography (PET) [29], [30].

Surgery and radiation therapy are standard for localised prostate carcinoma. For metastatic disease, agents reducing the circulating androgen levels are being used, including darolutamide and enzalutamide [24]. Docetaxel chemotherapy is the gold standard for patients not responding to androgen deprivation therapy (ADT). However, as resistance caused by upregulation of the multidrug resistance (MDR) 1 gene became a problem, cabazitaxel, a second-generation therapy is also used. Moreover, different combination therapies based on ADT and docetaxel have been used and tested (e.g. radiation, thalidomide, apalutamide or gemcitabine) [28], [31].

1.2 Cancer Therapy

Cancer represents a global health problem and the development, as well as improvement of cancer therapy, have become an important task. The primary conventional methods today include surgery, chemotherapy, and radiotherapy [32]. Surgery is most effective only in the early stages of the disease, while chemotherapy and radiation therapy can harm healthy cells and tissues. Another challenge is the development of drug resistance by cancer cells, leading to a decrease in sensitivity and a reduction in the effect of chemotherapy. Furthermore, the lack of specificity, adverse side effects, and rapid drug metabolism exacerbate the situation [32], [33].

However, significant progress has been made with advancements in hormone therapy, targeted therapy, drug delivery systems (DDS), gene therapy, and immunotherapy. Understanding the various molecular pathways in cancers enabled further development of new approaches, which dramatically improved the therapy of some cancers [33].

1.2.1 Surgery

Surgery, i.e. resection was the first method to remove a tumor and even today is considered one of the most promising treatments for many malignant and benign tumors. The earliest mention of using surgery in cancer treatment dates back thousands of years ago to ancient

Egypt, with historical records describing the removal of breast tumors around 1600 BC [34], [35].

The primary objective of cancer surgery is to remove the tumor along with a surrounding margin of healthy tissue, rather than incising into the cancerous tissue. Compared to radiation therapy or chemotherapy, surgery assures minimal systemic damage to the body [34], [35].

Furthermore, surgery is followed by histology to determine staging, a process for assessing the extent of the disease and whether it has spread into regional lymph nodes and other parts of the body (formed metastases) [36], [37].

In addition, surgeons also play a crucial role in early diagnosis and cancer prevention. They are integral to most screening services, including cervical, breast, colorectal and gastric cancer. Their contribution is not only by providing therapy but also by participating in screening research. As a result, huge improvements can be seen in the survival rates of breast or colorectal cancer [34].

1.2.2 Radiotherapy

The beginning of radiation therapy traces back to 1895 when X-rays were discovered by Wilhelm Conrad Röntgen. Subsequent important discoveries were made by Marie Curie in 1898 during her research on radium. This knowledge paved the way for the integration of radiation therapy into cancer treatment [38], [39]. Despite accounting for only about 5 % of the total cost of cancer care, it is utilized by more than half of all cancer patients as part of their treatment plan [40].

Ionizing radiation is a physical agent employed to eradicate cancer cells. Three main forms of ionizing radiation are released during radioactive decay: alpha and beta particles, and gamma rays. While alpha particles, consisting of two neutrons and two protons, are large and highly energetic, they lose energy over short distances and can be stopped by human skin. Beta particles are negatively charged electron-like particles. They are smaller, faster, and more penetrating than alpha particles, but cause less damage. Gamma rays, a form of electromagnetic radiation, have no mass but possess the greatest energy, enabling them to penetrate through the entire body and making them the most potent for cancer treatment [41].

Ionizing radiation deposits energy by interacting with atoms in cells and tissues as it passes through them. This energy can kill cancer cells by causing changes in DNA, disabling their ability to divide and proliferate [38]. Radiation can damage the cell DNA directly or by producing free radicals. Based on the observed dose in the cell, the outcomes

include DNA base changes, DNA-protein cross-links, DNA-DNA cross-links, and single/double-strand breaks [40].

Radiation therapy is used to treat various types of cancer, including skin cancers, breast/prostate/lung/cervix carcinomas, lymphomas, and head and neck carcinomas [38]. It serves as both a primary treatment and as a neoadjuvant or adjuvant therapy, either preceding or following other treatments like surgery or chemotherapy, respectively. Advancements in recent decades have enabled radiation delivery more accurately and at higher doses to the tumor while preserving the healthy tissue [40].

1.2.3 Immunotherapy

Cancer is a disease that can be characterised by genomic instability, leading to the accumulation of many point mutations that can result in the expression of tumour-specific or tumor-associated antigens in cancer cells. These antigens may be identified by the immune system as foreign and trigger cellular immune responses [42]. In cancer, both innate and adaptive immune systems play crucial roles. Components of the innate system, particularly natural killer (NK) cells, neutrophils, macrophages, monocytes and dendritic cells (DC), along with the members of the adaptive immune system, mostly T cells, may contribute to the elimination of cancer cells [42], [43].

However, tumors often develop various mechanisms to evade immune surveillance, including defects in antigen presentation, the recruitment of immunosuppressive cells, and increased activation of inhibitory pathways. These strategies result in the diminished effectiveness of immune cells and the suppression of anti-tumor immune reactions [42].

There are 6 major categories of immunotherapy: cancer vaccines, adoptive T cell transfer, cytokine therapies, immune checkpoint inhibitors, oncolytic virus therapies, and agonistic antibodies against co-stimulatory receptors [42], [44]. Cancer vaccines aim to trigger T-cell-mediated anti-tumor responses by providing tumor-specific or tumor-associated antigens. Adoptive cell transfer involves an *ex vivo* preparation of autologous T-cells, which could be further genetically engineered and reintroduced into patients to eradicate cancer cells [42]. Immune checkpoint inhibitors are engineered to reinvigorate anti-tumor immune responses by blocking inhibitory signaling pathways. The primary targets of these molecules are cytotoxic T lymphocyte-associated molecule-4 (CTLA-4), programmed cell death-1 (PD-1), and programmed cell death ligand 1 (PD-L1) [44]. Cytokine therapies are mainly used to enhance the activity of the immune system and coordinate immune responses. In contrast, oncolytic virus therapies destroy cancer cells directly or create a proinflammatory environment inside a tumor to boost systematic

anti-tumor immunity [42]. Agonistic antibodies are engineered to bind specifically to costimulatory receptors on T cells. They can activate intracellular signaling pathways promoting the growth of T cells, activate effector function against tumor cells, and promote survival [44].

1.2.4 Hormone Therapy

Hormone therapy is commonly used in the treatment of hormone-dependent cancers, such as breast, prostate, and endometrial cancers [45], [46], [47].

The four main types of breast cancer differ in terms of prognosis and the therapeutic agents currently employed. Tumors that are positive for estrogen and/or progesterone receptor (luminal A/B) are less responsive to cytotoxic chemotherapy and can benefit from neoadjuvant endocrine therapy (NET) [20], [45]. Approximately 60-75 % of all breast cancer cases are hormone receptor-positive. The treatment includes aromatase inhibitors, selective estrogen receptor modulators, progestin, and selective estrogen receptor degraders [48].

As the growth and development of the prostate gland rely on androgens, androgen deprivation therapy (ADT) serves as the primary pillar of treatment. The therapy includes gonadotropin-releasing hormone agonists, androgen biosynthesis inhibitors, and nonsteroidal androgen receptor antagonists [46].

Endometrial carcinoma ranks as the fourth most common malignancy in women but with an optimistic prognosis, as the majority of cases are diagnosed in the early stage [47]. Surgery is the main method of treatment, supplemented by radiotherapy and chemotherapy in more advanced cases [49]. Approximately 85 % of all cases arise from prolonged exposure to exogenous and endogenous estrogens with inadequate progesterone activity. These cases can be managed in the early stages without surgery through hormonal manipulation, such as high-dose progestogens or estrogen withdrawal [47].

1.2.1 Chemotherapy

Chemotherapy is a treatment based on a wide array of anti-cancer drugs and natural compounds that can inhibit cell proliferation and destroy cancer cells through various mechanisms. Certain compounds target some of the essential cellular enzymes or structural proteins, while others target DNA, either directly or indirectly, or modulate cell metabolism [50], [51]. Chemotherapeutics demonstrated the ability to disrupt important cellular processes, including DNA replication, and DNA damage repair, and induce programmed cell death (apoptosis), or immune reaction [50].

Chemotherapy primarily works by inhibiting DNA synthesis and cell division, tumor growth and metastasis. Cancer cells are usually under much higher physiological endogenous stress and divide more frequently compared to normal cells. For these reasons, the drugs can affect cancer cells more effectively. However, the toxic effects also impact healthy cells and tissues [50], [52]. The therapy can be given as major treatment per se or in neoadjuvant and adjuvant forms [52]. Adjuvant chemotherapy involves the administration of cytostatic drugs after primary surgery to eliminate or suppress micrometastases, while neoadjuvant chemotherapy is applied before the surgery to reduce tumor volume [53], [54].

Chemotherapy is usually administered as a combination of multiple agents, which are selected for a given type and stage of cancer. The two crucial aspects that need to be considered are the schedule of the treatment and the dosage. It has been observed that very high doses can cause severe side effects and damage normal cells and that prolonged exposure to the drugs can lead to the development of drug resistance and also affect patient's mental and physical health. Therefore, a team of radiologists, psychologists, oncologists, and nutritionists collectively plan the treatments [50].

Conventional chemotherapeutics are categorised into several groups depending on their mechanism of action, including alkylating agents, antimetabolites, intercalators, mitotic inhibitors, topoisomerase inhibitors, radiomimetics, proteasome inhibitors, and polyadenosine diphosphate-ribose polymerase (PARP) inhibitors [50], [51], [55].

1.2.1.1 Alkylating Agents

Alkylating agents are among the oldest and most frequently used drugs employed in cancer treatment, with their first documented use dating back to the early 1940s [56]. The potential of sulphur and nitrogen mustards as anticancer agents was recognized following the use of yperite during World War I, which led to a massive reduction of white blood cells [57]. While most of them share similar mechanisms of action, they vary in their clinical efficacy. Alkylating agents directly target DNA throughout all cell cycle phases by forming intra- or inter-DNA molecule crosslinks. This process inhibits cell division and eventually leads to cell death [56].

These drugs are utilized in the treatment of various cancers, demonstrating significant efficacy against aggressive cancers [58]. Due to their effect on replication, they are also toxic to normal cells that divide frequently, leading to acute suppression of the bone marrow [59]. Prolonged use of alkylating agents can lead to several side effects, such as permanent infertility due to reduced sperm production in males and cessation of menstruation in females. Furthermore, some of the agents have been linked to the

development of secondary malignancies. Thus intense efforts are focused on improving the selectivity of alkylating agents, reducing the side effects, and exploring new combinations with other anticancer drugs [56].

Alkylating agents are classified into six classes: nitrogen mustards, triazenes, ethylenimine, nitrosourea derivates, platinum-containing antineoplastic agents, and alkyl sulfonates. They initiate intramolecular cyclization reactions within cells, forming highly reactive electrophilic cations. These cations can interact with nitrogen, oxygen, sulphur, and phosphorus atoms on biological molecules, leading to their alkylation. Based on this mechanism, alkylating agents mostly act by crosslinking or modifying DNA and ribonucleic acid (RNA), which can lead to the inhibition of DNA replication, transcription and translation. Additionally, they can trigger other molecular alterations, such as oxidative stress induced by glutathione depletion and lipid peroxidation. They also deplete the nicotinamide adenine dinucleotide ($NAD^{+)}$ pool by activating DNA repair enzyme PARP-1. These effects collectively contribute to apoptosis [60].

Among the most frequently used ones are cisplatin, oxaliplatin, carboplatin, chlorambucil, cyclophosphamide, ifosfamide, melphalan, temozolomide, and busulfan [61].

1.2.1.2 Intercalators

Intercalators are drugs that reversibly interact with the DNA double helix and include primarily anti-tumor antibiotics. They belong to a group of anticancer drugs produced by microorganisms, including fungi, and bacteria, as well as derived from animals and plants with antimicrobial properties. These compounds can inhibit aggressive tumor growth and prevent the formation of cancer metastases [62], [63].

The group includes predominantly anthraquinones (i.e. anthracyclines) and peptides (i.e. bleomycin, mitomycin, and actinomycin) [62]. Anthracyclines are aromatic polyketides with a polyhydroxy anthraquinone structure, such as doxorubicin, daunorubicin, epirubicin, idarubicin, and valrubicin. After passive diffusion into the cells, they localize primarily in the nuclei. While the precise mechanisms through which anthracyclines affect tumors are not completely understood, they are believed to employ multiple molecular mechanisms. These include intercalation into DNA, poisoning of topoisomerase II, formation of DNA adducts, and altering the redox state of a cell resulting in torsional stress, destabilization of nucleosomes, and generation of reactive oxygen species (ROS) [64], [65]. Bleomycin is a glycopeptide capable of binding DNA and producing highly reactive free radicals that cause DNA single-strand breaks [66]. The mechanism of mitomycin involves an enzymatic reduction to its active form, which can form cross-links between the complementary strands

of the DNA, leading to cell death, while actinomycin forms a stable complex with double-stranded DNA and inhibits RNA synthesis [67], [68].

Additionally, anti-tumor antibiotics can inadvertently eradicate beneficial bacterial strains, including *Lactobacillus* and *Bifidobacterium*. Given the critical role of the intestinal microbiome in cancer treatment, the use of antibiotics may lead to its disruption, and promotion of inflammation. Consequently, this might dampen the effect of cancer treatment [62].

1.2.1.3 Mitotic Inhibitors

Cell division is a critical process in tumor growth, thus presenting a significant target for effective treatment. The mitotic spindle is at the core of cell division and represents an essential structure that binds to chromosomes, aligns them, and evenly distributes them into daughter cells. Comprised of microtubules, the mitotic spindle represents a key target in cancer therapy [69].

Microtubules, composed of α- and β-tubulin, are highly dynamic polymers and essential components of the cell cytoskeleton. They play pivotal roles in various molecular processes, including mitosis and intracellular trafficking. Microtubules grow by adding Guanosine triphosphate (GTP)-tubulin dimers to their ends, forming a protective stabilizing cap. Loss of this cap triggers rapid microtubule shrinkage, known as catastrophe. However, occasional rescue events can revert this shrinkage to growth. This process is called dynamic instability and cells harness it to generate force during chromosome segregation in mitosis [70]. Mitotic inhibitors, such as taxanes and vinca alkaloids, modulate microtubule dynamics in a dose-dependent manner through different mechanisms [69].

Taxanes are a group of antineoplastic drugs, which include paclitaxel, initially isolated from the bark of the western yew (*Taxus brevifolia*), and semisynthetic derivates like docetaxel and cabazitaxel. After observing its anticancer activity, paclitaxel was first tested in preclinical studies in the 1970s. However, its efficacy was hindered by poor solubility and insufficient substance content in the bark. Therefore, its clinical use remained limited until advancements in chemical synthesis. Today, taxanes are primarily used for the treatment of ovarian, breast, bladder, head and neck, gastric, prostate, and non-small cell lung carcinomas. These drugs exert their effect by binding to β-tubulin with high affinity, stabilizing microtubules and the mitotic spindle. This stabilization leads to the blockade of cell division. Additionally, they bind to Toll-like receptor 4 (TLR-4) in macrophages, leading to the expression of pro-inflammatory cytokines (i.e. IFN-β, TNFα, and IL-1),

and their interaction with microtubules triggers apoptosis and inhibits angiogenesis [71], [72], [73].

Vinca alkaloids are anti-cancer drugs with a hypoglycemic effect isolated from the Madagascar periwinkle plant (*Catharanthus roseus*). Moreover, they have been used to treat high blood pressure and diabetes. Four major representatives used in the clinic are vinblastine, vinorelbine, vincristine, and vindesine. Like taxanes, they interact with microtubules, however, they cause the interruption of microtubule congregation and blockade of polymerization, leading to mitotic arrest. They are mainly used for the treatment of osteosarcoma, breast cancer, acute lymphocytic leukemia, rhabdomyosarcoma, neuroblastoma, and testicular carcinoma [74], [75].

1.2.1.4 Topoisomerase Inhibitors

Topoisomerase inhibitors represent a class of anti-cancer drugs, initially derived from plants. They function by targeting topoisomerases, enzymes capable of altering DNA topology, a crucial process for many cellular functions, including the cell cycle [76]. These compounds are often used in the treatment of small-cell lung, colorectal, ovarian, and haematological cancers [77].

All cells possess two types of topoisomerases: type 1 and type 2. The main function of these enzymes is the relaxation of DNA by inducing temporary breaks to relieve strain created due to supercoiling and regulation of the topological changes in the structure of the double-stranded DNA. The break is formed by an interaction between a phosphate diester of DNA and a tyrosine residue of the enzyme (transesterification). Afterwards, a second transesterification process follows to re-anneal the DNA strands and release the tyrosine residue. Whether a single-strand or double-strand break is formed, depends on the type of topoisomerase [76], [78], [79].

There are two main groups of topoisomerase inhibitors. The first group, primarily affecting type I topoisomerases, includes camptothecin, topotecan, irinotecan, and belotecan. Generally, they exert their effects on DNA by preventing strand rotation, inhibiting the process of re-ligation in the reaction, and stabilizing the bond between DNA and topoisomerase. Camptothecin induces single-strand DNA breaks, while topotecan and irinotecan can reversibly bind to DNA and the topoisomerase I, leading to the formation of a ternary complex. Belotecan, a newer class of inhibitors, shares similar mechanisms with the other members but exhibits reduced toxicity [79]. These drugs are used to treat ovarian, colorectal, and small-cell lung cancers [80].

The second group of inhibitors targets type II topoisomerases. This group includes etoposide, teniposide, doxorubicin, and epirubicin. Etoposide and teniposide modify the activity of topoisomerase II, resulting in breaks in the DNA strands. Doxorubicin and epirubicin primarily function as intercalators but also have the ability to inhibit topoisomerase II. Topoisomerase II inhibitors are employed in the treatment of breast, lung, and testicular cancers, lymphomas, and sarcomas [79], [81].

1.2.1.5 Antimetabolites

It was first observed in the 1940s that antimetabolites exhibit clinical antitumor activity when S. Faber discovered remission in acute leukemia with the use of aminopterin. This discovery was followed by the addition of methotrexate, 5-fluorouracil and 6-mercaptopurine into clinical practice in the next decade [82], [83].

Antimetabolites comprise a class of anticancer drugs that are synthetic derivatives of naturally occurring compounds found in the human body [84]. These drugs can be further divided based on their chemical structure into analogues of purine and pyrimidine bases (compounds crucial for nucleic acid synthesis), vitamins (folic acid/hormones/coenzymes analogues), and non-natural amino acids or peptides (i.e. phosphopeptide-mimetics) [85]. They inhibit vital metabolic processes by interfering with the synthesis and utilization of endogenous compounds. While these drugs influence various enzymatic processes, the majority of them disrupt the synthesis of nucleic acids [84].

Human cells possess the capability to recycle purines and pyrimidines, utilizing them to synthesise deoxyribonucleotides necessary for DNA synthesis. Antimetabolites, which are analogues of these nucleotide precursors, have emerged as a crucial class of anticancer drugs. In 2009, 14 antimetabolites were approved by the FDA for cancer treatment, constituting nearly 20 % of all anti-cancer agents [86]. In recent years, pharmaceutical industries have developed and characterised numerous novel drugs based on nucleoside analogues. As of 2023, there were 18 antimetabolite drugs approved for cancer treatment in the U.S. [87], [88].

There are two important antimetabolite sub-groups: folic acid and purine/pyrimidine analogues. Folic acid is a crucial compound that, in its reduced form, can transfer one-carbon groups to other molecules. This process is essential, for example, in converting deoxyuridine monophosphate to deoxythymidine monophosphate. Folic acid is reduced by dihydrofolate reductase, an enzyme, that has become a target for many folic acid antagonists (e.g. methotrexate). The effect of methotrexate combines the inhibition of dihydrofolate reductase and the inhibition of enzymes necessary for pyrimidine synthesis (thymidylate

synthase). It is used to treat many cancers, including acute childhood leukemia, as well as breast, testicular, and lung cancers in adults [85], [89].

The other sub-group comprises analogues of natural purine and pyrimidine bases or nucleosides. These antimetabolites are imported into cells, usually by a membrane transporter, and are transformed into analogues of nucleoside triphosphates that can interfere with DNA synthesis, leading to DNA damage, replication blockage and apoptosis [86].

Antimetabolites of purine and pyrimidine bases primarily target the DNA polymerases involved in DNA replication, including DNA polymerase α, δ, and ε. These compounds exert their activity by competing or substituting for the natural nucleotides, interfering with DNA synthesis and ultimately leading to chain termination. This sub-group comprises several drugs, including 6-mercaptopurine, 5-fluorouracil, capecitabine, cytarabine, and gemcitabine. They are commonly used in the treatment of various cancers, such as childhood acute lymphocytic leukemia, and colorectal, breast, stomach, pancreatic, or non-small-cell lung cancers [86].

1.2.1.5.1 Gemcitabine

Gemcitabine (2′,2′-difluorodeoxycytidine, Gemzar®) is a cytidine analogue with two fluorine atoms (**Fig. 1**) and one of the most prescribed anticancer drugs in the world [90]. Initially developed as an antiviral agent, but is now primarily used to treat pancreatic adenocarcinoma, breast, ovarian, bladder, and non-small-cell lung cancer [90], [91].

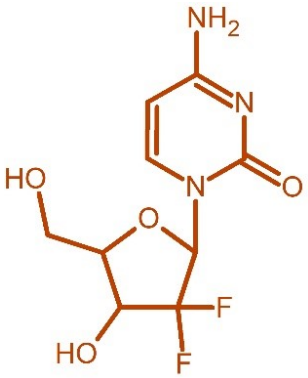

Figure 1. A cytidine analogue gemcitabine with two fluorine atoms replacing the hydroxyl in the ribose. Created in ChemSketch.

The most frequently used schedule in clinical practice involves the intravenous administration of 1 000 mg/m^2 weekly for 3 weeks, followed by a one-week break. In addition to adult patients, gemcitabine is often prescribed to children due to mild toxicity [90], [92]. The most common side effects include anaemia, thrombocytopenia, fatigue,

and vomiting. Importantly, these adverse effects are clinically manageable, and fatal treatment-related occurrences are reported in only 1 to 4 % of patients [93].

It has become the standard treatment for locally advanced and metastatic pancreatic cancer. Pancreatic cancer is one of the most devastating malignancies, characterised by a median survival rate of fewer than 5 months post-diagnosis and a 5% five-year survival rate. This poor prognosis is mainly attributed to late prognosis, limited efficacy of drugs due to poor penetration, tumor cell chemoresistance, aggressive tumor behaviour, and the inability to perform the surgical intervention in the majority of patients [93], [94].

Gemcitabine is administered as a prodrug, meaning that after administration, it requires to be metabolised into its active triphosphate form. It enters cells through a group of membrane proteins known as human nucleoside transporters (hNTs) [94]. Subsequently, three phosphate groups are added to it by the enzymes deoxycytidine kinase, pyrimidine nucleoside monophosphate kinase, and nucleoside diphosphate kinase [90], [94].

Gemcitabine's primary mechanism of action is the inhibition of DNA synthesis by incorporating its triphosphate form (dFdCTP) into DNA. This incorporation is followed by the addition of a single deoxynucleotide, leading to the termination of chain elongation as the DNA polymerase is incapable of proceeding. This process is also known as masked chain termination (**Fig. 2**) [94]. Moreover, gemcitabine blocks the activity of repair enzymes, preventing its removal from DNA. Furthermore, gemcitabine diphosphate inhibits ribonucleotide reductase, a crucial enzyme responsible for the synthesis of deoxynucleotides [90], [94].

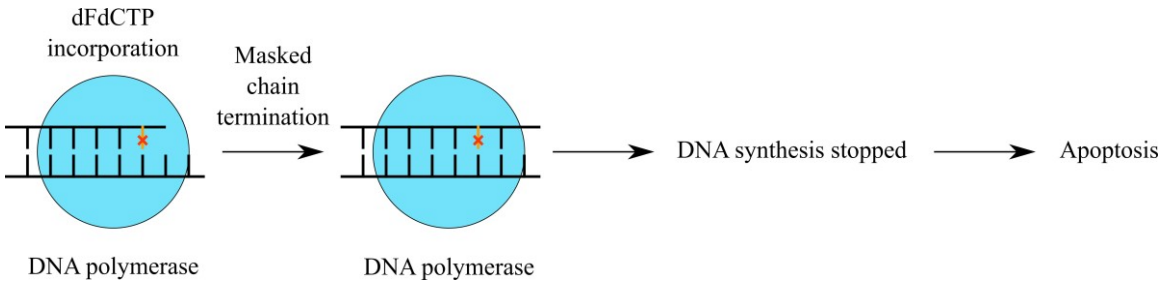

Figure 2. Masked chain termination. After the incorporation of dFdCTP and another deoxynucleotide, DNA polymerase is unable to proceed and the chain elongation is stopped, ultimately leading to apoptosis. Adapted from [94]. Created in Inkscape.

Gemcitabine undergoes deactivation through several mechanisms, including deamination by cytidine deaminase, which exhibits a significantly high affinity for gemcitabine. Additionally, deoxycytidylate deaminase metabolizes the monophosphate form, and the monophosphate can also be dephosphorylated to a nucleoside [94]. Of these

processes, inactivation by cytidine deaminase is the most significant, as this enzyme is highly expressed in the liver and plasma, resulting in the inactivation of the majority of the administered drug [90], [94].

Over 75 % of gemcitabine is excreted in the urine within the first 24 h after being metabolised to 2′,2′-difluoro-deoxyuridine by cytidine deaminase. Furthermore, no changes in pharmacokinetics were observed when gemcitabine was administered in combination with cisplatin or paclitaxel [90]. Collectively, these findings suggest that enhanced anti-tumor efficacy could be achieved by prolonging systematic exposure of tumors to gemcitabine through a DDS. This has been demonstrated, for example, through the use of poly(ethylene glycol), hydrogel polymers composed of a pentablock terpolypeptide, or covalent coupling of squalene, a natural lipid. Many of these modifications have shown prolonged circulation time, reduced metabolic degradation, and improved gemcitabine stability [91], [93], [95].

1.3 Chemotherapy Limitations and Multidrug Resistance

In cancer treatment, chemotherapy serves as a cornerstone in managing various types of cancer across different disease stages. As a result, developing resistance to chemotherapy may lead to treatment ineffectiveness and adverse outcomes, including death [96]. Statistical data indicates that the majority of cancer-related deaths are linked to drug resistance [97]. Chemotherapy resistance is a multifactorial phenomenon caused by alterations in the metabolism and genomic processes of cancer cells. It has become one of the main targets in cancer research. Over the years, numerous mechanisms of chemotherapy resistance have been discovered, such as alterations in drug metabolism, increased drug efflux and changes in apoptotic pathways [96], [97].

1.3.1 Drug Metabolism

Drug metabolism is a crucial process involving alterations in drug polarity (hydrophilicity) to facilitate its removal from the body. It comprises two main processes aimed at increasing the polarity of the drug. The initial step entails reactions such as hydroxylation, reduction, and oxidation, while the subsequent step involves binding the drug to structures, such as glutathione, glucuronic acid, or an amino acid [96]. While drug metabolism primarily functions as a detoxification mechanism diminishing the effect of the drug, it can lead to drug activation in some cases. Moreover, these modifications can also alter the

pharmacokinetics of the metabolite, resulting in enhanced efficacy [96], [98]. The primary group of enzymes responsible for this process are cytochromes P450 [96]. They play an important role in activating many anti-cancer agents, such as cyclophosphamide or tamoxifen [99], [100]. However, their overexpression has been also associated with resistance to chemotherapy due to the rapid inactivation of other drugs, including irinotecan [101].

1.3.2 Multidrug Resistance

Multidrug resistance (MDR) is another critical mechanism that enables cancer cells to survive exposure to a wide array of anti-cancer drugs. This type of resistance is often mediated by the upregulation of the expression of specific membrane proteins known as ATP-binding cassette transporters (ABC transporters) [97]. The three most important members of the ABC transporters are P-glycoprotein (P-gp), multi-drug resistance-associated protein 1 (MRP1), and breast cancer resistance protein (BCRP) [102]. These proteins are responsible for the absorption, regulation of distribution, and excretion of numerous chemical compounds within the body [97]. P-gp, for instance, normally functions as a biological barrier, actively removing toxins from cells, however, it can also bind and pump out a range of chemotherapy agents, including vinblastine, methotrexate, doxorubicin, and paclitaxel, using energy from ATP hydrolysis [97], [102]. Elevated expression of P-gp has been observed in approximately 50 % of tumors [97].

Another challenge in cancer treatment is mutations or downregulation of solute carrier (SLC) proteins, which facilitate the uptake of drugs into cells. In many cancers, mutations and downregulation of these proteins hinder the efficient import of anti-cancer drugs, further contributing to drug resistance [102].

1.3.3 Apoptosis

Programmed cell death, or apoptosis, is an evolutionarily conserved process fundamental for organism development and maintaining tissue homeostasis. Additionally, it serves as a response to cell damage and external stress. This genetically programmed process is characterised by several features, including fragmentation of DNA in the nucleus, condensation of chromatin material, loss of adhesion to extracellular matrices, and cell shrinkage [103]. Furthermore, apoptosis involves the expression of phosphatidylserine on the outer membrane and the activation of caspases, which are cysteine aspartyl proteases capable of degrading different substrates, such as actin and nuclear lamin [102], [103].

However, when cancer cells lose the ability to undergo apoptosis, they may become capable of uncontrolled proliferation. Numerous proteins are responsible for apoptosis resistance, and many of them have been observed to be overexpressed in various tumors. Apoptosis occurs through both extrinsic and intrinsic pathways [103]. Additionally, another pathway involving T-cell-mediated cytotoxicity has been observed. This process entails the effects of granzyme B and perforin, ultimately leading to cell death [104].

1.3.3.1 Intrinsic Apoptosis

The intrinsic pathway, which originates in mitochondria, is mediated through pro-apoptotic proteins (Bax, Bak, Bim, Bid, PUMA) and anti-apoptotic proteins (Bcl-2, Bcl-xL, Bcl-w, MCL1). Various intra and extra-cellular stressors causing DNA damage, including irradiation, oxidative stress, and exposure to anti-cancer agents trigger this pathway [102], [103].

The detection of DNA damage is facilitated by DNA damage response (DDR) pathways, which serve as defence mechanisms to protect the genome. These pathways involve various proteins and complexes, including MRN, ATM, and MDC1, leading to the activation of signaling pathways and molecules that modulate DNA repair, cell cycle progression, cell death, and cell metabolism. Among these, p53, also known as the guardian of the genome, is the most important effector molecule. As a transcription factor, p53 activates the expression of numerous genes involved in the intrinsic apoptosis pathway, such as Bax, Bid, and PUMA [105], [106].

Upon activation by Bim/Bid, Bax/Bak proteins are inserted into the mitochondrial membrane, causing the release of cytochrome c into the cytosol. Bax and Bak play a crucial role in this process by forming macropores in the outer mitochondrial membrane, leading to mitochondrial outer membrane permeabilization. Conversely, anti-apoptotic proteins hinder this process by binding and inhibiting Bax and Bak. Subsequently, an apoptosome is formed through the interaction between cytochrome c, Apaf-1, ATP and procaspase-9. This formation leads to the cleavage of caspase-9, which activates executioner caspases, such as caspase-3, caspase-6, and caspase-7, ultimately resulting in cleavage of cell-death substrates (PARP, nuclear lamins) [105], [107], [108].

Additionally, proteins like SMAC (Second mitochondria-derived activator of caspases), IAPs (Inhibitors of apoptosis), and MYC, an oncogene, modulate this process. Following apoptosis initiation, SMAC is released alongside cytochrome c from the mitochondria. SMAC acts as an antagonist of IAPs, blocking their function as negative regulators of apoptosis. Dysregulation of the expression of anti-apoptotic and pro-apoptotic

genes has been observed in many cancers, contributing to the development of drug resistance [105], [107].

1.3.3.2 Extrinsic Apoptosis

The extrinsic pathway is initiated by the binding of ligands such as tumor necrosis factor (TNF), Fas ligand (FasL), and TNF-related apoptosis-inducing ligand (TRAIL) to their respective transmembrane receptors. These ligands bind to the Type 1 TNF receptor (TNFR1), Fas, and TRAIL receptors (Death receptors 4 and 5), leading to receptor trimerization. Upon TNF binding, the receptor undergoes trimerization and recruits the TNF receptor-associated death domain (TRADD), which binds TNF receptor-associated factor (TRAF), receptor-interacting protein kinase (RIP1 or RIPK1), and cellular inhibitor of apoptosis proteins (cIAPs), forming Complex I. In the Fas-mediated pathway, binding of a Fas ligand to Fas receptors initiates the formation of a death-inducing signaling complex (DISC), consisting of a Fas-associated death domain (FADD), cellular FLICE inhibitory proteins (c-FLIPs), procaspase-8, and procaspase-10. Formation of DISC activates caspase-8 and caspase-10, leading to its dissociation from the complex and subsequent activation of effector caspases (-3, -6- and -7). Caspase-8 activation also triggers the activation of BID protein, which translocates to the mitochondrial membrane and contributes to cytochrome c release. TRAIL signaling mechanism closely resembles that of the Fas-mediated pathway. [102], [103], [107].

Numerous proteins serve as negative regulators of cell death and are frequently overexpressed in different types of cancer. Therefore, many of these proteins have become targets in cancer therapy, intending to induce apoptosis in cancer cells. Among these proteins are death signal receptors (TNFR1, Fas, and TRAIL receptor), anti-apoptotic Bcl-2 proteins (Bcl-2, Bcl-XL, and Mcl-1), as well as members of the IAP family [103], [109].

1.4 Inhibitor of Apoptosis Proteins

IAPs constitute a family of proteins initially discovered in insect cells during baculoviral infections, where they act as crucial inhibitors of cell death [110], [111]. In mammalian cells, they possess the same role, working as negative regulators of caspases. Furthermore, IAPs play a significant role in ubiquitin (Ub)-dependent signaling processes, acting as E3 ubiquitin ligases. This function involves facilitating the transfer of Ub from E2 enzymes to target substrates. These processes include the modulation of key pathways such as mitogen-activated protein kinase (MAPK) and nuclear factor-κB (NF-κB), which regulate the

expression of genes essential for numerous processes, such as inflammation, cell migration, immunity, and cell survival [111].

Dysregulation of various cellular processes controlled by IAPs is frequently observed in cancer, contributing to disease initiation, tumor progression, and maintenance [111]. Additionally, aberrant expression of IAPs, along with the downregulation of their natural inhibitor SMAC, is frequently detected in many cancers [112]. Consequently, IAPs have emerged as promising targets in cancer therapy [111].

1.4.1 IAP Family and Structure

The family consists of eight members, each differing in structure and function (**Fig. 3, p. 33**) [112]. The first member discovered was NRL family apoptosis inhibitory protein (NAIP) in 1995, found in type I spinal muscular atrophy patients, where it was proposed to contribute to the pathogenesis of the disease [113]. The following year, X chromosome-linked IAP (XIAP), cellular inhibitor of apoptosis 1 (cIAP1), and cellular inhibitor of apoptosis 2 (cIAP2) were identified, followed by the discovery of Apollon, Survivin, melanoma IAP (ML-IAP), and IAP-like protein 2 (ILP-2) [112], [114].

The main characteristic shared by all members of the IAP protein family is the presence of the baculovirus inhibitor of the apoptosis protein repeat (BIR) domain. This domain is approximately 70 residues long and is essential for protein-protein interactions. There are 3 such BIR domains (BIR1, BIR2, BIR3) in IAP proteins, usually located in their N-terminus portion, although their arrangement may vary among individual IAPs. In addition to the BIR domain, XIAP, cIAP1, cIAP2, ILP-2, and ML-IAP also contain a RING (Really Interesting New Gene) domain, which contributes to their E3 ubiquitin ligase activity. Furthermore, XIAP, cIAP-1, cIAP-2, and ILP-2 possess a ubiquitin-associated domain (UBA), crucial for the binding of IAPs to Lysine-linked polyubiquitination. A caspase-recruitment domain (CARD) is a distinctive feature of cIAPs, contributing to the regulation of E3 activity by inhibiting RING-mediated dimerization and E2 binding [111], [112]. Additionally, the ubiquitin-conjugating domain (UBC) is unique for Apollon, facilitating the covalent attachment of ubiquitin to target proteins (**Fig. 3, p. 33**) [111], [115].

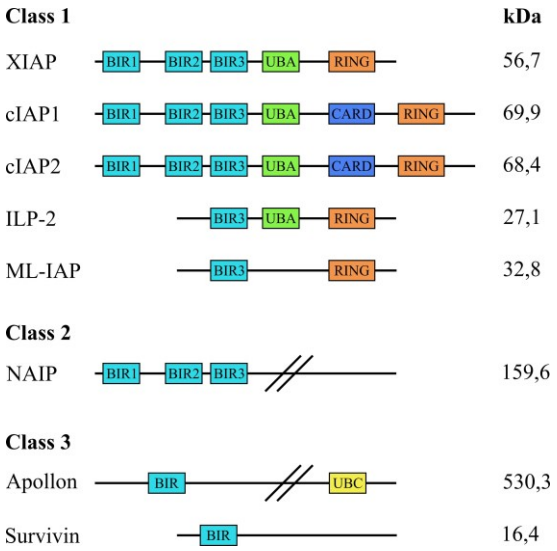

Figure 3. IAP family. This protein family consists of 8 members found in the human body differing in their structure and functions. Adapted from [116]. Created in Inkscape.

1.4.2 BIR Domain

The BIR domain stands as the cornerstone of IAPs, providing them with the ability to interact with other proteins, including binding to target proteins and adaptor molecules. The domain features specific invariant amino acid residues, including a conserved histidine and three cysteines, crucial for the coordination of a zinc ion. This coordination is necessary for stabilizing the BIR tertial structure. Besides these residues, there are differences in the structure of the three BIR domains (BIR1, BIR2, BIR3), explaining the variability in their functions [111], [117].

There are two distinct types of BIR domains, distinguished by the presence of a deep peptide-binding groove. Type-I BIR (BIR1) domains possess a shallow binding groove and lack a peptide-binding groove. In contrast, type-II BIR (BIR2/3) domains feature a distinctive hydrophobic groove enabling them to bind IAP-binding motifs (IBMs) found in caspases and IAP-inhibitory molecules like SMAC [111]. A crucial part of an IBM is an N-terminal alanine or serine, which inserts into the hydrophobic groove and forms hydrogen bonds with neighbouring residues, securing the binding of IBM-carrying proteins to an IAP [111], [118].

Apoptosis-regulatory IAPs like XIAP, cIAP1, and cIAP2 contain two type-II BIR domains arranged in tandem. This structure serves two purposes: it expands the range of proteins they can interact with, and it enhances their affinity for specific IBM-containing target proteins, particularly those that are dimeric or oligomeric. Additionally, these IAPs possess a type-I BIR domain, which employs distinct strategies to interact with a diverse set

of target proteins [111]. For instance, BIR1 of XIAP binds to TAB1, an adaptor protein of transforming growth factor-β activated kinase 1 (TAK1), while BIR1 of cIAPs interacts with TRAF2, an adaptor protein in the TNF signaling pathway (discussed further in the Physiological Role of IAPs chapter). Therefore, type-I BIR domains play a crucial role in connecting IAPs to specific signaling processes [119], [120], [121].

1.4.3 RING Domain

The RING domain, another distinguishing characteristic of apoptosis-regulatory IAPs, is located at the C-terminal region. It functions as a ubiquitin ligase (E3) enzyme, facilitating the transfer of Ub to target proteins [111]. Ub, a small protein, can be covalently bound to target proteins through a process involving 3 enzymes: ubiquitin-activating enzyme (E1), ubiquitin-conjugating enzyme (E2), and E3 [122].

Ub activation occurs when E1 utilizes ATP hydrolysis to form a thioester bond between its active-site cysteine residue and the C-terminus of Ub. Subsequently, Ub is transferred to the active-site cysteine of E2. The last step involves the interaction between Ub-charged E2 and E3, which facilitates the transfer of Ub to different substrates depending on its specificity. There are three subfamilies of E3 enzymes based on their mechanism of Ub transfer. The RING subfamily can simultaneously interact with Ub-charged E2 and substrate, providing direct transfer of Ub to the target. In contrast, HECT and RBR E3 ligases facilitate a two-step mechanism of Ub transfer [122], [123].

E3 ligases can transfer Ub to lysine, cysteine, serine, and threonine residues, as well as the free amino group of the N-terminus of target proteins, forming isopeptide, thioester, hydroxyester, and peptide bonds, respectively. After the initial ubiquitination, more Ub molecules can be linked to the first Ub molecule creating polyubiquitin chains. During this elongation, the C-terminal glycine of the first Ub molecule can be linked to one of seven lysine residues of other Ub via an isopeptide bond (Lys6, Lys11, Lys27, Lys29, Lys33, Lys48 or Lys63). Moreover, Ub can be linked to the N-terminus of another Ub, forming Methionine1 (M1)-linked Ub chains [122], [123].

These diverse Ub chains result in different cellular outcomes. For example, K48-linked poly-Ub chains typically target proteins for proteasomal degradation, whereas M1- and K63-linked chains regulate various biological processes, including MAPK and NF-κB signaling pathways [111], [124].

The activity of the E3 domain in IAPs is tightly regulated through signaling pathways, such as TNF, and NF-κB. In the absence of any signal, cIAP1 remains in

an inactive monomeric state, formed through an intramolecular interaction between the BIR3 and RING domains, which blocks the activation (dimerization) of the RING domain. This autoinhibition is further enhanced by the interactions with the CARD domain [111], [125], [126].

Activation of E3 ligase activity is initiated by binding of IAP to a substrate through the BIR3 domain, which disrupts the interaction between the BIR3 and RING domains. Furthermore, it induces dimerization of the RING domain, crucial for the transfer of Ub from E2 to the substrate [111], [127].

However, the binding of SMAC or SMAC mimetics (anti-cancer drugs) to one of the BIR domains triggers autoubiquitination and subsequent degradation of cIAPs (**Fig. 4**). By mimicking the presence of a substrate, SMAC/SMAC mimetics facilitate the transfer of Ub to one of the lysine residues in cIAPs, leading to its proteasomal degradation [128], [129].

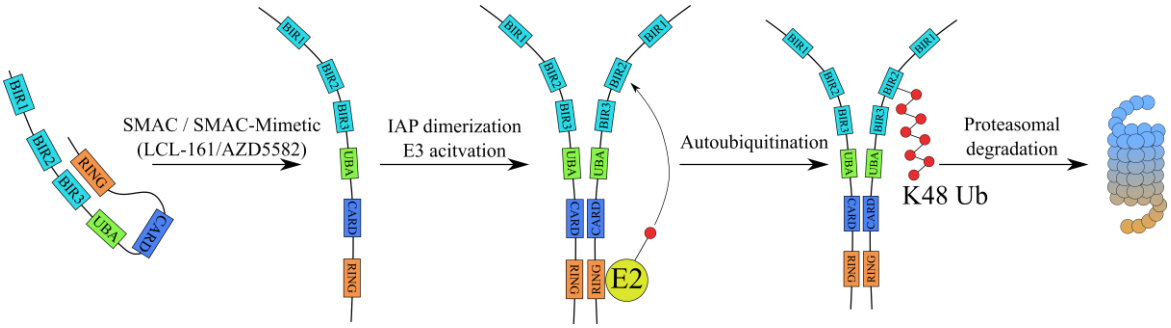

Figure 4. Effect of SMAC/SMAC mimetic on cIAP1/2. In the presence of these molecules, RING-RING interaction leads to cIAP dimerization, leading to autoubiquitination and proteasomal degradation of cIAP1/2. Adapted from [111]. Created in Inkscape.

1.4.4 Physiological Role of IAPs

The primary function of IAPs is to prevent apoptosis by inhibition of caspases. Among the IAP family, XIAP is the only member known to directly bind and inhibit caspase-3, -7, and -9 [117]. XIAP achieves inhibition of caspases-3 and -7 through a key-lock mechanism, where the BIR2 domain binds next to the active-site pocket, thus preventing the binding of the substrate. In contrast, XIAP inhibits caspase-9 by the interaction of the BIR3 domain with the enzyme, thereby blocking the dimerization of caspase-9, a critical step for its activity (**Fig. 5, p. 36**) [111].

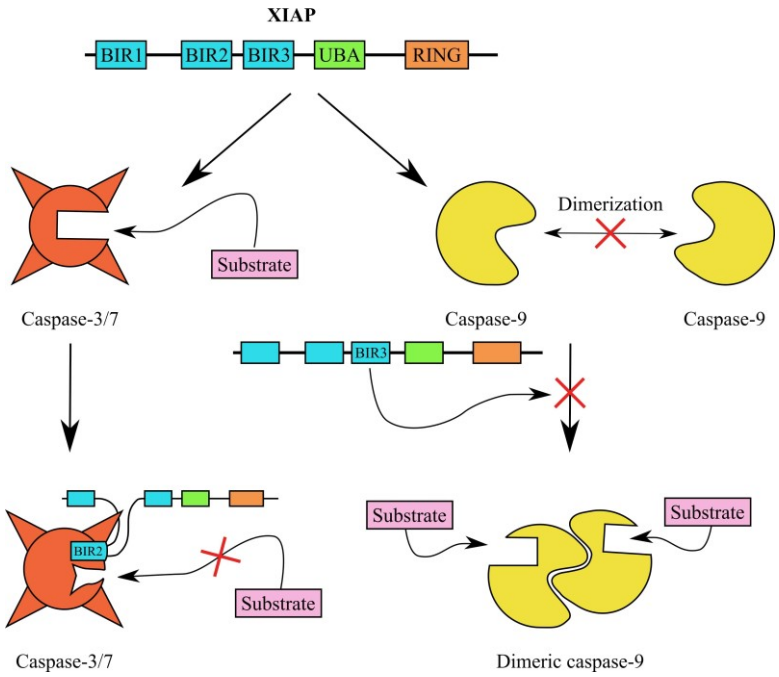

Figure 5. Mechanisms of XIAP-mediated inhibition of caspase-3/7 and caspase-9. A key-lock mechanism of the BIR2 domain in caspases-3/7 and a blockade of dimerization by the BIR3 domain in the case of caspase-9. Adapted from [111]. Created in Inkscape.

Additionally, cIAPs play a crucial role in mediating the activation of the MAPK and NF-κB pathways triggered by TNF-receptor (TNFR) family members (**Fig. 6, p. 37**) [130]. Upon the binding of TNF to TNFR1, Complex I is formed, consisting of TRADD, TRAF2, cIAP1/cIAP2, and RIP1 [111], [131]. The ubiquitination of RIP1 by cIAPs recruits the Linear Ub chain assembly complex (LUBAC), comprising heme-oxidized IRP ubiquitin ligase 1 (HOIL1), HOIL-1L-interacting protein (HOIP), and SHANK-associated RH-domain interactor (SHARPIN). This recruitment also involves the kinase complex composed of transforming growth factor beta-activated kinase 1 (TAK1), TAK1-binding protein 1 (TAB1), and TAK-1 binding protein 2 (TAB2), as well as the IKK complex, which consists of NF-κB essential modulator (NEMO), inhibitor of kappa B kinase α (IKKα), and inhibitor of kappa B kinase β (IKKβ) [132]. Once recruited, LUBAC modifies RIP1 and NEMO with M1-linked Ub chains, stabilizing the signaling. Moreover, the ubiquitination of NEMO induces a conformational change in the IKK complex, potentially facilitating its activation. Consequently, the degradation of inhibitors of NF-κB occurs, resulting in the translocation of NF-κB to the nucleus and initiation of expression of target genes involved in cell proliferation and survival, as well as expression of pro-inflammatory molecules in immune cells [111], [116]. The MAPK pathway is activated by the complex of three kinases TAK1, TAB1, and TAB2. The polyubiquitin chains produced by LUBAC serve as a docking platform for this complex, thus activating it [126].

Furthermore, XIAP, cIAP1, and cIAP2 collectively regulate the formation of the Ripoptosome, an upstream cell-death-inducing platform. This complex forms due to the degradation of IAP proteins, which serve as negative regulators. The Ripoptosome complex includes RIP1, Fas-associated death domain (FADD), and caspase-8, leading to apoptosis [133], [134]. The activation of caspase-8 triggers the cleavage and subsequent activation of Bid, initiating the intrinsic pathway of apoptosis [135]. However, in the absence of caspase-8, a Ripopstosome-derived complex is formed, comprising FADD, RIPK1, and RIPK3/RIP3, ultimately triggering necroptotic cell death (**Fig. 6**) [116].

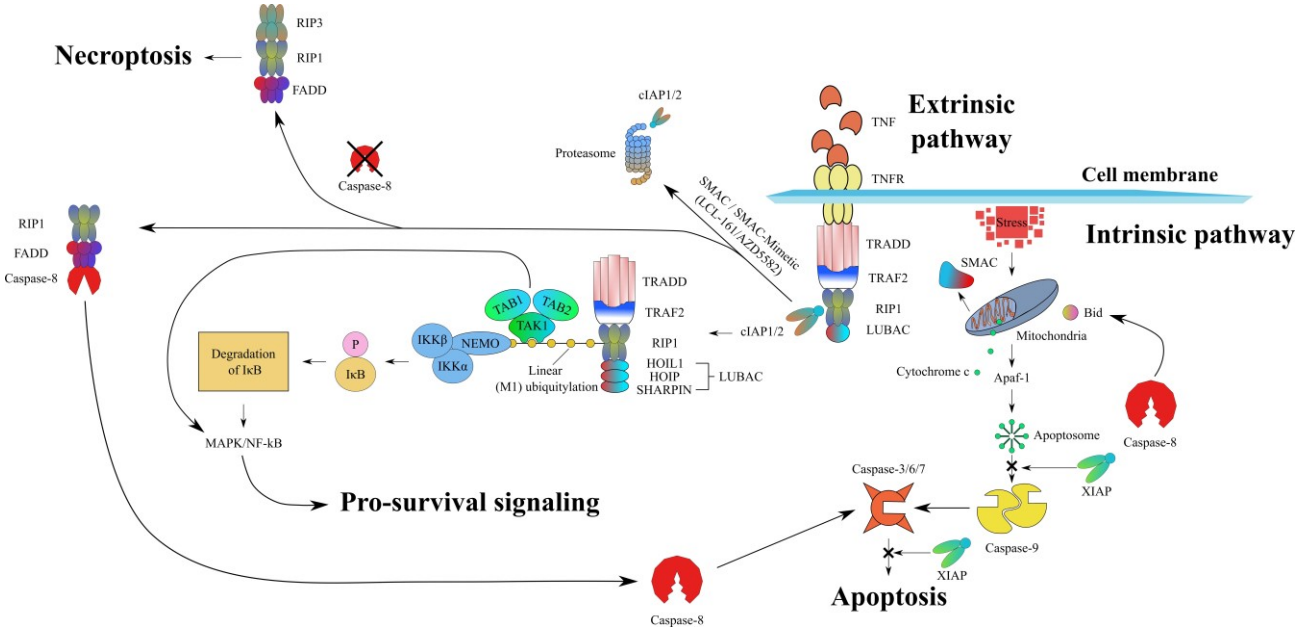

Figure 6. Overview of extrinsic and intrinsic pathways of apoptosis and the role of IAP proteins in these processes. Adapted from [111], [116], [116], [126], [131], [132], [133], [134], [135]. Created in Inkscape.

1.4.5 IAPs and Cancer

IAPs have emerged as potential druggable targets in cancer treatment due to their pivotal role in apoptosis regulation and signaling pathways, coupled with their observed overexpression in various types of cancer [112].

Similar levels of IAPs expression have been observed in healthy and cancerous tissue in breast carcinoma, but increased levels of XIAP and survivin have been associated with advanced disease stages [136]. In pancreatic carcinoma, elevated expression of cIAP2, survivin, ML-IAP, and XIAP have been documented. Furthermore, a correlation between an increased expression of cIAP2 and resistance to paclitaxel, doxorubicin, and 5-fluorouracil has been found [137]. Similarly, elevated expression of multiple IAPs has been observed in prostate cancers [138].

1.4.6 IAP Inhibitors

The discovery of SMAC, a natural inhibitor of IAPs, and the findings of its downregulation in many cancers, have sparked interest in developing new compounds that mimic the structure of SMAC to target IAPs for inhibition and degradation [112].

The mature form of SMAC consists of 184 amino acids and it is released from mitochondria during the intrinsic apoptotic pathway along with cytochrome c [112], [139]. Upon dimerization through a hydrophobic interface, SMAC interacts with IAP domains BIR2 and BIR3, neutralizing their inhibitory effects on caspases [140]. The crucial part of the interaction is the first four N-terminal residues, also referred to as the alanine-valine-proline-isoleucine (AVPI) domain (**Fig. 7, p. 39**). Following the interaction, the AVPI domain activates the RING activity of IAP, leading to the inhibition or degradation of cIAP1, cIAP2, XIAP, or ML-IAP [129].

In response to the evasion of apoptosis and SMAC downregulation in cancer cells, SMAC mimetics (IAP inhibitors) have been developed. They replicate the AVPI domain structure to optimize their pharmacological properties. These mimetics are categorised into four generations, including GDC-0512, SM-406, Birinapant, LCL-161, and AZD5582 [112]. However, most of these drugs have shown low efficacy in Phase I/II clinical trials and therefore are being tested in combination with different cytotoxic agents, including paclitaxel, docetaxel, irinotecan, gemcitabine, and carboplatin [116].

LCL-161 (**Fig. 7, p. 39**), an orally bioavailable compound, exhibits binding affinity for cIAP1, cIAP2, and XIAP [141]. It demonstrated a promising potential to induce cell death in leukemia and hepatocellular carcinoma cells [142], [143]. Moreover, LCL-161 showed good tolerability in solid tumors patients in the phase I study [112], [144]. However, this study also revealed poor efficacy as a single drug with a maximum tolerated dose determined to be 1800 mg [144]. Conversely, positive outcomes were observed when LCL-161 was combined with paclitaxel [112].

AZD5582 (**Fig. 7, p. 39**), a dimeric IAP inhibitor, binds to cIAP1, cIAP2, and XIAP. It demonstrated efficacy in breast and pancreatic cancer cell lines by inducing apoptosis [145], [146]. Interestingly, it also showed potential in HIV treatment by activating the NF-kB pathway. The mechanism involves breaking the latency of the virus by inducing the expression of HIV protein, thereby activating the immune system [147].

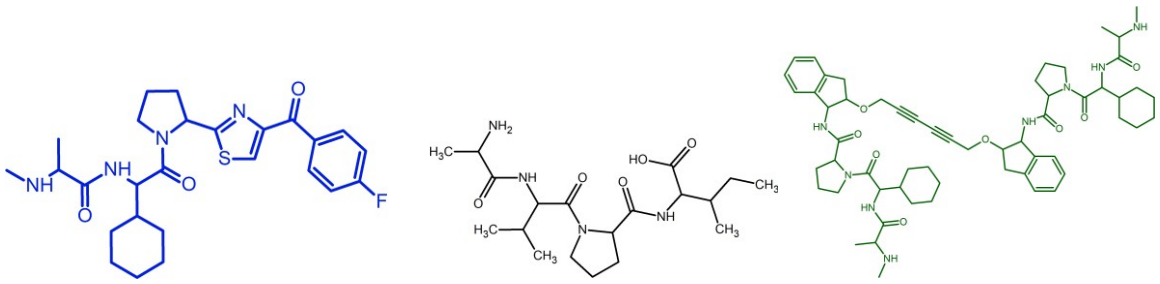

Figure 7. AVPI domain of SMAC in black, LCL-161 in blue, and AZD5582 in green. LCL-161/AZD5582 works as mimetics of the AVPI tetrapeptide. Compared to LCL-161, AZD5582 is a dimeric molecule connected through a linker. Created in ChemSketch.

1.5 Drug Delivery Systems for Cancer Therapy

In recent decades, significant progress has been made in cancer treatment, largely attributed to an improved understanding of the underlying mechanisms of cancer development and progression. Despite these advancements, numerous cancers remain difficult to treat effectively, with a need for novel approaches [148]. As developing new drugs is time-consuming and expensive, researchers have increasingly focused on enhancing the efficacy and safety of existing medications through various strategies, including individualized drug therapy or the utilization and development of DDS [149].

The primary objectives for all DDS are to reduce drug toxicity, enhance the accumulation at the target site to maximize the therapeutic efficacy, and minimize drug accumulation in healthy tissues [150]. Currently, numerous DDS in cancer therapy are employed for various anti-cancer agents. Examples include nab-paclitaxel and pegylated liposomal doxorubicin, which passively target tumors through modifications in their physicochemical characteristics. Based on these passive targeting approaches, the second generation of drug delivery systems actively targeting drugs to tumors by utilizing small organic molecules and peptides specific to cancer cells is under development [151].

1.5.1 Types of Drug Delivery Systems

In recent years, there has been a significant increase in research focused on exploring a wide range of inorganic (metal and nonmetallic) and organic materials, including liposomes, exosomes, natural polymers, and synthetic polymers, for their applications in drug delivery. These DDS have shown promise in addressing the challenges of cancer therapy demonstrating selective accumulation in tumors and improved treatment efficacy [151].

Metal nanoparticles are derived from a range of materials, such as gold, zinc oxide, or silver [152], [153], [154]. They can be characterised by their anticancer, antimicrobial, and magnetic properties, making them usable in various areas, including food science and

medicine [151]. In cancer treatment, they can be employed either per se for their cytotoxic effect or in combination with other drugs for enhanced therapeutic efficacy [155], [156]. Furthermore, metal nanoparticles are also used as DDS to deliver agents directly to tumor tissue. This is achieved by modifying the surface of nanoparticles with targeting ligands, including antibodies or nucleic acids [157].

Nonmetallic nanoparticles include silicon and carbon substances. Their main advantages are high biocompatibility, low cytotoxicity, and low cost for their preparation. They can work as part of photodynamic therapy due to their photoluminescence ability but are also used as nano-containers for hydrophobic drugs [151]. These include for example carbon nanotube DDS, which have been used in near-infrared photothermal ablation therapy and also have been investigated as drug delivery systems for their ability to cross biological barriers [158].

Liposomes stand as one of the most successful and versatile DDSs, offering several advantages such as biocompatibility, prolonged circulation time, controlled drug release, passive tumor targeting, and improved efficacy of various drugs. Moreover, they are used to enhance drug solubility and reduce toxicity. Liposomes are spherical vesicles formed by the self-assembly of phospholipids, creating a bilayer structure with an aqueous cavity inside for drug encapsulation [159]. Their size ranges from 30 nm to micrometres, with the phospholipid bilayer typically being 4-5 nm thick [160]. This unique structure facilitates fusion with cell membranes, enabling cargo delivery into cells [148]. The bilayer consists mainly of glycerophospholipids, sphingomyelin, and cholesterol, imparting negative or neutral charges at physiological pH [160]. Due to their size, surface charge, and modifications, liposomes are swiftly cleared upon recognition by the reticuloendothelial system. However, the bilayer can be covalently modified with polyethylene glycol (PEG), creating stabilized 'stealth' liposomes. This modification generates repulsive forces from the liposome surface, protecting liposomes from serum protein binding, reducing endocytosis by targeted cells, and avoiding clearance by the phagocytic system [160], [161]. Additionally, PEG can be further modified with antibodies and proteins to facilitate targeted tumour delivery [148]. These molecules can specifically bind receptors and certain moieties at the target size improving the delivery efficacy [162].

Exosomes are nanoscale extracellular vesicles surrounded by a lipid bilayer membrane, which can act as biological cargos transporting various biologically active molecules such as nucleic acids and proteins into target cells. They are secreted and absorbed by a wide range of eukaryotic cells, making them promising candidates for DDS. Compared to other delivery systems, exosomes offer advantages such as biocompatibility,

low toxicity, and low immunogenicity. Additionally, the presence of anchoring proteins naturally enhances the endocytosis of exosomes within target cells [163]. However, one of the challenges in exosome-based DDS research is their isolation. Various methods are employed for isolation, including ultracentrifugation, ultrafiltration, immunoaffinity, and density gradient centrifugation. Furthermore, the heterogeneity in origin, structure, storage, and production still limits their clinical application [164].

Natural polymer nanoparticles offer various advantages and can be exemplified by chitosan (glycan), albumin, and ferritin (proteins) [151]. Chitosan, derived from chitin, is a natural cationic polysaccharide and a promising material for DDS. Its main advantages include biocompatibility, mucoadhesion, nontoxicity, and biodegradability, as it can be degraded by internal lysosome enzymes and chitosanases [165], [166]. Challenges related to its poor solubility have been addressed through modifications of hydroxyl and amino groups, resulting in improved derivatives [167]. With its structure, chitosan might facilitate the passive delivery of numerous anticancer drugs. Additionally, modifications of various functional groups in chitosan by peptides, saccharides, and other molecules hold potential for active tumor-targeted therapies [168].

Synthetic polymeric systems represent fundamental components of soft material used in nanomedicine. This is mainly due to their tunable structure, which allows the creation of specific nanoparticles or water-soluble systems modified for various applications. These systems can be built from different molecules, such as poly(ε-caprolactone), poly(lactic acid), poly(lactic-co-glycolic acid), and N-(2-hydroxypropyl) methacrylamide (HPMA). These materials can encapsulate various drugs either by attachment to the polymer surface or dispersion within the polymer matrix. Their main advantage, compared to natural polymers, lies in their ability to provide continuous drug release over several days or weeks, due to their enhanced stability. These compounds have been tested in cancer therapy over the last years with some promising results [158].

1.5.2 HPMA Copolymers as Macromolecular Drug Carriers

HPMA copolymers are synthetic polymer-based nanomedicines that have been the subject of investigation in recent decades, showing significant potential in anti-cancer therapy. Interestingly, HPMA polymer was originally developed as a completely synthetic plasma expander marketed under the name Duxon™, which demonstrated no toxicity in several tested cell lines. A couple of years later, scientists found that HPMA homopolymer was not identified as a foreign macromolecule in mice, and no detectable antibodies were produced against it, making it a potential candidate for a delivery system.

HPMA copolymers can be nowadays characterised as non-toxic, biocompatible, and non-immunogenic delivery systems. Furthermore, as DDS, they exhibit enhanced pharmacokinetics and minimize the side effects of various drugs. They are water-soluble systems with a hydrophilic nature, capable of solubilizing water-insoluble drugs and preventing the adsorption of proteins and other macromolecules during blood circulation due to the tightly bound water layer. Additionally, HPMA copolymers have demonstrated prolonged blood clearance and improved accumulation in solid tumors, primarily attributed to the enhanced permeability and retention (EPR) effect. Moreover, a properly selected spacer and type of bond between the drug and copolymer facilitate the controlled release of the drug within cancer cells [169].

1.5.2.1 Enhanced Permeability and Retention Effect

More than three decades ago, scientists discovered vascular permeability associated with inflammation, which was triggered by microbial infection and mediated by the generation of bradykinin, a peptide that promotes inflammation. Subsequently, the presence of bradykinin and other mediators such as nitric oxide, collagenase, prostacyclins, prostaglandins, thromboxanes, and leukotrienes has been observed in tumors [170]. This discovery led to the development of a novel concept in selective cancer drug delivery of macromolecules, known as the EPR effect, which relies on the vascular permeability of tumor tissue [171].

The formation of new blood vessels, i.e. angiogenesis, is a crucial process during fast tumor growth. It is primarily mediated by vascular endothelial growth factor (VEGF), also known as vascular permeability factor (VPF). VEGF not only promotes angiogenesis but also enhances vascular permeability, ensuring an adequate supply of oxygen and nutrients to the tumor tissue. This increased permeability facilitates also the passive delivery of macromolecular anti-cancer drugs, characterised by a molecular weight larger than 40 kDa. Furthermore, impaired clearance of macromolecules from the tumor results in prolonged retention in the tumor interstitium, another defining key aspect of the EPR effect (**Fig. 8, p. 43**) [171]. Tumor blood vessels exhibit large fenestrations between endothelial cells, allowing macromolecules to leak into the interstitial space of tumor tissue. The EPR effect has been also validated *in vivo* using fluorescent macromolecules, demonstrating their accumulation primarily in tumor tissue. Similar results were obtained using HPMA copolymer conjugated with Zinc protoporphyrin, exhibiting ten times higher localization in tumors compared to other organs [170].

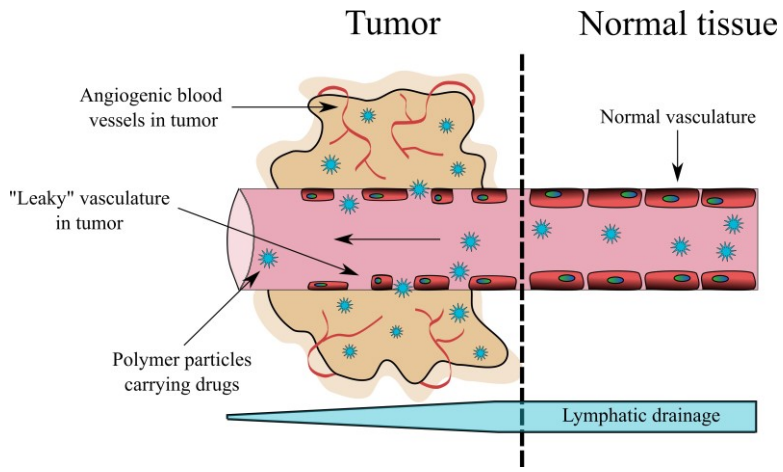

Figure 8. Enhanced retention and permeability (EPR) effect. Increased vascular permeability, mediated primarily by VEGF, facilitates a higher accumulation of macromolecules in tumors. Additionally, impaired clearance leads to prolonged retention of these compounds within tumors. Adapted from [170], [171], [172]. Created in Inkscape.

1.5.2.2 Design of HPMA Copolymer-bound Drug Conjugates

The overall therapeutic efficacy of HPMA copolymers is significantly influenced by their design, including polymer structure, molecular weight, spacer structure, and the bond between the polymer and the drug.

These systems rely on their molecular weight to accumulate in organisms, capitalizing on the EPR effect. Their high molecular weight facilitates uptake and accumulation in tumor tissues while also preventing rapid blood clearance. However, there is an upper limit to the molecular weight, as compounds exceeding 1 000 kDa can lead to severe side effects. Therefore, multiple types of HPMA copolymer structures ranging in molecular weight have been developed to optimize their activity.

The simplest form is a linear copolymer synthesized via the reversible addition-fragmentation transfer (RAFT) polymerization method. This method allows the synthesis of HPMA copolymers with tunable molecular weight and low dispersity. Experiments showed that linear HPMA copolymers with a molecular weight close to the renal filtration limit (30-50 kDA) appear to be the most promising [169], [173].

After recognizing that HPMA accumulation in solid tumors via the EPR effect can be optimized by higher molecular weight, a variety of more complex biodegradable conjugates, including star, diblock, and multi-block structures, has been designed [174], [175], [176], [177]. Since these DDS are primarily eliminated through renal filtration, the molecular weight of the non-degradable part of the conjugate should be below the renal filtration threshold.

Biodegradable diblock and multiblock conjugates contain spacers between individual parts and were synthesized to enhance accumulation in tumors and prolong blood circulation. These spacers, primarily enzymatically degraded (GFLG spacer) in lysosomes or reductively degraded (disulfide spacer) in the cytoplasm, enable intracellular degradation of the DDS and subsequent elimination of the resulting shorter fragments [169].

HPMA-based star-like copolymers consist of a hyperbranched dendrimer core and polymer arms, linked together through enzymatically or reductively degradable linkers. Star-like conjugates with a molecular weight ranging from 150 to 300 kDa demonstrated superior accumulation in solid tumors compared to other types of HPMA conjugates mentioned [178].

Another type of high molecular weight and long-circulating DDS is HPMA polymer micelles [179]. These supramolecular structures surpass the renal filtration threshold. Below their critical micellar concentration, they disassemble into individual polymer chains that can be released. Their core comprises a hydrophobic block made of poly(lauryl methacrylate) or poly(ε-caprolactone), surrounded by a hydrophilic shell of HPMA. Drugs can be encapsulated within the hydrophobic core or bound by a biodegradable linker [169].

Another factor influencing the activity is the bond between the HPMA copolymer and the drug, which is chosen to exploit the properties of cancer cells [174]. Tumors are characterised by a slightly acidic extracellular pH which promotes tumor progression and results primarily from anaerobic glycolysis, leading to lactate secretion [180]. HPMA copolymers are internalized by cells through endocytosis and processed in lysosomes, which have a low pH and contain numerous enzymes [181]. Consequently, HPMA copolymers can enhance drug release in tumor tissue through pH- or enzymatically-sensitive bonds [169]. Enzymatically degradable bonds (e.g., amide bond, ValCitPab) undergo degradation in lysosomes of cancer cells, while pH-sensitive bonds (e.g., hydrazone) remain stable at physiological pH but undergo hydrolysis in the acidic pH of the tumor microenvironment or lysosomes [169], [174].

Drawing from insights into the intricate design features of HPMA copolymers, including molecular weight, spacer, and the bond between the copolymer and the drug, researchers have developed potent systems capable of carrying various drugs. Among these drugs are notable chemotherapeutic agents such as doxorubicin, docetaxel, and paclitaxel, which have exhibited remarkable antitumor activity [182], [183].

2 Aims

The primary aim of this diploma thesis was to characterize the anticancer activity of two SMAC mimetics (LCL-161 and AZD5582) as single agents and explore their potential in combination with gemcitabine across five different human cancer cell lines (pancreatic carcinomas: PANC1, BxPC-3, and MiaPaca-2, prostatic carcinoma: PC-3, breast carcinoma: MDA-MB-231). Additionally, our aim was to develop and characterize the anticancer properties of HPMA copolymer conjugates bearing LCL-161 and AZD5582. We decided to achieve this aim through the following objectives.

1) To determine *in vitro* cytostatic and cytotoxic activities of LCL-161 and AZD5582 using [^{3}H]-thymidine incorporation assay, Annexin V-binding and caspase-3 activity assay.

2) To determine the expression levels of cIAP1, cIAP2, and XIAP in above listed human cancer cell lines by real-time PCR, and to correlate their expression to sensitivity to SMAC mimetics.

3) To investigate the potential of LCL-161 and AZD5582 to boost the cytostatic and cytotoxic activities of gemcitabine through assays mentioned above.

4) To characterize the cytostatic and cytotoxic activities of HPMA-copolymer conjugates bearing gemcitabine, LCL-161, and AZD5882 using the [^{3}H]-thymidine incorporation and Annexin V-binding assays.

5) To assess the *in vivo* toxicity of HPMA copolymer conjugates bearing LCL-161, AZD5582, and gemcitabine as single agents and in combination.

3 Material and Methods

3.1 Material

3.1.1 Chemicals

[^{3}H]-thymidine	PerkinElmer, USA
Agarose	SigmaAldrich, USA
Annexin V Dyomics 647	Exbio, Czech Republic
AZDD5582	Cayman Pharma, Czech Republic
Calcium chloride (CaCl2)	Lachema, Czech Republic
Dioxyribonucleotide triphosphate mix	Thermo Fisher Scientific, USA
Disodium hydrogen phosphate (Na_2HPO_4)	Lachner, Czech Republic
Dithiothreitol (DTT, 10 mM)	Thermo Fisher Scientific, USA
DNase	Thermo Fisher Scientific, USA
DNase buffer	Thermo Fisher Scientific, USA
Ethanol	VWR, USA
Ethylenediaminetetraacetic acid (EDTA), 0.5 M, pH 8.0	Thermo Fisher Scientific, USA
GB SG PCR master mix	Generi Biotech, Czech Republic
Gemcitabine	Acros Organics, USA
Hoechst 33258	Thermo Fisher Scientific, USA
Hydroxyethylpiperazineethanesulfonic acid (HEPES)	Sigma-Aldrich, USA
Isopropanol	Sigma-Aldrich, USA
LCL-161	Cayman Pharma, Czech Republic
PCR mix PPP master mix (Taq DNA polymerase in reaction buffer)	Top-Bio, Czech Republic
Potassium chloride (KCl)	Lachema, Czech Republic
Reverse transcriptase buffer (5x concentrated)	Thermo Fisher Scientific, USA
Ribonuclease inhibitor RNase OUT	Thermo Fisher Scientific, USA
Sodium chloride (NaCl)	Lachner, Czech Republic
Sodium dihydrogen phosphate (NaH_2PO_4)	Lachner, Czech Republic
SuperScript IV reverse transcriptase	Thermo Fisher Scientific, USA

SYBR safe dye for agarose electrophoresis	Thermo Fischer Scientific, USA
Tris-Acetate-EDTA buffer (TAE, 50x concentrated)	Omega Bio-Tec, USA
TRIzol, nucleic acid isolation reagent	Ambion, USA
Trypan blue, 0.4% (v/v) solution	Thermo Fisher Scientific, USA
Trypsin, 0.5% (v/v) solution	Preparation of media, Institute of Molecular Genetics of the Czech Academy of Sciences, Czech Republic
Ultra-pure water for PCR	Top-Bio, Czech Republic

3.1.2 Primers for Real-Time PCR

Sense and antisense primers for real-time PCR were designed by RNDr. Petra Procházková, PhD, from the Laboratory of Cellular and Molecular Immunology team at the Institute of Microbiology of the Czech Academy of Sciences and synthesized in Generi Biotech (Czech Republic). In this diploma thesis, primers for the amplification of these human genes were used: cIAP1, cIAP2, HSPCB, RPS13, XIAP, and YWHAZ.

3.1.3 Buffers and Gels

Buffer for Annexin V binding:
10 mM HEPES
4.09 g NaCl
140 mg $CaCl_2$
dH_2O

To prepare 500 mL of the buffer, the salt components were dissolved in 495 mL of dH_2O. Subsequently, 5 mL of 1M HEPES was added to the solution, and the pH of the buffer was adjusted to 7.4.

Gel for agarose electrophoresis:
1.3 g agarose
1x concentrated TAE
SYBR safe

To prepare the agarose gel, the agarose was dissolved in 100 mL of 1x concentrated TAE and then 10 μL of SYBR-safe dye was added to the resulting solution.

Phosphate buffer
(PBS, from Phosphate Buffered Saline): pH 7.4
137 mM NaCl
2.7 mM KCl
8 mM Na_2HPO_4
2 mM KH_2PO_4

The buffer was prepared by the Media Preparation Facility, Institute of Molecular Genetics of the Czech Academy of Sciences.

TAE buffer (1x concentrated): 50x concentrated TAE
dH_2O

To prepare 1 L of TAE buffer, 20 mL of 50x concentrated TAE was mixed with 980 mL of dH_2O.

3.1.4 Cell Lines and Cultivation Media

Cell lines used in this project include BxPC-3, MiaPaca-2, PANC1 (human pancreatic carcinomas), MDA-MB-231 (human breast adenocarcinoma), and PC-3 (human prostatic carcinoma). They were obtained from ATCC (American Type Culture Collection). Specific media were prepared and used for these cell lines.

3.1.4.1 Cultivation Medium for Cell Lines MiaPaca-2, PANC1, MDA-MB-231, and PC-3:

DMEM (Dulbecco's Modified Eagle's Medium) basic medium (Sigma-Aldrich, USA), 1:10 FTS (Gibco, USA), 1:100 Pen/Strep (Gibco, USA).

3.1.4.2 Cultivation Medium for Cell Line BxPC-3:

RPMI-1640 basic medium (Sigma-Aldrich, USA), 1:10 FTS (Gibco, USA), 1:100 Pen/Strep (Gibco, USA), 1:100 nonessential amino acids (NEA, prepared by the Institute of Molecular Genetics of the Czech Academy of Sciences, Czech Republic).

3.1.5 HPMA copolymer conjugates

In this diploma thesis, 4 HPMA copolymer conjugates were tested besides gemcitabine, AZD5582 and LCL-161. One linear conjugate was prepared for Gemcitabine and two for LCL-161. An HPMA-based micelle was prepared for AZD5582. Structures and physical-chemical characteristics are listed below. All of these samples were prepared by the Institute of Macromolecular Chemistry by Bc. Kevin Kotalík and Ing. Robert Pola, PhD.

3.1.5.1 Gemcitabine

In this diploma thesis, we utilized a linear HPMA copolymer bearing gemcitabine (P-Gem), which demonstrated significant potential (results to be published). Gemcitabine is bound to the HPMA copolymer via an aminocaproic acid linker through an enzymatically degradable amide bond (**Fig. 9**). The average molecular weight of the compound is 49 000 g/mol, with a dispersity of 1.38, and an active substance content of 14.0 %. The sample was stored in the fridge and prepared by dissolving it in PBS before use.

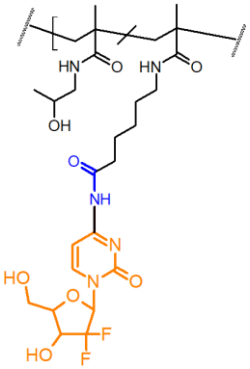

Figure 9. Structure of linear HPMA copolymer bearing gemcitabine (highlighted in orange). Gemcitabine is bound through an aminocaproic acid linker by an enzymatically degradable amide bond (highlighted in blue). Created in ChemSketch.

3.1.5.2 AZD5582

Due to the hydrophobic nature of AZD5882 and its dimeric structure, a micelle carrying the compound was prepared (**Fig. 10, p. 51**). The micelle is formed by amphiphilic graft copolymer poly(ε-caprolactone)-graft-poly(HPMA). The hydrophobic core is biodegradable and the grafts are formed by hydrophilic PHPMA copolymer bearing protected hydrazide groups (Boc protecting group). The compound has an active substance content of 7.0 % (AZD5582). To prepare for use, the sample was thawed from a -20°C freezer and allowed to reach room temperature. It was then dissolved in PBS for 30 min with constant shaking, followed by a 2-min sonication to facilitate micelle formation and filtration through a 0.45μm filter (VWR, USA).

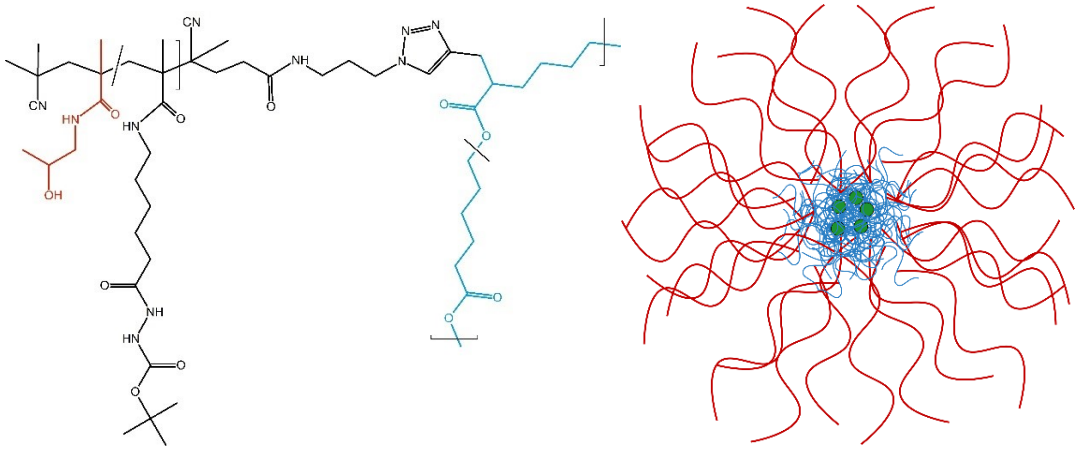

Figure 10. Structure of HPMA-based micelle carrying AZD5582 (referred to as Micelle AZD5582). The polymer consists of HPMA (highlighted in red), forming the hydrophilic part, boc protecting groups (highlighted in black), and polycaprolactone (highlighted in blue), forming the hydrophobic core where AZD5582 (highlighted in green) is encapsulated. Created in ChemSketch and Inkscape.

3.1.5.3 LCL-161

For LCL-161, two linear HPMA copolymers were prepared. In Hydrazone-HPMA copolymer, LCL-161 (P-LCL161$_{HYD}$) is bound via a pH-sensitive hydrazone bond (**Fig. 11**). The average molecular weight of the compound is 53 000 g/mol, with a dispersity of 1.23, and an active substance content of 5.1 %. The HPMA-ValCitPab copolymer (P-LCL161$_{VCP}$) utilizes an enzymatically cleavable linker for the release of LCL-161 within lysosomes (**Fig. 12, 13, p. 52**). The compound has an average molecular weight of 279 000 g/mol, with a dispersity of 1.029, and an active substance content of 7.93 %. Both samples sample were stored in a - 20°C freezer and prepared by dissolving them in PBS before use.

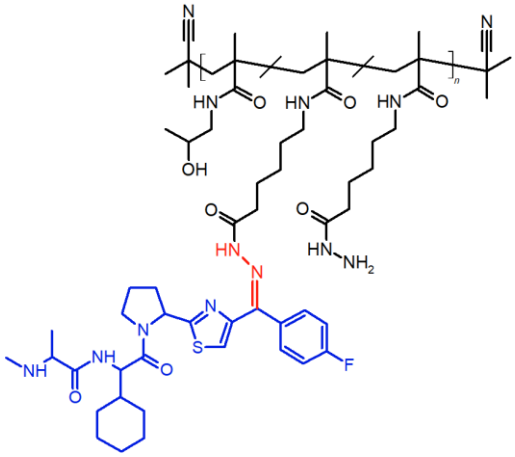

Figure 11. Structure of linear HPMA copolymer bearing LCL-161 (highlighted in blue, referred to as P-LCL161$_{HYD}$). The compound is bound through an aminocaproic acid linker and a pH-sensitive hydrazone bond (highlighted in red). Created in ChemSketch.

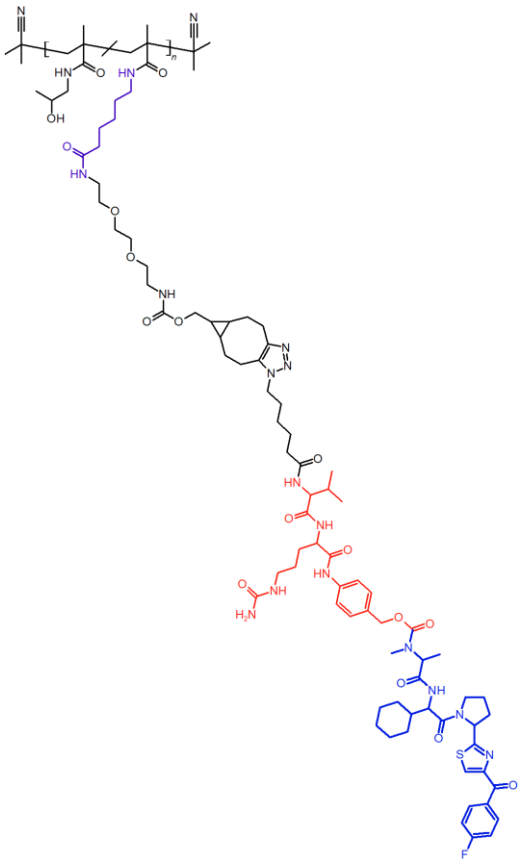

Figure 12. Structure of linear HPMA copolymer bearing LCL-161 (highlighted in blue, referred to as P-LCL161$_{VCP}$). The compound is bound through an aminocaproic acid linker (highlighted in purple) followed by valine, citrulline, and para-aminobenzylalcohol (highlighted in red), which are important for the release of LCL-161. Created in ChemSketch.

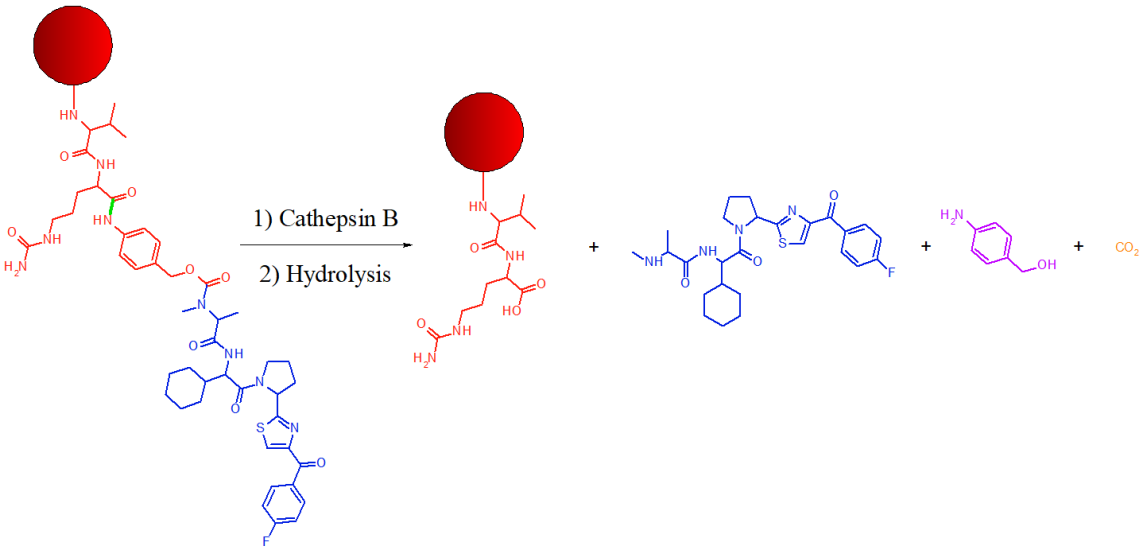

Figure 13. Mechanism of the release of P-LCL161$_{VCP}$. After the uptake of the copolymer (highlighted as red circle) carrying LCL-161 into lysosomes, Cathepsin B cleaves the bond between citrulline and para-aminobenzylalcohol (highlighted in green). Subsequently, acidic hydrolysis occurs, resulting in the formation of para- aminobenzylalcohol (highlighted in purple), LCL-161 (highlighted in blue), and CO_2 (highlighted in orange). Created in ChemSketch.

3.1.6 Experimental Animals

For the *in vivo* experiments Athymic Nude-Foxn1nu and NSG mice aged 8-10 weeks and weighing a minimum of 20 g were used. Athymic Nude-Foxn1nu mice were obtained from AnLab, Czech Republic, while NSG mice were obtained from The Jackson Laboratory, USA and bred in the breeding facility of the Institute of Microbiology of the Czech Academy of Sciences. Mice had ad libitum access to food and water and were housed in ventilated cages (Tecniplast, USA). The handling of the animals was conducted in a laminar flow cabinet CS5 EVO (Tecniplast, USA). Experimental activities involving animal work were strictly performed according to protocols approved by the Expert Committee for Ensuring Good Living Conditions for Laboratory Animals of the Institute of Microbiology of the Czech Academy of Sciences and all experiments were carried out in compliance with local and European regulations. Animals were handled in the animal facility of the Institute of Microbiology, CAS (Decision on granting authorization No. 52105/2018-MZE-17214, file number: 16OZ10910/2018-17214), and experiments were conducted with the appropriate permit (decision dated April 26, 2021, No. AVCR 2755/2021 SOV II). All animal work was performed by a person with the corresponding certification.

3.2 Devices

-80 °C freezer	Panasonic, Japan
-150 °C freezer	PHCbi, Japan
Analytical scales Pioneer	OHAUS, USA
Cell harvester Harvester 96	TOCMEC, Germany
Centrifuge Eppendorf centrifuge 5810 R	Eppendorf, Germany
Centrifuge Jouan BR4i	Thermo Fischer Scientific, USA
CO_2 incubator PHCbi MCO-170AICUV	PHC, Japan
CountlessTM cell counting chamber slides	Thermofischer, USA
Cycler Biometra Tadvanced	Analytik Jena, Germany
EVE Automatic cell counter	NanoEnTek, South Korea
Flow cytometer LSR II	BD, USA
Ice maker	BREMA, Czech Republic
Laminar box Safe FAST Classic	Faster, Italy

Laminar flow cabinet CS5 EVO	Techniplast, USA
Magnetic stirrer RH basic KT/C	IKA, Germany
Microscope Olympus CK 30	Olympus, Japan
pH meter 3510	JENWAY, UK
Pipettes	Eppendorf, Germany
Pipettes	Gilson, USA
Real-time PCR instrument CFX 96 Touch RT-PCR	BioRad, USA
Rocker 3D shaker	IKA, Germany
Scintillation detector Microbeta 2450 Microplate counter	PerkinElmer, USA
Serological (sterile) pipettes 10/25 mL	VWR International, USA
Shaker IKA Rocker 3D Digital	Verkon, Czech Republic
Sliding scale 0.2-100 mm	Koh-i-noor Hardtmuth, Czech Republic
Spectrophotometer BioPhotometr	Eppendorf, Germany
Spectrophotometer Infinite 200 Pro	Tecan, Switzerland
Spectrophotometer NanoDrop 2000c	Thermo Fischer Scientific, USA
Vortex stuar	Cole-Parmer, USA

3.3 Methods

3.3.1 Cultivation of Cell Lines, Trypsinization and Subculturing

Cell lines were stored in 1 mL aliquots (containing 2 million cells per aliquot) at -150 °C. Upon thawing, the cell solution was mixed with 5 mL of cultivation medium and centrifuged at 1300 rpm for 5 min at 4 °C. The resulting pellet was resuspended in 5 mL of cultivation medium and transferred into cultivation flasks containing 20 mL of the appropriate medium. The cell lines were cultured in a CO_2 incubator under conditions of 5% CO_2, 37 °C, and 100% relative humidity.

Subculturing was performed every 3-5 days. Adherent cell lines (all cell lines used in this project) were transferred into suspension by washing them with 0.05% (v/v) 0.5M EDTA solution. Subsequently, the cells were incubated for 6 min with 0.5% (v/v) trypsin solution in a CO_2 incubator. The cells were then resuspended in 10 mL of medium, and 80-90 % of the solution was removed. Subsequently, 20 mL of the appropriate medium was

added to the cultivation flask containing the remaining cells. All cell manipulations were performed within a laminar flow cabinet.

3.3.2 Counting of the Cells

The EVE Automatic cell counter was utilized to determine the number of cells for specific experiments. 10 µL of cell suspension was mixed with 10 µL of Trypan blue solution. Subsequently, 10 µL of the mixture was transferred onto a counting chamber slide and inserted into the automated cell counter. Following this, the viability and the number of cells in 1 mL of suspension were determined.

3.3.3 Investigating mRNA Levels of IAP Genes by Real-time PCR

3.3.3.1 RNA Isolation

RNA was isolated from all cell lines (BxPC-3, MiaPaca-2, PANC1, MDA-MB-231, and PC-3) using a TRIzol nucleic acid isolation reagent. Approximately 2 to 5 million cells were used for each isolation. After trypsinization and centrifugation of the cells at 357 g for 5 min at 4 °C, the cell pellet was resuspended and homogenized in 1 mL of TRIzol reagent, followed by a 5-min incubation at room temperature. Subsequently, 200 µL of chloroform was added, and the mixture was incubated for an additional 3 min before centrifugation at 10 000 g for 20 min at 4 °C.

Following centrifugation, the mixture was divided into a colourless upper aqueous phase, interphase, and a lower red phenol-chloroform phase. The upper aqueous phase containing RNA was carefully transferred into a new tube, and 500 µL of isopropanol was added to precipitate the RNA. The mixture was then incubated on ice for 10 min and centrifuged at 10 000 g for 20 min at 4 °C. The resulting white gel-like RNA pellet at the bottom of the tube was washed twice with 1 mL of 75% ethanol. The remaining supernatant was discarded and the RNA pellet was air-dried for 5-10 min. Finally, the pellet was resuspended in 40 µL of RNase-free water and incubated on a heat block at 60 °C for 10 min. The prepared RNA solution was stored at -80 °C until further use.

3.3.3.2 Reverse Transcription

For reverse transcription, 2 µg of RNA was utilized, with RNA concentration determined by NanoDrop 2000c spectrophotometer at 260 nm. The RNA solution was treated with DNAse reagent to remove genomic DNA. 2 µL of DNase buffer and 1 µL of DNAse

(TURBO DNA-free kit, Thermo Fischer Scientific) were added to 17 µL of RNA solution, followed by a 30-min incubation at 37 °C. After incubation, 2 µL of inactivation buffer was added, and the solution was centrifuged at 10 000 g for 2 min at 4 °C. The resulting supernatant was transferred to a new tube and combined with oligodeoxythymidine, deoxyribonucleotide triphosphate mixture, and PCR water in an 8:1:1:3 ratio, followed by a 5-min incubation at 65 °C.

Subsequently, the reverse transcription mixture, consisting of 5x concentrated reverse transcriptase buffer, 10 mM DTT, ribonuclease inhibitor RNAse OUT and SuperScript IV reverse transcriptase (SSIV) (in a 4:1:1:1 ratio), was added to the samples. The reaction mixture was incubated in a PCR cycler (10 min/50 ºC), followed by inactivation of SSIV (10 min/80 ºC). The purity of cDNA was assessed through PCR and agarose gel electrophoresis. Negative controls included RNA incubated without reverse transcriptase and cDNA without specific housekeeping gene primers.

3.3.3.3 Real-time PCR

Real-time PCR was conducted on FrameStar plates (4titude, Germany) to quantify mRNA levels of target genes (HSPCB, RPS13, YWHAZ, cIAP1, cIAP2, XIAP). A reaction mixture was prepared, consisting of gb SG PCR master mix, sense and antisense primers, PCR water, and 10x diluted cDNA in a ratio of 12.5:1:1:9.5:1.

Amplification was carried out using a CFX 96 Touch RT-PCR instrument following the program: initial denaturation at 95 ºC for 10 min, followed by 40 cycles of denaturation at 94 ºC for 10 seconds, annealing at 58 ºC for 25 seconds, and extension at 72 ºC for 35 seconds.

Additionally, a melting curve analysis was performed from 54 ºC to 95 ºC. The expression levels of cIAP1, cIAP2, and XIAP were normalized to three house-keeping genes (HSPCB, RPS13, YWHAZ) and presented as relative expression compared to the PANC1 cell line, with SD indicated. Additionally, the expression levels of the three IAP proteins were compared across all cell lines. The expression levels were normalized to three housekeeping genes (HSPCB, RPS13, YWHAZ) and presented as relative expression compared to cIAP2. The evaluation was performed using CFX Manager software (BioRad, USA).

3.3.4 [^{3}H]-Thymidine Incorporation Assay

All tested samples were initially diluted according to the experimental requirements. Subsequently, 50 µL of each diluted sample was dispended in quadruplicate into wells of a 96-well plate (NunclonTM Delta Surface, Thermofisher, USA). Cells were harvested by

trypsinization, and upon centrifugation at 357 g for 5 min, the resulting pellet was resuspended in 5 mL of medium to determine the cell concentration.

A cell suspension of a concentration of 5 000 cells/200 μL (per well) was prepared, and 200 μL of this suspension was added to each well of the prepared 96-well plate containing the diluted samples. For control groups, 50 μL of the medium was added to each well instead of the sample. The plates were incubated in a CO_2 incubator for 72 h.

After incubation, a solution of [^{3}H]-thymidine in a medium (1:250) was prepared, and 50 μL of this solution was added to each well. The cells were further incubated in a CO_2 incubator for an additional 8 h. Subsequently, the cells were harvested onto a membrane (1450-421 Printed Filtermat, PerkinElmer, USA), sealed into plastic bags (1450-432 Sample Bag, PerkinElmer, USA) using a cell harvester (Harvester 96, TOMTEC, Germany), and the radioactivity of the samples was measured using a scintillation detector (Microbeta2 2450 Microplate Counter, PerkinElmer, USA).

Based on the measured values, the IC_{50} value was determined as the concentration of the tested sample causing a 50% inhibition in cell proliferation, with standard deviation (SD) indicated. Each experiment was conducted in quadruplicate and was independently repeated at least two times.

3.3.5 Sensitization to Cytostatic Activity of Gemcitabine by IAP Inhibitors: Finding The Synergy

The potential of IAP inhibitors LCL-161 and AZD5582 to enhance the activity of gemcitabine was evaluated using a [^{3}H]-thymidine incorporation assay. The assay protocol closely followed that described above. Gemcitabine was appropriately diluted based on the specific cell line and experimental conditions, with 50 μL of the diluted solution added to each well.

Concurrently, diluted solutions of LCL-161 or AZD5582 were prepared. 50 μL of a solution at a specific concentration was added across the entire titration range of gemcitabine. Following this, a cell suspension with a concentration of 5 000 cells per 150 μL was prepared, with 150 μL dispended into each well.

Control samples were included, with 50 μL of an appropriately concentrated IAP inhibitor together with 50 μL of the medium instead of gemcitabine. The subsequent steps mirrored those described in the previous section outlining the [^{3}H]-thymidine incorporation assay. Experiments were conducted in quadruplicate, with a minimum of two independent experiments performed for each condition.

The interaction between the drugs (LCL-161/AZD5582 and gemcitabine) was assessed using the online tool SynergyFinder 3.0, a web application designed for interactive analysis and visualization of multi-drug and multi-dose combination response data. Leveraging the obtained proliferation data from the [^{3}H]-thymidine incorporation assay and the Zero Interaction Potency (ZIP) model, this software categorizes drug combinations as either antagonistic (resulting in a lower-than-expected effect) or synergetic (resulting in a higher-than-expected effect). The ZIP model captures drug interaction relationships by comparing the change in potency (effect at a certain dose level) of dose-response curves between individual drugs and their combinations.

Data were uploaded in a table format, following a protocol outlined on the SynergyFinder webpage. The summary synergy score for a drug combination is derived from an average of all dose combination measurements. Scores less than 0 suggest an antagonistic interaction, scores around 0 indicate an additive interaction and scores greater than 0 suggest a synergetic interaction. The 2D synergy map highlights synergetic and antagonistic dose regions in red and green colours, respectively. These summary synergy scores quantify the average excess response due to drug interactions (i.e., a synergy score of 20 corresponds to a 20% response beyond expectation) [184].

3.3.6 Annexin V-binding Assay

Cells were harvested by trypsinization, followed by the addition of 10 mL of appropriate medium. After centrifugation at 357 g for 5 min, the resulting pellet was resuspended in 5 mL of medium, and cell concentration was determined. Cell suspensions containing $0.3 \cdot 10^6$ (BxPC-3), $0.15 \cdot 10^6$ (MiaPaca-2), $0.2 \cdot 10^6$ (PANC1), $0.1 \cdot 10^6$ (MDA-MB-231), or $0.15 \cdot 10^6$ (PC-3) cells per 1 mL were prepared.

Next, 1 mL of the cell suspension was transferred into each well of a 6-well plate (BioLite, Thermofischer, USA). The tested samples were diluted, and 500 µL was added to each well, while 500 µL of the medium was added to control samples. The final volume was adjusted to 2,5 mL by the addition of appropriate medium (1 mL for controls or when drugs were used as single agents, and 500 µL in combination). Plates were then incubated in a CO_2 incubator for 72 h.

Following incubation, the medium was collected into 15 mL tubes on ice through a 30 µm filter (CelltricsTM, Sysmex, Japan), and cells were harvested by trypsinization into these tubes. After centrifugation for 5 min at 357 g at 5 ºC, the pellets were resuspended in leftover medium, and the suspensions were pipetted onto a 96-well conical bottom plate (Nunc™ 96-Well Polystyrene Conical Bottom MicroWell™ Plates, Thermofisher, USA).

The plate was centrifuged for 5 min at 357 g at 5 ºC, and the well contents were washed twice with 200 µL of Annexin buffer.

A solution of Annexin V conjugated with Dyomics 647 fluorochrome (Annexin V Dyomics 647, exbio, CZ) in annexin buffer was prepared at a ratio of 1:50. The pellets were then resuspended in 20 µL of this solution, and the plate was incubated for 30 min on ice in the dark. Afterward, 100 µL of annexin buffer was added to each well, mixed, and 100 µL of this solution was transferred to a tube for flow cytometry.

Flow cytometry analysis was conducted on 5 0000 cells for each sample. Before measurement, Hoechst 33258 (0.1 µg/mL) was added to each sample for the detection of dead cells. At least two independent experiments were performed. The results were analyzed using the FlowJoTM software (version 10.8.1). The strategy for selecting cell populations and the analysis procedure are illustrated in **Fig. 14**.

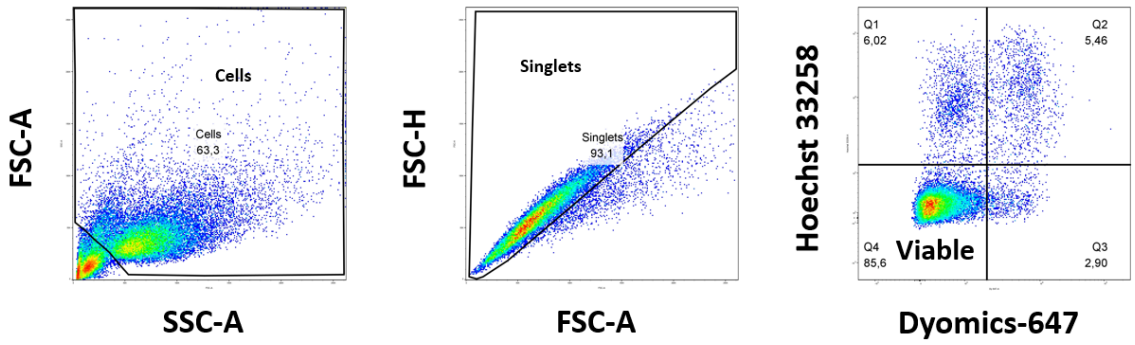

Figure 14. Strategy for flow cytometry analysis. In the analysis of flow cytometry results, live cells were initially selected based on the dependence of Forward Scatter Area (FSC-A) values on Side Scatter Area (SSC-A) values. Next, the population was assessed based on the dependence of Forward Scatter Height (FSC-H) values on FSC-A values to identify and exclude multiplets. Finally, the selected population was further characterised by plotting the Hoechst 33258 fluorescence signal against the Annexin V Dyomics-647 fluorescence signal.

3.3.7 Caspase-3 Activity Assay

The cytotoxic effects of gemcitabine, LCL-161, and AZD5582, either alone or in combination, were tested on MiaPaca-2 and MDA-MB-231 cell lines by measuring caspase-3 activity. The EnzCheck Caspase-3 Assay Kit (Thermo Fisher Scientific, USA) was employed to perform the assay. Cell solutions were prepared at concentrations of $0.8 \cdot 10^6$ (MiaPaca-2) and $0.5 \cdot 10^6$ (MDA-MB-231) per Petri dish.

The cell solution, diluted drug samples, and medium were combined in a Petri dish to a total volume of 10 mL, with three Petri dishes prepared for each sample. Control

samples contained only cells and medium. Cells were then incubated for 72 h in a CO_2 incubator to ensure consistent conditions, as in the Annexin V-binding assay.

Following incubation, the medium was collected into 50 mL tubes on ice through a 70 µm filter (VWR, USA), and cells were harvested by trypsinization into these tubes. After centrifugation for 5 min at 357 g at 5 ºC, cell counts were determined, and all tubes were adjusted to contain the same number of cells. The tubes were washed with 5 mL PBS and centrifuged again. The resulting pellets were then resuspended in 140 µL of lysis buffer and left on ice for 30 min.

Subsequently, the suspensions were transferred to 1.5 mL tubes and centrifuged at 10 000 g for 5 min. The supernatant was then transferred in quadruplicate to new tubes. 50 µL of the supernatant was pipetted into the wells of a transparent flat-bottom microtiter plate (Nunc, Denmark). To each sample, 50 µL of 2x concentrated reaction buffer (composed of 400 µL 5x concentrated reaction buffer, 10 µL 1M DTT, 590 µL dH2O) containing Z-DEVD-AMC substrate in a 1:50 ratio (kit ingredients) was added. A negative control consisting of 50 µL of lysis buffer was included.

The plate was incubated in the dark at laboratory temperature for 30 min. Fluorescence measurements were then performed using an Infinite 200 Pro (excitation at 342 nm, emission at 441 nm). Results are presented as relative caspase-3 activity compared to the control sample.

3.3.8 In Vivo Experiments

3.3.8.1 Determination of Toxicity In Vivo

Athymic Nude-Foxn1nu/NSG mice were injected with 300 µL of the tested substances or PBS (control group) on day 0. Subsequently, their body weight was recorded every two or three days over the next 2 weeks. To assess toxicity, the dosage was considered not toxic if the body weight of the mice did not drop below 85 % of their initial body weight, and if no mice died during the observation period.

4 Results

4.1 IAPs Expression in Selected Cancer Cell Lines

The expression levels of three IAP genes – cIAP1, cIAP2, and XIAP – were investigated across five selected human cancer cell lines: BxPC-3, MiaPaca-2, PANC1 (human pancreatic adenocarcinomas), MDA-MB-231 (human breast adenocarcinoma), and PC-3 (human prostatic carcinoma). These cell lines were selected based on the primary use of gemcitabine in treating pancreatic cancer, its frequent use in breast carcinoma treatment, and its modest activity in prostate cancer. We aimed to investigate whether the activity of gemcitabine could be boosted by IAP inhibitors across this panel of cell lines and whether the sensitivity of these cell lines to IAP inhibitors correlated with the expression of three IAP genes.

To achieve this, three housekeeping genes (HSPCB, RPS13, and YWHAZ) were used for normalization of the expression levels, and the results are presented as relative expression compared to the PANC1 cell line.

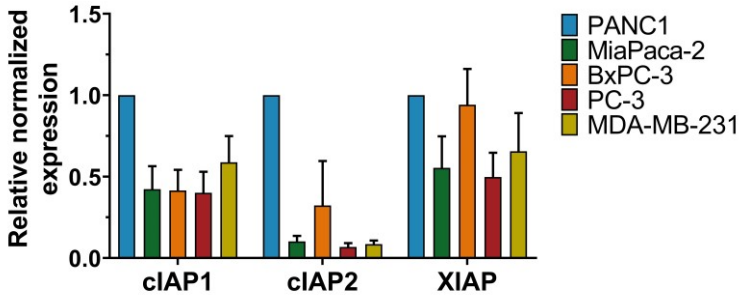

Tukey's multiple comparisons test	Summary	P Value
cIAP1		
PANC1 vs. MiaPaca-2	****	<0.0001
PANC1 vs. BxPC-3	****	<0.0001
PANC1 vs. PC-3	****	<0.0001
PANC1 vs. MDA-MB-231	**	0.0025
cIAP2		
PANC1 vs. MiaPaca-2	****	<0.0001
PANC1 vs. BxPC-3	****	<0.0001
PANC1 vs. PC-3	****	<0.0001
PANC1 vs. MDA-MB-231	****	<0.0001

Tukey's multiple comparisons test	Summary	P Value
XIAP		
PANC1 vs. MiaPaca-2	***	0.0009
PANC1 vs. PC-3	***	0.0002
PANC1 vs. MDA-MB-231	*	0.0164
MiaPaca-2 vs. BxPC-3	**	0.0051
BxPC-3 vs. PC-3	***	0.001

Figure 15. Relative normalized expression of IAP genes. After the isolation of RNA and reverse transcription, gene expression was evaluated by real-time PCR. The expression levels of cIAP1, cIAP2, and XIAP were normalized to the expression of three housekeeping genes (HSPCB, RPS13, YWHAZ) and are presented relative to the PANC1 cell line. Statistical significance was determined using One-way ANOVA with Tukey's multiple comparisons tests (n.s. P > 0.05, * P ≤0.05, ** P ≤0.01, *** P ≤0.001, **** P ≤0.0001). The experiment was performed three times with comparable results.

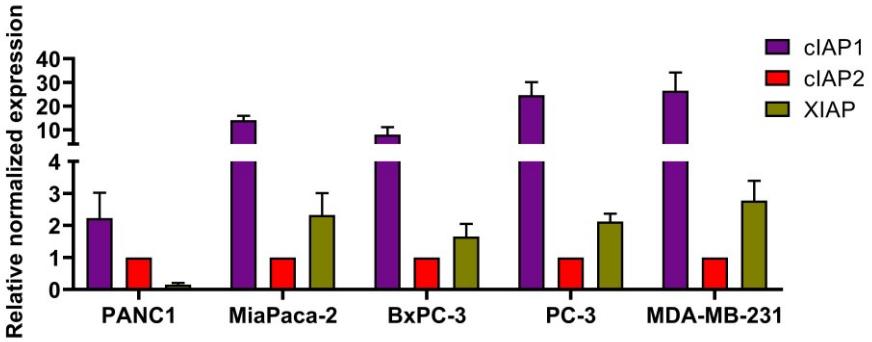

Figure 16. Comparison of IAP expression levels in selected human cancer cell lines. The expression levels of cIAP1, cIAP2, and XIAP were normalized to the expression of three housekeeping genes (HSPCB, RPS13, YWHAZ) and are presented relative to cIAP2 expression for each cell line. The experiment was performed three times with comparable results.

The results (**Fig. 15, p. 61**) revealed significantly elevated expression of cIAP1 in the PANC1 cell line compared to the other four cell lines (P≤0.0001). Additionally, a higher expression of cIAP1 was observed in MDA-MB-231 compared to MiaPaca-2, BxPC-3, and PC-3, although this difference did not reach statistical significance.

Similarly, significantly elevated expression of cIAP2 was observed in PANC1 compared to MiaPaca-2, BxPC-3, PC-3, and MDA-MB-231 (P≤0.0001). This difference was more pronounced than that observed for cIAP1.

PANC1 displayed significantly higher expression of XIAP compared to MiaPaca-2, PC-3 (P ≤0.001), and MDA-MB-231 (P ≤0.05) cell lines. Furthermore, BxPC-3 exhibited significantly elevated XIAP expression compared to MiaPaca-2 (P ≤0.01) and PC-3 (P ≤0.001).

Moreover, the results in **Fig. 16 (p. 62)** show a consistent trend in IAP gene expression across the selected cell lines. Specifically, in four out of the five cell lines (BxPC-3, MiaPaca-2, PC-3, and MDA-MB-231), mRNA levels of XIAP were slightly higher, while mRNA levels of cIAP1 were observed to be 10-30 times higher compared to cIAP2. However, in the PANC1 cell line, while a twofold increase in cIAP1 mRNA levels relative to cIAP2 was observed, the mRNA level of XIAP was notably low compared to cIAP2.

4.2 The Cytostatic Activity of the Tested Compounds

The cytostatic activity of gemcitabine, P-Gem, SMAC mimetics (LCL-161 and AZD5582), P-LCL161$_{HYD,}$ P-LCL161$_{VCP,}$ and Micelle AZD5582 was assessed using the [^{3}H]-thymidine incorporation assay. The primary objective of these experiments was to determine the sensitivity of our panel of human cancer cell lines to these anticancer agents and to observe any differences in cytostatic activity between the free drugs and the HPMA copolymers carrying these drugs.

4.2.1 The Cytostatic Activity of Gemcitabine and P-Gem

All tested human cancer cell lines showed high sensitivity to the cytostatic activity of gemcitabine. The activity of P-Gem was ~ 10 times lower compared to the free drug.

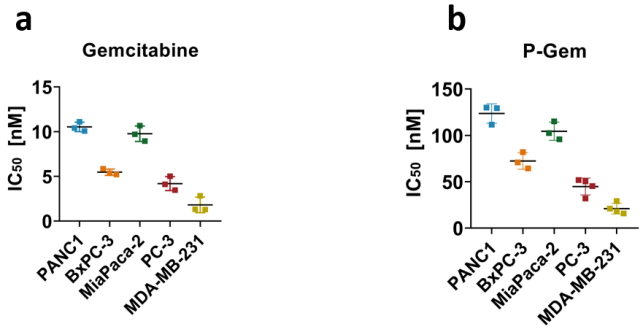

c

Gemcitabine	
Cell line	**IC_{50} ± SD [nM]**
PANC1	10.5 ± 0.53
BxPC-3	5.47 ± 0.35
MiaPaca-2	9.77 ± 0.87
PC-3	4.19 ± 0.78
MDA-MB-231	1.82 ± 0.88

P-Gem	
Cell line	**IC_{50} ± SD [nM]**
PANC1	123.6 ± 10.5
BxPC-3	72.4 ± 8.87
MiaPaca-2	104.5 ± 9.85
PC-3	44.9 ± 9.06
MDA-MB-231	21.0 ± 5.85

Figure 17. Cytostatic activity of gemcitabine (**a**) and gemcitabine P-Gem (**b**) determined by [^{3}H]-thymidine incorporation assay. The IC_{50} value represents the concentration of the sample (drug equivalent) causing a 50% inhibition of cell proliferation after 72h incubation. Cells incubated in the medium alone were used as

a control. IC_{50} values (**c**), determined in at least three independent experiments, are listed in the table along with SD.

The results demonstrated that all five cell lines exhibit high sensitivity to gemcitabine (**Fig. 17a, c, p. 63**), with IC_{50} values ranging from 1.8 to 10.5 nM. The less sensitive cell lines, PANC1 and MiaPaca-2, exhibited IC_{50} values of ~ 10 nM, while cell lines BxPC-3, PC-3, and MDA-MB-231 were more sensitive.

The sensitivity of all five cell lines to P-Gem (**Fig. 17b, c, p. 63**) was observed to be lower to that of free gemcitabine. In all cases, the IC_{50} values were ~ 10 times higher for P-Gem compared to gemcitabine. The less sensitive cell lines, PANC1 and MiaPaca-2, exhibited IC_{50} values of ~ 110 nM, while the more sensitive cell lines (BxPC-3, PC-3, and MDA-MB-231) displayed IC_{50} values of 21-72 nM.

4.2.2 The Cytostatic Activity of IAP Inhibitors

Both SMAC mimetics, LCL-161 and AZD5582, demonstrated cytostatic activity, while AZD5582 emerged as the more potent. Additionally, our results revealed that two cell lines exhibited notably higher sensitivity to SMAC mimetics compared to the others.

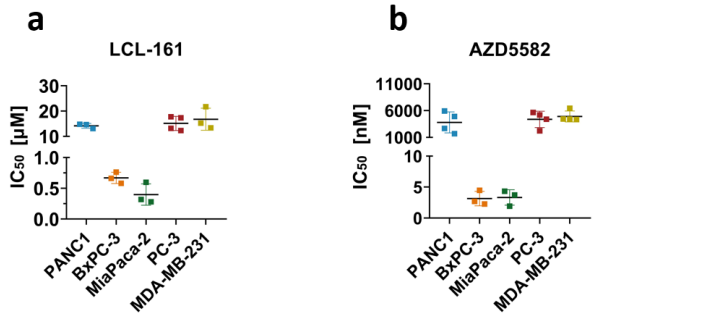

c

LCL-161

Cell line	IC_{50} ± SD
PANC1	14.2 ± 0.94 μM
BxPC-3	0.67 ± 0.09 μM
MiaPaca-2	0.40 ± 0.17 μM
PC-3	15.2 ± 2.80 μM
MDA-MB-231	16.8 ± 4.37 μM

AZD5582

Cell line	IC_{50} ± SD
PANC1	3.80 ± 1.95 μM
BxPC-3	3.14 ± 1.17 nM
MiaPaca-2	3.33 ± 1.25 nM
PC-3	4.36 ± 1.51 μM
MDA-MB-231	4.90 ± 1.02 μM

Figure 18. Cytostatic activity of LCL-161 (**a**) and AZD5582 (**b**) determined by [^{3}H]-thymidine incorporation assay. The IC_{50} value represents the concentration of the sample (drug equivalent) causing a 50% inhibition of cell proliferation after 72h incubation. Cells incubated in the medium alone were used as a control. IC_{50} values (**c**), determined in at least three independent experiments, are listed in the table along with SD.

The cytostatic activity of two IAP inhibitors was evaluated in all five selected human cancer cell lines by a [^{3}H]-thymidine incorporation assay. The sensitivity of these cell lines was

similar for both SMAC mimetics, though LCL-161 and AZD5582 showed very different efficacy.

For the less sensitive cell lines (PANC1, PC-3, and MDA-MB-231), the IC_{50} value for LCL-161 (**Fig. 18a, c, p. 64**) was ~ 15 μM, while the two sensitive cell lines, BxPC-3 and MiaPaca-2, displayed IC_{50} values of 0.7 μM and 0.4 μM.

A similar trend was observed for AZD5582 (**Fig. 18b, c, p. 64**), the second IAP inhibitor used in this study. The sensitive cell lines (BxPC-3 and MiaPaca-2) exhibited IC_{50} values of 3.1 nM and 3.3 nM, which were ~ 200 and 100 times lower than those for LCL-161. The IC_{50} values for the less sensitive cell lines were 3.8 μM for PANC1, 4.3 μM for PC-3, and 4.9 μM for MDA-MB-231. These values represented ~ a 3 to 4-fold decrease compared to LCL-161.

4.2.3 The Cytostatic Activity of HPMA Copolymer-bound LCL-161 conjugates

Both HPMA copolymers bearing LCL-161 exhibited significantly lower activity compared to free LCL-161. Specifically, P-LCL161$_{HYD}$ demonstrated a slightly more pronounced effect compared to P-LCL161$_{VCP}$.

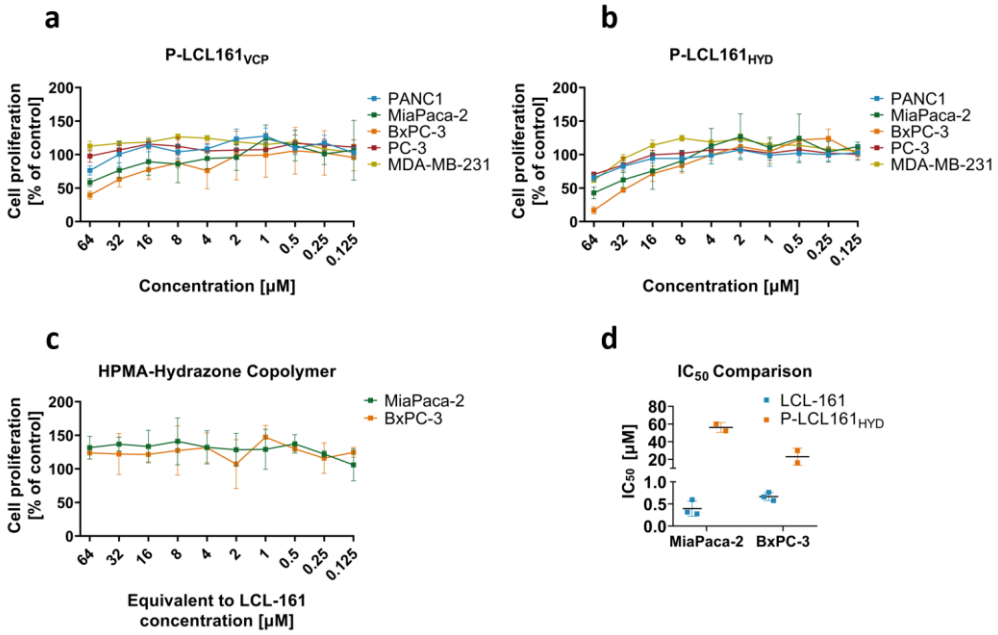

Figure 19. Cytostatic activity of HPMA copolymer conjugates bearing LCL-161 and bound via either an enzymatically cleavable (P-LCL161$_{VCP}$) linker (**a**) or a pH-sensitive hydrazone bond (P-LCL161$_{HYD}$) (**b**) was determined by [^{3}H]-thymidine incorporation assay. HPMA copolymer without the drug but bearing hydrazide group was used as a control conjugate (**c**). The IC_{50} value (**d**) represents the concentration of the sample (drug equivalent) causing a 50% inhibition in cell proliferation after 72h incubation. IC_{50} values are presented for LCL-161 and P-LCL161$_{HYD}$ in sensitive cell lines (BxPC-3 and MiaPaca-2). Cells incubated

in the medium alone were used as a control. Two independent experiments with comparable results were performed.

[^{3}H]-thymidine incorporation assay was employed to evaluate the cytostatic activity of HPMA copolymer conjugates carrying LCL-161 across five selected human cancer cell lines.

The cytostatic activity of the HPMA copolymer bearing LCL-161 bound via an enzymatically cleavable linker (P-LCL161$_{VCP}$) is depicted (**Fig. 19a, p. 65**). Minimal activity was observed in the cell lines less sensitive to IAP inhibitors (PANC1, PC-3, and MDA-MB-231), while a modest effect was found in the sensitive cell lines BxPC-3 and MiaPaca-2.

Similar trends were observed in the experiments with the HPMA copolymer bearing LCL-161 bound via a pH-sensitive hydrazone bond (P-LCL161$_{HYD}$) (**Fig. 19b, p. 65**). Some very weak effect was observed at the highest concentrations (32 and 64 μM) for the less sensitive cell lines, whereas a more pronounced effect was noted for BxPC-3 and MiaPaca-2.

Additionally, the cytostatic activity of the control HPMA copolymer without the drug but bearing hydrazide groups was investigated (**Fig. 19c, p. 65**). The same concentration range of HPMA copolymer as in **Fig. 19b (p. 65**) was used but without LCL-161 present at the end of the hydrazone bond. The two sensitive cell lines were chosen for this experiment and no cytostatic effect on the cells was observed, thus confirming that the carrier is non-toxic and the cytostatic activity observed above is attributed to the carried drug.

A comparison of the IC_{50} values for LCL-161 and the P-LCL161$_{HYD}$ in the two sensitive cell lines, BxPC-3 and MiaPaca-2, is shown in **Fig. 19a (p. 65)**. The IC_{50} values for P-LCL161$_{HYD}$ were 56 μM for MiaPaca-2 and 23 μM for BxPC-3, representing ~ 140-fold (MiaPaca-2) and 35-fold (BxPC-3) increases, compared to those obtained for LCL-161.

4.2.4 The Cytostatic Activity of Micelle AZD5582

Micelle AZD5582 demonstrated similar cytostatic activity to free AZD5582 in the PANC1 cell line. To ascertain that this effect is attributable only to the drug entrapped inside the HPMA copolymer-based micelle, we further investigated the activity of empty micelles.

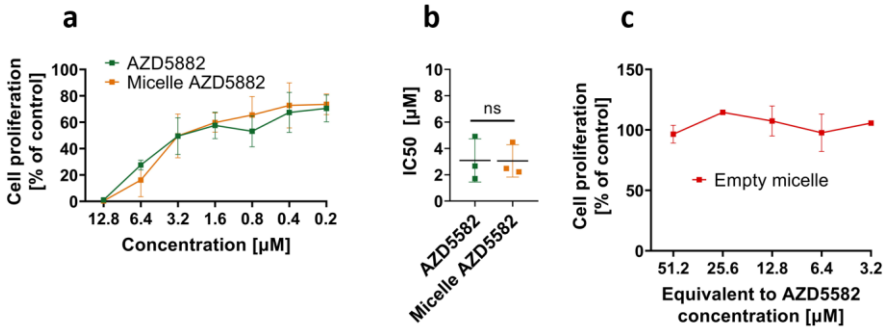

Figure 20. Cytostatic activity of HPMA copolymer-based micelle with entrapped AZD5582 (Micelle AZD5582). The cytostatic activity of AZD5582 and Micelle AZD5582 (**a**) was determined by [^{3}H]-thymidine incorporation assay in the PANC1 cell line. IC_{50} values (**b**) for both drug formulations in the PANC1 cell line were calculated from 3 independent experiments representing the concentrations of the samples that led to a 50% inhibition of cell proliferation after 72h incubation. The cytostatic effect of the HPMA copolymer-based micelle alone was evaluated in the PANC1 cell line (**c**). Statistical significance was determined using the t-test (n.s. $P > 0.05$, * $P \leq 0.05$, ** $P \leq 0.01$, *** $P \leq 0.001$, **** $P \leq 0.0001$).

[^{3}H]-thymidine incorporation assay was employed to evaluate the cytostatic activity of Micelle AZD5582, free AZD5582, and the empty HPMA copolymer micelles in the PANC1 cell line (**Fig. 20**). This cell line was selected for the *in vitro* experiments with Micelle AZD5582 due to its low sensitivity since Micelle AZD5582 possesses high critical micellar concentration. Therefore, BxPC-3 or MiaPaca-2 cell lines could not be used for their high sensitivity to AZD5582.

Micelle AZD5582 demonstrated comparable activity to free AZD5582 (**Fig. 20a**), with the IC_{50} values (**Fig. 20b**) being 3 μM for both free AZD5582 and Micelle AZD5582.

Furthermore, empty HPMA copolymer-based micelles were also tested (**Fig. 20c**), and no cytostatic activity was found.

4.3 Induction of apoptosis by IAP inhibitors and polymer conjugate bearing LCL-161

The ability of free IAP inhibitors and P-LCL161$_{HYD}$ to induce apoptosis as single agents was assessed using the Annexin V-binding assay following a 72h incubation period with tested compounds. The strategy for flow cytometry analysis is shown in **Fig. 21**.

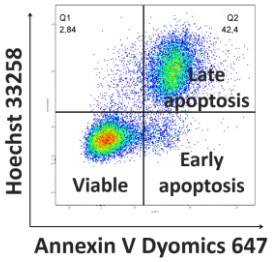

Figure 21. Strategy for flow cytometry analysis. Following the separation of single cells via FSC-A vs. SSC-A and FSC-H vs. FSC-A, the selected population was further characterised for apoptosis induction in cancer cell lines *in vitro* by plotting the Hoechst 33258 fluorescence signal against the Annexin V Dyomics-647 fluorescence signal. This process resulted in the classification of cells into three distinct populations: viable cells (Hoechst 33258$^-$ and Annexin V Dyomics 647$^-$), early apoptotic cells (Hoechst 33258$^-$ and Annexin V Dyomics 647$^+$), and late apoptotic cells (Hoechst 33258$^+$ and Annexin V Dyomics 647$^+$).

4.3.1 LCL-161

LCL-161 demonstrated cytotoxic activity and induced apoptosis in four out of five cell lines in a concentration-dependent manner.

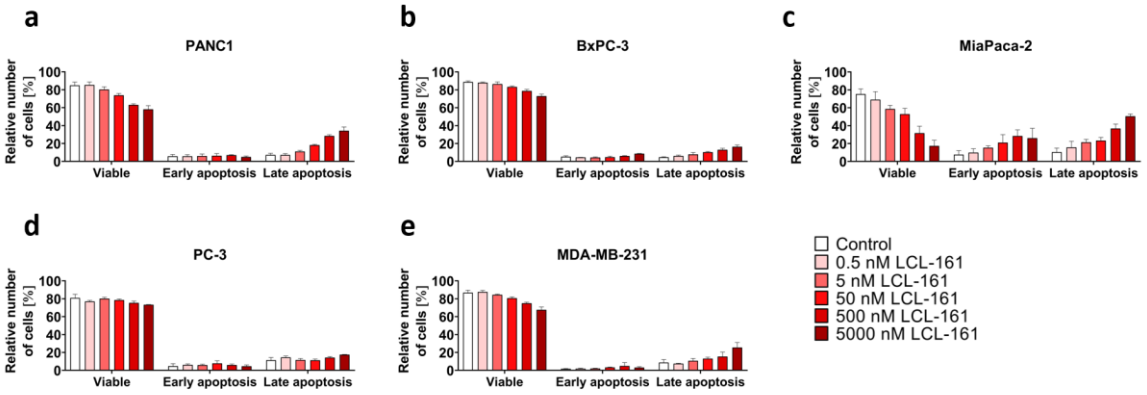

Figure 22. Induction of apoptosis in selected cancer cell lines by LCL-161. Cells were incubated for 72 h in a 6-well plate with titrated concentrations (0.5-5 000 nM) of LCL-161. Cells were harvested, labelled by Annexin V Dyomics 647 + Hoechst 33258, and analysed by flow cytometry. Cells incubated in the medium alone were used as a control. All five selected human cancer cell lines were employed: PANC1 (**a**), BxPC-3 (**b**), MiaPaca-2 (**c**), PC-3 (**d**), and MDA-MB-231 (**e**). The measurements were performed in triplicate, and each experiment was independently performed at least twice. Results are presented as the percentage of cells in the three states (viable, early apoptosis, and late apoptosis) ± SD.

The ability of LCL-161 to induce apoptosis was assessed across all five selected human cancer cell lines using the Annexin V-binding assay.

Interestingly, the results (**Fig. 22, p. 68**) revealed differences in sensitivity to apoptosis induction in comparison to the cytostatic activity measured via [^{3}H]-thymidine incorporation assay. The most sensitive cell line, MiaPaca-2 (**Fig. 22c, p. 68**), exhibited ~ 55 % of cells in the late apoptosis phase at the highest concentration of LCL-161 used, while the second most sensitive cell line to the cytostatic activity of LCL-161, BxPC-3 (**Fig. 22b, p. 68**), displayed minimal sensitivity with only ~ 20 % of cells in the late apoptosis phase.

Among the less sensitive cell lines in terms of cytostatic activity (PANC1, PC-3, and MDA-MB-231), varying responses were observed in the apoptosis induction. While LCL-161 demonstrated low activity in the PC-3 cell line (**Fig. 22d, p. 68**), a more pronounced effect was observed in PANC1 (**Fig. 22a, p. 68**) and MDA-MB-231 (**Fig. 22e, p. 68**) cell lines, with ~ 40 and 30 % of cells in the late apoptosis phase at the highest concentration of the IAP inhibitor tested, respectively.

4.3.2 AZD5582

AZD5582 exhibited cytotoxic activity in a concentration-dependent manner in four out of five selected human cancer cell lines, similar to LCL-161. Consistent with its cytostatic activity, AZD5582 was shown to be a more potent SMAC mimetic compared to LCL-161.

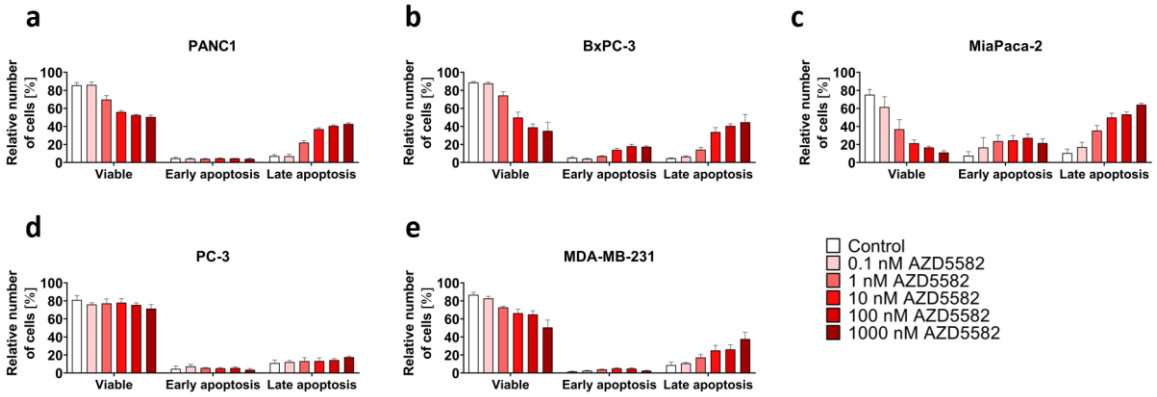

Figure 23. Induction of apoptosis in selected cancer cell lines by AZD5582. Cells were incubated for 72 h in a 6-well plate with titrated concentrations (0.1-1 000 nM) of AZD5582. Cells were harvested, labelled by Annexin V Dyomics 647 + Hoechst 33258, and analysed by flow cytometry. Cells incubated in the medium alone were used as a control. All five selected human cancer cell lines were employed: PANC1 (**a**), BxPC-3 (**b**), MiaPaca-2 (**c**), PC-3 (**d**), and MDA-MB-231 (**e**). The measurements were performed in triplicate, and each experiment was independently performed at least twice. Results are presented as the percentage of cells in the three states (viable, early apoptosis, and late apoptosis) ± SD.

The ability of AZD5582 to induce apoptosis was evaluated across all five selected human cancer cell lines using the Annexin V-binding assay.

The results (**Fig. 23, p. 69**) showed a similarity in sensitivity to apoptosis induction by AZD5582 compared to the cytostatic activity of this IAP inhibitor measured by the [^{3}H]-thymidine incorporation assay. The most sensitive cell lines, MiaPaca-2 (**Fig. 23c, p. 69**) and BxPC-3 (**Fig. 23b, p. 69**) exhibited ~ 65 % and 45 % of cells in the late apoptosis phase at the highest concentration of AZD5582 tested.

Among the less sensitive cell lines in terms of cytostatic activity (PANC1, PC-3, and MDA-MB-231), very distinct responses were observed in the apoptosis induction. While AZD5582 showed no activity in the PC-3 cell line (**Fig. 23d, p. 69**), a more notable effect was observed in PANC1 (**Fig. 23a, p. 69**) and MDA-MB-231 (**Fig. 23e, p. 69**) cell lines, with ~ 40 % of cells in the late apoptosis phase at the highest concentration of the IAP inhibitor used.

4.3.3 P-LCL161$_{HYD}$

The cytotoxic activity of P-LCL161$_{HYD}$ was significantly reduced compared to the free drug. Only the highest tested concentration showed minimal induction of apoptosis in the MiaPaca-2 cell line.

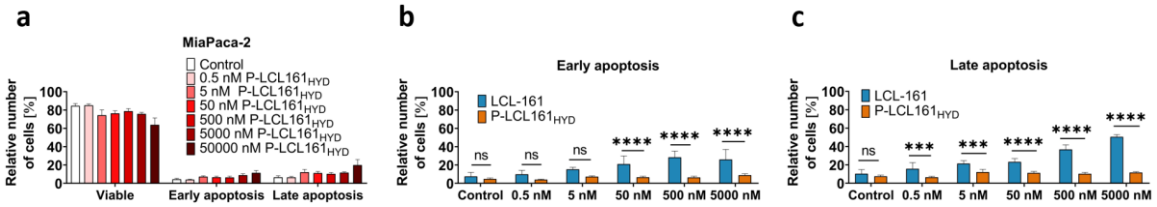

Figure 24. Induction of apoptosis in selected cancer cell lines by P-LCL161$_{HYD}$. Cells were incubated for 72 h in a 6-well plate with titrated concentrations (0.5-50 000 nM) of P-LCL161$_{HYD}$ (**a**). Cells were harvested, labelled by Annexin V Dyomics 647 + Hoechst 33258, and analysed by flow cytometry. Cells incubated in the medium alone were used as a control. The measurements were performed in triplicate, and each experiment was independently performed at least twice. Results are presented as the percentage of cells in the three states (viable, early apoptosis, and late apoptosis) ± SD. The percentage of MiaPaca-2 cells in the early and late phases of apoptosis was compared between P-LCL161$_{HYD}$ and free LCL-161 (**b**, **c**). Statistical significance was determined using One-way ANOVA with Sidak's multiple comparisons test (n.s. $P > 0.05$, * $P \leq 0.05$, ** $P \leq 0.01$, *** $P \leq 0.001$, **** $P \leq 0.0001$).

To assess the cytotoxic effect of HPMA copolymer conjugate bearing LCL-161, the Annexin V-binding assay was employed. P-LCL161$_{HYD}$ was selected for this experiment based on its higher potency compared to P-LCL161$_{VCP}$, as determined by the cytostatic activity measured by the [^{3}H]-thymidine incorporation assay. We decided to use the MiaPaca-2 cell

line, previously shown to be highly sensitive to LCL-161, to evaluate the cytotoxic activity of the conjugate.

The results (**Fig. 24a, p. 70**) revealed minimal cytotoxic activity P-LCL161$_{HYD}$, with only ~ a 5% increase in the late apoptotic cells at concentrations tested to 5 000 nM (LCL-161) in comparison to the control. However, a more notable effect was observed at a 50 000 nM (LCL-161) concentration, with ~ 20 % of cells in late apoptosis and 12 % in early apoptosis.

Comparison between LCL-161 and P-LCL161$_{HYD}$ showed a significant difference in cytotoxic activity across the concentrations range from 50 to 5 000 nM (LCL-161) for the early apoptosis phase and from 0.5 to 5 000 nM (LCL-161) for the late apoptosis phase (**Fig. 24b, c, p. 70**). While LCL-161 as a single agent effectively induced apoptosis in the MiaPaca-2 cell line, the HPMA copolymer compound demonstrated very low activity.

4.4 Potentiation of the Cytostatic And Cytotoxic Activities of Gemcitabine by IAP Inhibitors

4.4.1 Potentiation of Gemcitabine Cytostatic Activity by IAP Inhibitors

The potential synergy between IAP inhibitors (LCL-161 or AZD5582) and gemcitabine was determined using [^{3}H]-thymidine incorporation assay. The interaction between the drugs (LCL-161 or AZD5582 and Gemcitabine) was further analyzed using the online tool SynergyFinder 3.0 designed for interactive analysis and visualization of multi-drug and multi-dose combination response data. The summary synergy score for a drug combination is derived from an average of all dose combination measurements. The 2D synergy map highlights synergetic and antagonistic dose regions in red and green colours, respectively [184].

4.4.1.1 LCL-161

LCL-161 demonstrated the ability to sensitize four out of five cell lines to the cytostatic activity of gemcitabine, with the most pronounced synergy observed in the MiaPaca-2 and MDA-MB-231 cell lines.

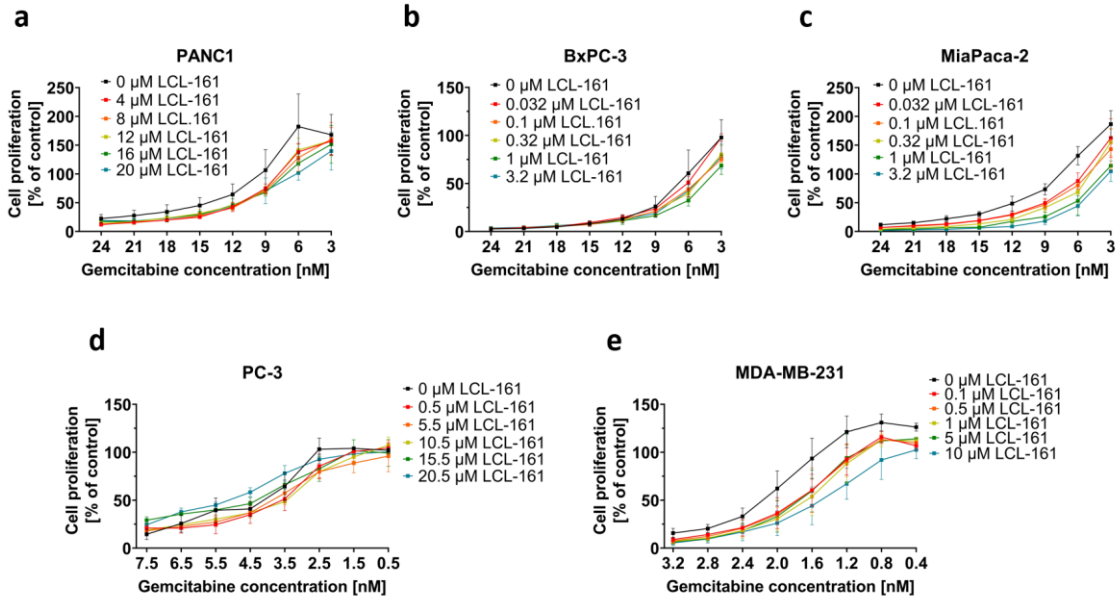

Figure 25. Sensitization to the cytostatic activity of gemcitabine by LCL-161. The [^{3}H]-thymidine incorporation assay was employed to determine the potential of LCL-161 to enhance the cytostatic activity of gemcitabine. Cells were incubated with titrated concentrations of gemcitabine and a constant concentration of LCL-161 for 72 h. Different concentrations of LCL-161 were used for the tested cell lines: 4-20 µM for PANC1 (**a**), 0.032-3.2 µM for BxPC-3 (**b**) and MiaPaca-2 (**c**), 0.5-20.5 µM for PC-3 (**d**), and 0.1-10 µM for MDA-MB-231 (**e**). Concentration ranges of gemcitabine were as follows: 3-24 nM for PANC1, BxPC-3, and MiaPaca-2, 0.5-7.5 nM for PC-3, and 0.4-3.2 nM for MDA-MB-231. Controls were cells incubated with appropriate concentrations of LCL-161 and no gemcitabine. Measurements were performed in quadruplicate, with each experiment conducted independently at least twice.

The results demonstrated the ability of LCL-161 to enhance the cytostatic activity of gemcitabine in some of the selected human cancer cell lines (**Fig. 25**), as measured by the [^{3}H]-thymidine incorporation assay. Notably, a potentiation of gemcitabine by LCL-161 was observed in four cell lines, except for the PC-3 cell line (**Fig. 25d**).

LCL-161 sensitised the PANC1 cells to the effects of gemcitabine across all concentrations (**Fig. 25a**). However, within the concentration range of 9-24 nM gemcitabine, no difference in potentiation was observed with varying concentrations of LCL-161. The most notable sensitization was observed at gemcitabine concentration range 3 to 9 nM.

LCL-161 also demonstrated the ability to sensitize BxPC-3 (**Fig. 25b, p. 72**) cells to the cytostatic activity of gemcitabine, particularly within the concentration range of gemcitabine from 3 to 9 nM.

MiaPaca-2 (**Fig. 25c, p. 72**) exhibited the highest sensitivity among the tested cell lines to the combination of LCL-161 and gemcitabine, with a synergetic effect observed across all gemcitabine concentrations.

Interestingly, the MDA-MB-231 (**Fig. 25b, p. 72**) cell line, which showed previously low sensitivity to LCL-161, displayed sensitivity to the combination effect of the two drugs. The synergetic effect was observed across almost all concentrations of gemcitabine, with the most pronounced combination effect noted at the highest concentration of LCL-161 used (10 µM).

4.4.1.2 AZD5582

AZD5582 sensitized all selected human cancer cell lines to the cytostatic activity of gemcitabine. Notably, the most significant sensitization was once again observed in the MiaPaca-2 and MDA-MB-231 cell lines.

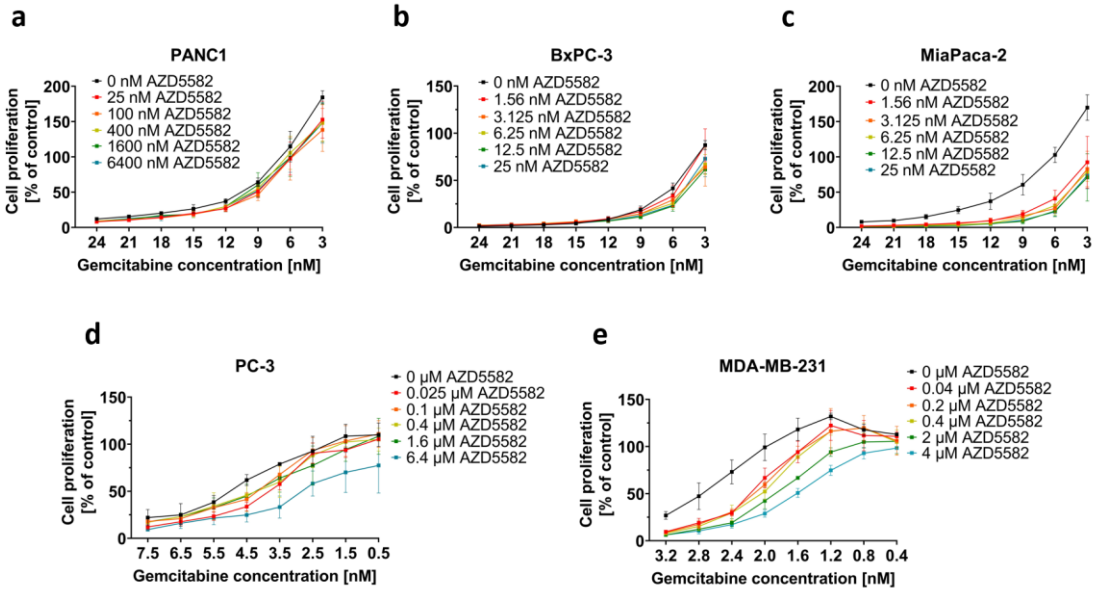

Figure 26. Sensitization to the cytostatic activity of gemcitabine by AZD5582. The [^{3}H]-thymidine incorporation assay was employed to determine the potential of AZD5582 to enhance the cytostatic activity of gemcitabine. Cells were incubated with titrated concentrations of gemcitabine and a constant concentration of AZD5582 for 72 h. Different concentration ranges of AZD5582 were utilized for the tested cell lines: 25-6400 nM for PANC1 (**a**), 1.56-25 nM for BxPC-3 (**b**) and MiaPaca-2 (**c**), 0.025-6.4 µM for PC-3 (**d**), and 0.04-4 µM for MDA-MB-231 (**e**). Concentration ranges of gemcitabine were as follows: 3-24 nM for PANC1, BxPC-3, and MiaPaca-2, 0.5-7.5 nM for PC-3, and 0.4-3.2 nM for MDA-MB-231. Controls were cells incubated with appropriate concentrations of AZD5582 and no gemcitabine. Measurements were performed in quadruplicate, with each experiment conducted independently at least twice.

We found that AZD5582 increased the sensitivity to the cytostatic activity of gemcitabine in all five tested cancer cell lines (**Fig. 26, p. 73**). However, this combination showed only a low effect in the PANC1 (**Fig. 26a, p. 73**) and BxPC-3 (**Fig. 26b, p. 73**) cell lines.

In contrast, MiaPaca-2 (**Fig. 26c, p. 73**) and MDA-MB-231 (**Fig. 26e, p. 73**) cell lines demonstrated a pronounced synergy between these two drugs across all concentrations tested.

The PC-3 cell line (**Fig. 26d, p. 73**) also exhibited a synergetic effect, which was most evident at the highest concentration of AZD5582.

4.4.1.3 SynergyFinder: LCL-161 or AZD5582 + Gemcitabine

SynergyFinder 3.0 was used to further analyze the interaction between LCL-161 or AZD5582 and gemcitabine. We used the ZIP model, which generates a 2D synergy map and calculates the overall synergy score based on the effect of all tested combinations. Scores below 0 indicate an antagonistic interaction, those near 0 represent an additive interaction, and scores above 0 suggest synergy. The synergistic regions are highlighted in red, while the antagonistic regions are depicted in green.

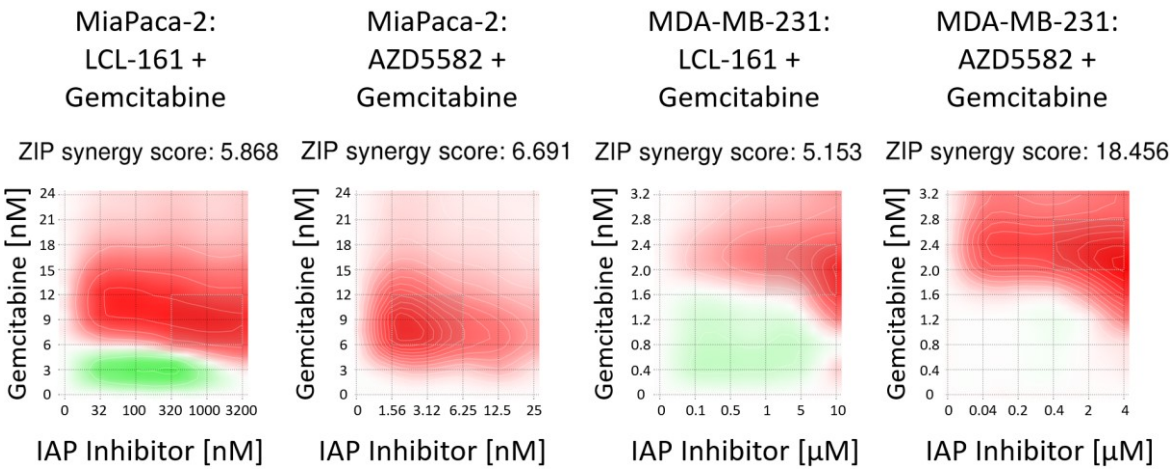

Figure 27. Synergy between LCL-161 or AZD5582 and gemcitabine. MiaPaca-2 and MDA-MB-231 which exhibited the most significant potentiation of gemcitabine cytostatic activity by the IAP inhibitors were selected for the analysis. Data obtained from the [^{3}H]-thymidine incorporation assay were analyzed using the online tool SynergyFinder 3.0. The summary synergy score for the drug combination is derived from an average of all dose combination measurements. Scores less than 0 suggest an antagonistic interaction, scores around 0 indicate an additive interaction and scores greater than 0 suggest a synergetic interaction. The 2D synergy map highlights synergetic and antagonistic dose regions in red and green colours, respectively [184].

2D heatmaps generated by the use of SynergyFinder 3.0 and the ZIP model indicate a synergetic effect between IAP inhibitors and gemcitabine in both cell lines (**Fig. 27, p. 74**). The most significant synergy in MiaPaca-2 cells was found within the gemcitabine concentration range of 6 to 16 nM, while in MDA-MB-231 cells, it was observed within the range of 1.6 to 3.2 nM. Interestingly, synergy was observed across the entire concentration range of IAP inhibitors. Notably, the combination of AZD5582 and gemcitabine exhibited the highest synergy score of 18.5 in the MDA-MB-231 cell line. The combinations of LCL-161/gemcitabine and AZD5582/gemcitabine in the MiaPaca-2 cell line, as well as LCL-161/gemcitabine in the MDA-MB-231 cell line, scored around 5, indicating a moderate synergetic effect.

4.4.2 Potentiation of Gemcitabine Cytotoxic Activity by IAP Inhibitors

The potential of IAP inhibitors LCL-161 and AZD5582 to enhance the cytotoxic effect of gemcitabine was assessed using the Annexin V-binding assay as well as the caspase-3 activity assay. MiaPaca-2 and MDA-MB-231 cell lines, identified as the most sensitive to the combination of gemcitabine and IAP inhibitors via the [^{3}H]-thymidine incorporation method, were selected for these experiments. The concentrations of both drugs that demonstrated the highest synergistic effect in the Annexin V-binding assay were used for the caspase-3 activity assay.

To determine the interaction between the IAP inhibitors (LCL-161/AZD5582) and gemcitabine, we compared the expected effect of the combination (sum of the effects of the single agents) to the observed combination effect. This comparison allowed us to assess whether the combination exhibited synergy (resulting in a greater-than-expected effect), additivity (where the effects of the two drugs sum together), or antagonism (resulting in a lower-than-expected effect).

To calculate this, the number of cells in late apoptosis for the control group, single-agent groups, and combination groups was determined. Subsequently, we subtracted the number of cells in late apoptosis for the control group from each treatment group. Then, we summed the effects of the IAP inhibitor and gemcitabine as single agents and compared this number with the number of cells in late apoptosis in the combination group.

4.4.2.1 MiaPaca-2: Gemcitabine + LCL-161

LCL-161 enhanced the cytotoxic activity of gemcitabine in the MiaPaca-2 cell line. This finding was further supported by the increased activity of caspase-3 at the concentration of gemcitabine and LCL-161 which exhibited the highest synergistic effect in the Apoptosis V-binding assay.

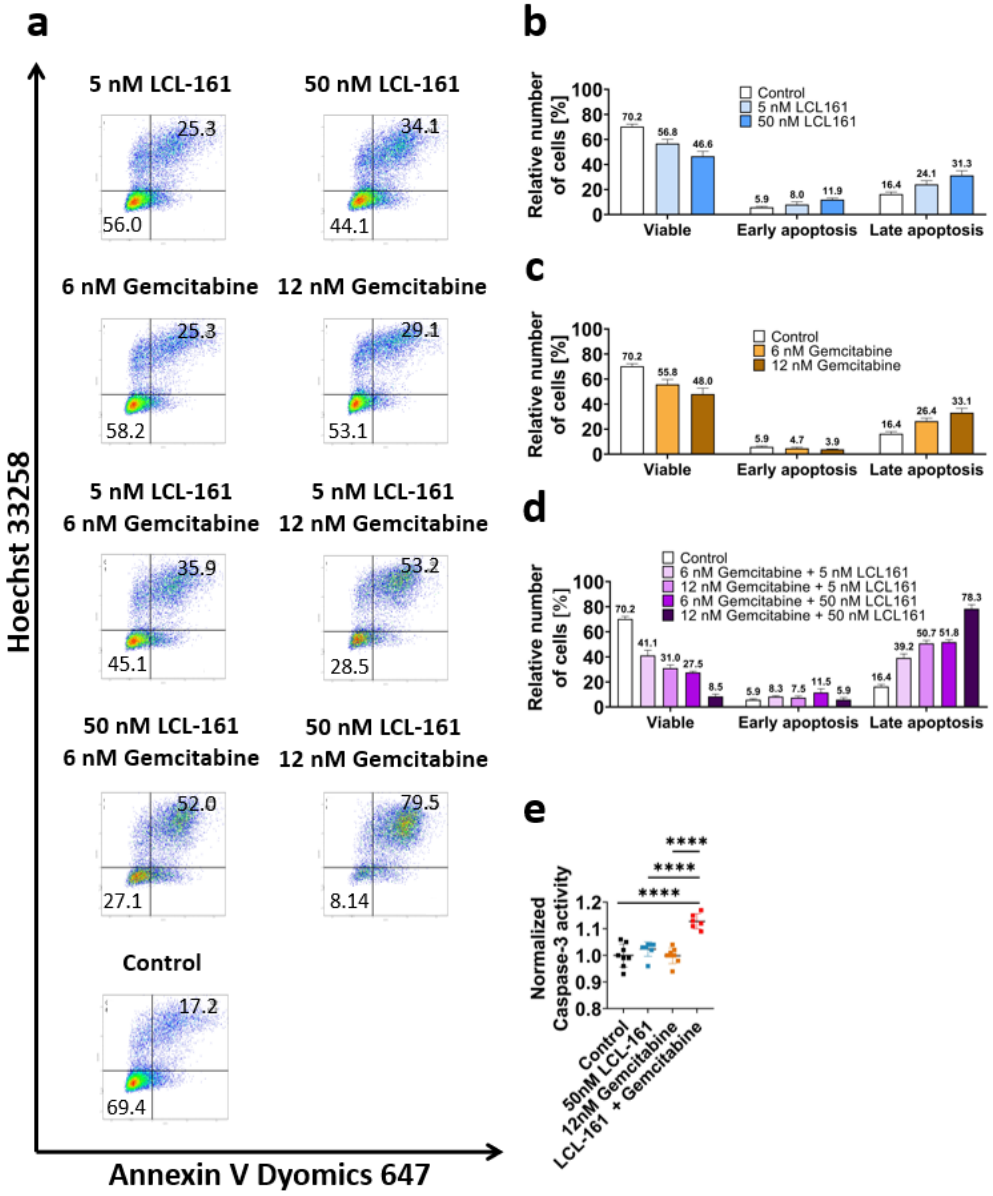

Figure 28. Potentiation of cytotoxic activity of gemcitabine by LCL-161. MiaPaca-2 cells were incubated with either gemcitabine (6 and 12 nM) or LCL-161 (5 and 50 nM) or both compounds for 72 h in a 6-well plate. The cells were labelled by Annexin V Dyomics 647 and Hoechst 33258 and analysed by flow cytometry (**a**). Cells incubated in the medium alone served as a control. Each experiment condition was performed in triplicate, and the experiment was performed at least twice with similar results. Results are presented as the percentage of cells in the three states (viable, early apoptosis, and late apoptosis) ± SD for LCL-161 treatment alone (**b**), gemcitabine treatment alone (**c**), and combined gemcitabine + LCL-161 (**d**). MiaPaca-2 cells were treated as in (**a**), harvested and cell lysates with the same number of cells were prepared. Caspase-3 activity in the lysates was determined using The EnzCheck Caspase-3 Assay Kit. Fluorescence measurements were

performed in quadruplicates using an Infinite 200 Pro (excitation 342 nm, emission 441 nm). Results are presented as caspase-3 activity relative to the control sample (**e**). The experiment was performed twice. Statistical significance was determined using One-way ANOVA with Tukey's multiple comparisons tests (n.s. $P > 0.05$, * $P \leq 0.05$, ** $P \leq 0.01$, *** $P \leq 0.001$, **** $P \leq 0.0001$).

The potentiation of gemcitabine cytotoxic activity by the IAP inhibitor LCL-161 was evaluated in MiaPaca-2 cells using Annexin V-binding and caspase-3 activity assays (**Fig. 28, p. 76**).

Treatment with a lower concentration of LCL-161 (5 nM) increased the percentage of cells in late apoptosis by 8 %, while the higher concentration (50 nM) led to a 15 % increase compared to the control group. Similarly, gemcitabine induced a 10 % increase in late apoptosis using the lower concentration (6 nM) and a 17 % increase using the higher concentration (12 nM).

A synergetic effect, resulting in a greater-than-expected increase in late apoptotic cells, was observed in all four combinations. Specifically, at the lower concentration of LCL-161, there was a 23 % increase compared to the expected 18 % (5 nM LCL-161 + 6 nM gemcitabine) and a 34 % increase compared to the expected 25 % (5 nM LCL-161 + 12 nM gemcitabine). Additionally, there was a 35 % increase compared to the expected 25 % (50 nM LCL-161 + 6 nM gemcitabine), and a 62 % increase compared to the expected 32 % (50 nM LCL-161 + 12 nM gemcitabine). Since the last combination demonstrated the most pronounced synergetic effect, it was selected for the caspase-3 activity assay.

The findings from the cytometry were further supported by the caspase-3 activity assay (**Fig. 28e, p. 76**), which showed minimal changes in caspase-3 activity when cells were exposed to gemcitabine or LCL-161 alone, but a significant increase in caspase-3 activity was found in combination treatment. However, this increase was rather moderate, with a ~ 15 % rise in caspase-3 activity.

4.4.2.2 MiaPaca-2: Gemcitabine + AZD5582

Similar to the effect of LCL-161, the IAP inhibitor AZD5582 enhanced the cytotoxic activity of gemcitabine in the MiaPaca-2 cell line. Synergistic results were observed in 3 out of 4 concentration combinations.

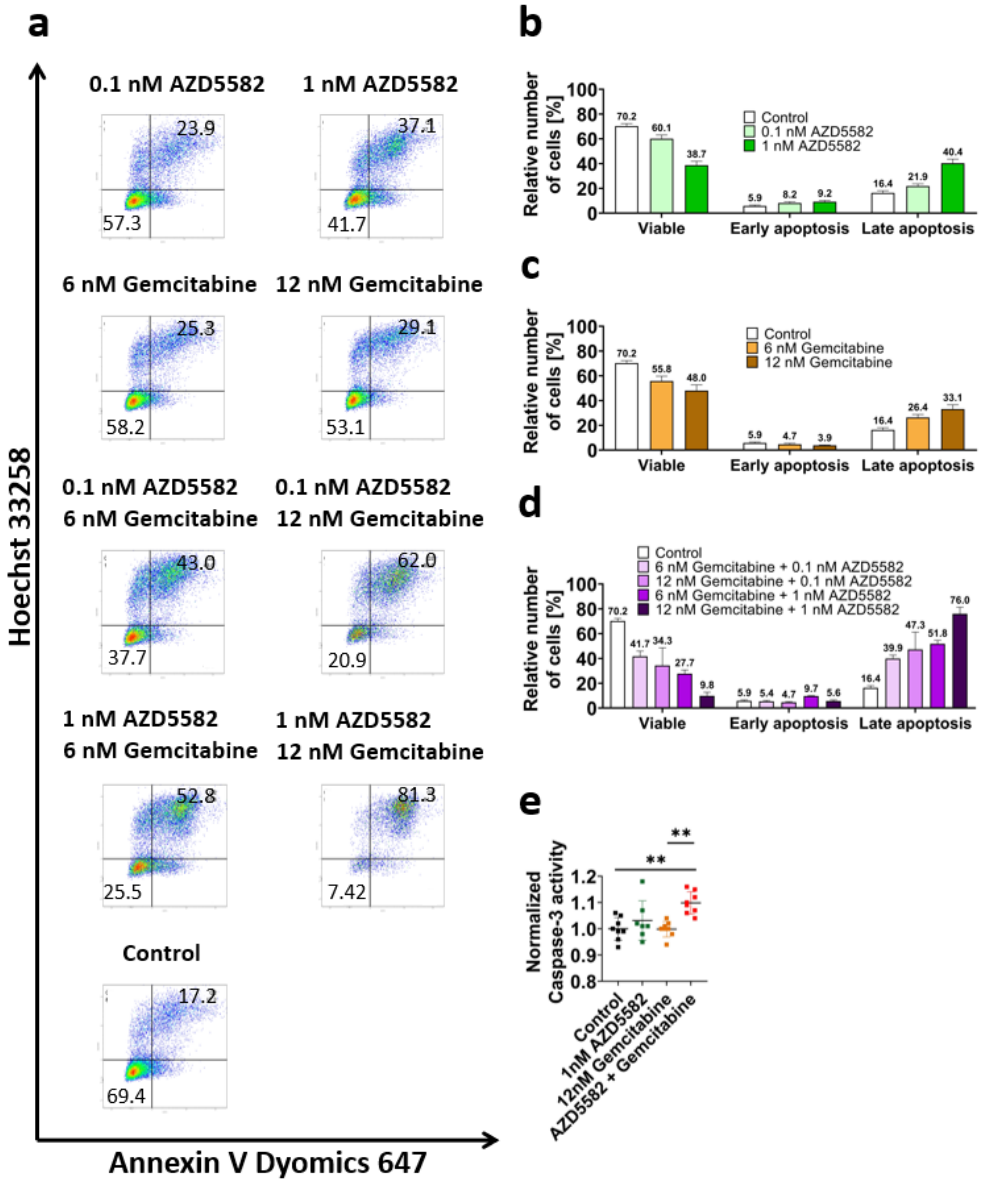

Figure 29. Potentiation of cytotoxic activity of gemcitabine by AZD5582. MiaPaca-2 cells were incubated with either gemcitabine (6 and 12 nM) or AZD5582 (0.1 and 1 nM) or both compounds for 72 h in a 6-well plate. The cells were labelled by Annexin V Dyomics 647 and Hoechst 33258 and analysed by flow cytometry (**a**). Cells incubated in the medium alone served as a control. Each experiment condition was performed in triplicate, and the experiment was performed at least twice with similar results. Results are presented as the percentage of cells in the three states (viable, early apoptosis, and late apoptosis) ± SD for AZD5582 treatment alone (**b**), gemcitabine treatment alone (**c**), and combined gemcitabine + AZD5582 (**d**). MiaPaca-2 cells were treated as in (**a**), harvested and cell lysates with the same number of cells were prepared. Caspase-3 activity in the lysates was determined using The EnzCheck Caspase-3 Assay Kit. Fluorescence measurements were performed in quadruplicates using an Infinite 200 Pro (excitation 342 nm, emission 441 nm). Results are

presented as caspase-3 activity relative to the control sample (**e**). The experiment was performed twice. Statistical significance was determined using One-way ANOVA with Tukey's multiple comparisons tests (n.s. $P > 0.05$, * $P \leq 0.05$, ** $P \leq 0.01$, *** $P \leq 0.001$, **** $P \leq 0.0001$).

Boosting of gemcitabine cytotoxic potential through the IAP inhibitor AZDD5582 was evaluated in MiaPaca-2 cells via Annexin V-binding and caspase-3 activity assays (**Fig. 29, p. 78**).

Treatment with a lower concentration of AZD5582 (0.1 nM) increased the percentage of cells in late apoptosis by 6 %, while the higher concentration (1 nM) led to a 24 % increase compared to the control group. Gemcitabine induced a 10 % increase in late apoptosis at the lower concentration (6 nM) and a 17 % increase at the higher concentration (12 nM).

A synergetic effect, i.e. greater-than-expected increase in late apoptotic cells, was observed in three combinations. There was a 24 % increase compared to the expected 16 % (0.1 nM AZD5582 + 6 nM gemcitabine) and a 31 % increase compared to the expected 23 % (0.1 nM AZD5582 + 12 nM gemcitabine). At the higher concentration of AZD5582, there was a 60 % increase compared to the expected 41 % (1 nM AZD5582 + 12 nM gemcitabine). The combination of 1 nM AZD5582 with 6 nM gemcitabine exhibited an additive effect, resulting in a 35 % increase in late apoptotic cells, closely aligning with the expected 34 % rise. Since the combination of 1 nM AZD5582 with 12 nM gemcitabine displayed the most substantial synergetic impact, it was chosen for the caspase-3 activity assay.

While minimal changes in caspase-3 activity levels were observed when gemcitabine or AZD5582 were administered alone, a statistically significant increase in caspase-3 activity was evident in combination treatment compared to both the control and gemcitabine-only groups (**Fig. 29e, p. 78**). However, this increase was decent, with a ~ 10% rise in caspase-3 activity.

4.4.2.3 MDA-MB-231: Gemcitabine + LCL-161

While LCL-161 and gemcitabine individually exhibited only moderate cytotoxic effects in the MDA-MB-231 cell line, their combination resulted in a significant increase in the cytotoxic activity and synergistic effect across all concentration combinations.

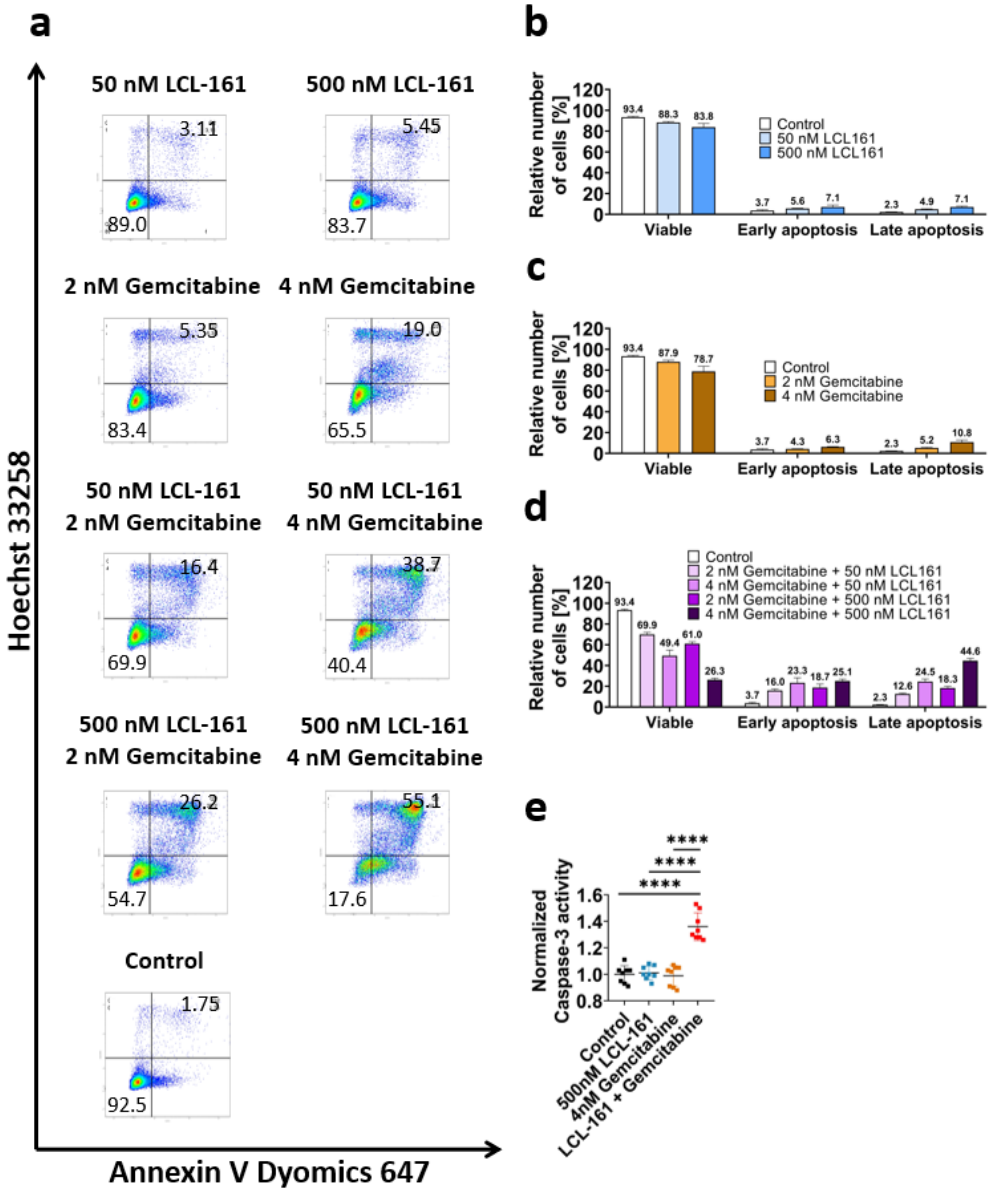

Figure 30. Potentiation of cytotoxic activity of gemcitabine by LCL-161. MDA-MB-231 cells were incubated with either gemcitabine (2 and 4 nM) or LCL-161 (50 and 500 nM) or both compounds for 72 h in a 6-well plate. The cells were labelled by Annexin V Dyomics 647 and Hoechst 33258 and analysed by flow cytometry (**a**). Cells incubated in the medium alone served as a control. Each experiment condition was performed in triplicate, and the experiment was performed at least twice with similar results. Results are presented as the percentage of cells in the three states (viable, early apoptosis, and late apoptosis) ± SD for LCL-161 treatment alone (**b**), gemcitabine treatment alone (**c**), and combined gemcitabine + LCL-161 (**d**). MDA-MB-231 cells were treated as in (**a**), harvested and cell lysates with the same number of cells were prepared. Caspase-3 activity in the lysates was determined using The EnzCheck Caspase-3 Assay Kit. Fluorescence measurements were performed in quadruplicates using an Infinite 200 Pro (excitation 342 nm, emission 441 nm). Results are

presented as caspase-3 activity relative to the control sample (**e**). The experiment was performed twice. Statistical significance was determined using One-way ANOVA with Tukey's multiple comparisons tests (n.s. $P > 0.05$, * $P \leq 0.05$, ** $P \leq 0.01$, *** $P \leq 0.001$, **** $P \leq 0.0001$).

The potentiation of gemcitabine cytotoxic activity by the IAP inhibitor LCL-161 was investigated in MDA-MB-231 cells using Annexin V-binding and caspase-3 activity assays (**Fig. 30, p. 80**).

Treatment with a lower concentration of LCL-161 (50 nM) increased the percentage of cells in late apoptosis by 2 %, while the higher concentration (500 nM) led to a 5 % increase compared to the control group. Gemcitabine induced a 3 % increase in late apoptosis at the lower dose (2 nM) and an 8 % increase at the higher dose (4 nM).

A synergetic effect was evident in all four combinations. There was a 10 % increase compared to the expected 5 % (50 nM LCL-161 + 2 nM gemcitabine) and a 22 % rise compared to the expected 10 % (50 nM LCL-161 + 4 nM gemcitabine). Furthermore, we observed a 16 % increase compared to the expected 8 % (500 nM LCL-161 + 2 nM gemcitabine), and a 42 % increase compared to the expected 13 % (500 nM LCL-161 + 4 nM gemcitabine). Since the combination of 500 nM LCL-161 and 4 nM, gemcitabine showed the most significant synergetic effect, it was chosen for the caspase-3 activity assay.

We found no increase in caspase-3 activity when cells were exposed to gemcitabine or LCL-161 alone, but a significant increase in caspase-3 was found with combination treatment, reaching ~ 35% increase (**Fig. 30e, p. 80**).

4.4.2.4 MDA-MB-231: Gemcitabine + AZD5582

AZD5582 demonstrated the most significant potentiation of gemcitabine cytotoxic activity in the MDA-MB-231 cell line. This observation was further supported by the highest caspase-3 activity observed across our experiments.

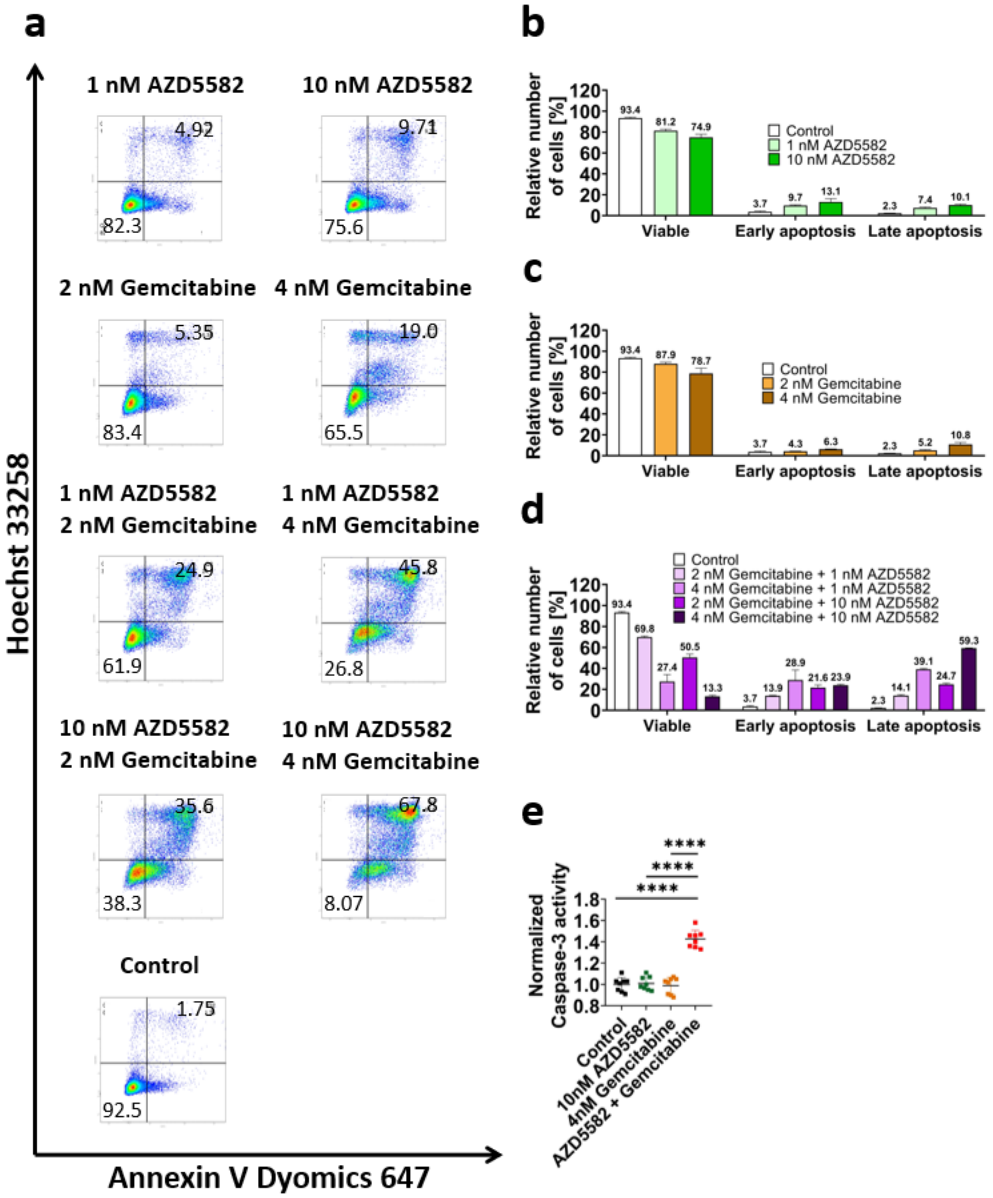

Figure 31. Potentiation of cytotoxic activity of gemcitabine by AZD5582. MDA-MB-231 cells were incubated with either gemcitabine (2 and 4 nM) or AZD5582 (1 and 10 nM) or both compounds for 72 h in a 6-well plate. The cells were labelled by Annexin V Dyomics 647 and Hoechst 33258 and analysed by flow cytometry (**a**). Cells incubated in the medium alone served as a control. Each experiment condition was performed in triplicate, and the experiment was performed at least twice with similar results. Results are presented as the percentage of cells in the three states (viable, early apoptosis, and late apoptosis) ± SD for AZD5582 treatment alone (**b**), gemcitabine treatment alone (**c**), and combined gemcitabine + AZD5582 (**d**). MDA-MB-231 cells were treated as in (**a**), harvested and cell lysates with the same number of cells were prepared. Caspase-3 activity in the lysates was determined using The EnzCheck Caspase-3 Assay Kit. Fluorescence measurements were performed in quadruplicates using an Infinite 200 Pro (excitation 342 nm, emission 441 nm). Results are

presented as caspase-3 activity relative to the control sample (**e**). The experiment was performed twice. Statistical significance was determined using One-way ANOVA with Tukey's multiple comparisons tests (n.s. $P > 0.05$, * $P \leq 0.05$, ** $P \leq 0.01$, *** $P \leq 0.001$, **** $P \leq 0.0001$).

Augmentation of the cytotoxic activity of gemcitabine by the IAP inhibitor AZD5582 was examined in MDA-MB-231 cells through Annexin V-binding and caspase-3 activity assays (**Fig. 31, p. 82**).

Exposure to a lower concentration of AZD5582 (1 nM) resulted in a 2 % increase of cells in late apoptosis, while the higher concentration (10 nM) led to a 5 % increase compared to the control group. Gemcitabine induced a 3 % elevation in late apoptosis at the lower dose (2 nM) and an 8 % increase at the higher dose (4 nM).

A synergetic effect was observed in all four combinations. There was a 12 % increase compared to the anticipated 8 % (1 nM AZD5582 + 2 nM gemcitabine), and a 37 % rise compared to the anticipated 13 % (1 nM AZD5582 + 4 nM gemcitabine). We observed also a 22 % increase compared to the anticipated 11 % (10 nM AZD5582 + 2 nM gemcitabine), and a 57 % increase compared to the anticipated 16 % (10 nM AZD5582 + 4 nM gemcitabine). Given the most pronounced synergetic effect observed in the last combination, it was selected for the caspase-3 activity assay.

The caspase-3 activity assay demonstrated no increase in caspase-3 activity when cells were exposed to gemcitabine or AZD5582 alone, but a significant increase in caspase-3 activity was found with combination treatment, reaching ~ 45 % increase in caspase-3 activity (**Fig. 31e, p. 82**).

4.5 In Vivo Experiments

4.5.1 Toxicity of Micelle AZD5582

The toxicity test of Micelle AZD5582, conducted on athymic Nude-Foxn1nu mice, revealed significant toxicity at the dose of 5 mg/kg (AZD5582).

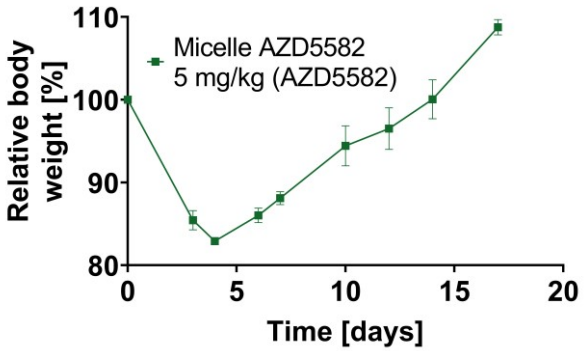

Figure 32. Toxicity of Micelle AZD5582 in mice. Athymic Nude-Foxn1nu mice (n=4) were i.v. injected with Micelle AZD5582 (5 mg/kg AZD5582) on day 0 in 300 µL PBS. Body weight was recorded every 2 or 3 days up to day 17.

To assess the toxicity of HPMA copolymer-based micelle loaded with AZD5582, the sample (Micelle AZD5582) was i.v. administered to athymic Nude-Foxn1nu mice at a dose corresponding to 5 mg/kg AZD5582 on day 0. The mice were monitored for body weight changes over 17 days. The average body weight of experimental mice had dropped to 85.4 % of the initial body weight on day 3, and by day 4, it had decreased further to 82.9 %. Additionally, one mouse died on day 1. These results indicate that Micelle AZD5582 exhibited significant toxicity at the dose of 5 mg/kg AZD5582 (**Fig. 32**).

4.5.2 Toxicity of P-LCL161$_{HYD}$ and P-Gem

We evaluated the toxicity of P-LCL161$_{HYD}$ and P-Gem in NSG mice. While both tested doses of P-LCL161$_{HYD}$ were non-toxic, the higher dose of P-Gem exhibited toxicity. Additionally, testing these two compounds in combination resulted in high toxicity.

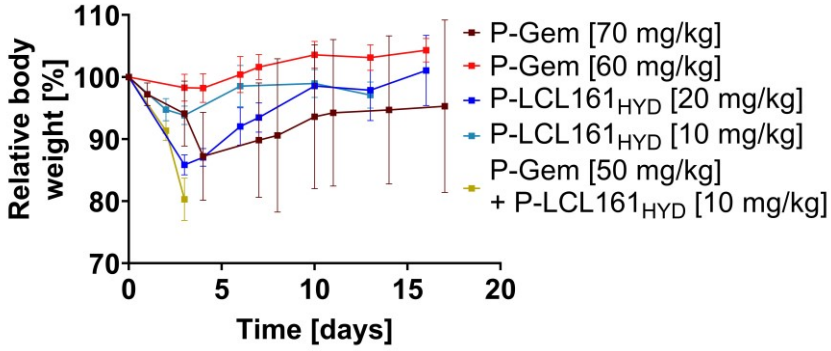

Figure 33. Toxicity of P-Gem conjugate, P-LCL161$_{HYD}$ conjugate and their combination in mice. NSG mice (n=4) were i.v. injected with P-Gem conjugate alone, P-LCL161$_{HYD}$ conjugate alone, or with both conjugates in 300 µL PBS. The dosage for each conjugate in a particular experiment group is shown in the graph. Body weight was recorded every 2 or 3 days for ~ 14 days.

The toxicity of P-LCL161$_{HYD}$ and P-Gem conjugates, both as single agents and in combination, was evaluated in NSG mice. The mice were monitored for body weight changes and overall health status over ~ 14 days.

In the group receiving 70 mg/kg gemcitabine, the average body weight dropped to 87 % on day 4, and one mouse died, indicating toxicity at this dosage. The dose of 60 mg/kg of gemcitabine caused only a negligible and very transient decrease in body weight (2 %) thus this dose could be considered a safe one.

Both doses of LCL-161 were considered non-toxic, as no mice died and the body weight dropped to 93 % (10 mg/kg LCL-161) and 86 % (20 mg/kg LCL-161) before rebounding. However, the combination of 50 mg/kg gemcitabine and 10 mg/kg LCL-161 proved to be highly toxic, as the average body weight of the group dropped to 80 % on day 3 and all 4 mice died on day 4. Thus, it seems that the toxicity of P-Gem and P-LCL161$_{HYD}$ conjugates potentiates each other and a significant reduction of the dose of each conjugate is required to reach a safe dosage (**Fig. 33**).

5 Discussion

In addition to targeting cancer cells, chemotherapy can also damage normal cells and lead to severe side effects [50]. For this reason, new approaches have been tested and introduced in cancer treatment, such as combination therapies. This method involves the simultaneous use of two or more therapeutic agents with distinct mechanisms of action and can enhance treatment efficacy by targeting crucial molecular pathways. Combination therapy presents several advantages, including reducing drug resistance and lowering the cytotoxic effects on normal cells. Additionally, it may enhance the anticancer effects of the therapeutic agents and allow for a more efficient treatment response, often requiring fewer treatment cycles or lower doses [185].

Another approach is the use of DDS. The main goals of these tools include reduction of drug toxicity, increasing drug accumulation at the target site for maximal therapeutic efficacy, and minimizing the accumulation in healthy tissues. Currently, various DDS are utilized in cancer therapy for numerous anti-cancer agents, such as liposomes or exosomes [150], [151].

The main objective of this thesis was to investigate the potential of two IAP inhibitors (SMAC mimetics) LCL-161 and AZD5582 to enhance the cytostatic and cytotoxic effects of gemcitabine. SMAC mimetics bind to multiple members of the IAP family, such as cIAP1, cIAP2, and XIAP, dampening their function of inhibiting caspases and thereby lowering the threshold to apoptosis induction. Additionally, they play a crucial role in the TNF, MAPK, and NF-κB signaling pathways. Despite promising preclinical results, Phase I/II human clinical trials of IAP inhibitors as single agents have shown low efficacy. Consequently, they are being investigated in combination therapies with various drugs, including paclitaxel, docetaxel, carboplatin, and irinotecan [116].

In this diploma thesis, we chose to combine IAP inhibitors with gemcitabine due to our long-term interest in this anticancer drug and the work of our group on the development of DDS for gemcitabine. Gemcitabine is a cytidine analogue with two fluorine atoms and primary therapy for various cancers. It inhibits DNA synthesis, which can lead to activation of DDR systems and increased TNF-alpha production, with both pathways involving IAPs (**Fig. 6, p. 37**) [186], [187]. However, several mechanisms deactivate gemcitabine and 75 % of gemcitabine is excreted in the first 24 h in urine [94]. These findings collectively indicate that the efficacy of gemcitabine could be enhanced by prolonging systematic exposure of tumors to the drug through a DDS. Additionally, its anticancer effects can be potentiated by combining it with IAP inhibitors.

IAP inhibitors and gemcitabine were tested as single agents and in combination in five human cancer cell lines: pancreatic (PANC1, MiaPaca-2, BxPC-3), prostatic (PC-3), and breast (MDA-MB-231). Additionally, HPMA copolymer-based DDS bearing these anti-cancer agents were prepared and characterised at the Department of Biomedical Polymers (Institute of Macromolecular Chemistry).

All five cancer cell lines exhibited high sensitivity to the cytostatic activity of gemcitabine (**Fig. 17, p. 63**). The IC_{50} values ranged from 2 to 11 nM. The *in vitro* cytostatic activity of P-Gem was found to be considerably lower, with IC_{50} values ~ 10 times higher in all tested cell lines. This reduction is attributed to the slow release of the drug caused by the structure of the spacer between the HPMA copolymer carrier and the drug. In this system, gemcitabine is linked through an amide bond to the aminocaproic acid spacer and copolymer backbone, resulting in enhanced stability and prolonged half-life in circulation compared to the free drug (data to be published).

Both IAP inhibitors LCL-161 and AZD5582 exhibited cytostatic activity in the [^{3}H]-thymidine incorporation assay as single agents (**Fig. 18, p. 64**). Interestingly, both inhibitors showed a similar pattern of efficacy in our panel of cancer cell lines. Specifically, MiaPaca-2 and BxPC-3 cell lines displayed significantly higher sensitivity to IAP inhibitors in comparison to the other three cell lines. Notably, dimeric SMAC mimetic AZD5582 demonstrated much higher potency than monomeric LCL-161, with IC_{50} values ~ 100-200 times lower for those two sensitive cell lines.

AZD5582 is a bivalent SMAC mimetic, comprising two parts of the same AVPI motif connected via a linker. AVPI is a crucial tetrapeptide of SMAC necessary for binding the BIR domains in IAPs. Bivalent SMAC mimetics, such as birinapant, APG-1387, and HGS1029, were developed based on observations that monomeric SMAC mutants exhibit much lower activation of caspase-3 compared to dimeric SMAC. The most significant advantage of bivalent SMAC mimetics is their ability to bind both BIR2 and BIR3 domains simultaneously, resulting in increased inhibitory effects on the IAPs [116], [188]. While AZD5582 has shown potency in cancer research and the treatment of HIV, it has not yet progressed to clinical trials contrary to LCL-161 [146], [147], [189].

Since elevated expression levels of cIAP1 and XIAP have been found to reduce the efficacy of IAP inhibitors, we investigated whether there is a correlation between the expression levels of cIAP1, cIAP2, and XIAP in our panel of cancer cell lines and their sensitivity to two selected SMAC mimetics for this study (**Fig. 15, p. 61-62**) [145]. Surprisingly, the data did not reveal any significant correlation and showed different patterns of IAP expression irrespective of the cell sensitivity to LCL-161 and AZD5582 among the

tested cancer cell lines. The PANC1 cell line exhibited elevated expression levels of both cIAP1 and cIAP2, while increased expression of XIAP was observed in both the PANC1 and BxPC-3 cell lines compared to others. In contrast, the comparison of the expression levels of the three IAP genes (**Fig. 16, p. 62**) in all five cell lines revealed a consistent pattern, with XIAP showing slight elevation and cIAP1 exhibiting significantly higher expression compared to cIAP2 in most cases (4 out of 5 cell lines). Notably, PANC1 showed a marginal increase in cIAP1 expression and a notable decrease in XIAP expression relative to cIAP2.

Similar to P-Gem and free gemcitabine, the activity of HPMA copolymers bearing LCL-161 was observed to be much lower than free LCL-161 (**Fig. 19, p. 65**). Out of the two prepared conjugates, P-LCL161$_{HYD}$, which comprises an aminocaproic spacer and pH-sensitive hydrazone bond between the spacer and LCL-161, exhibited slightly higher activity compared to P-LCL161$_{VCP}$, which utilizes an enzymatically cleavable linker and requires uptake into lysosomes for cathepsin B-mediated release of the drug. The IC_{50} values for P-LCL161$_{HYD}$ showed almost 140-fold (MiaPaca-2) and 35-fold (BxPC-3) increases, compared to those obtained for LCL-161. Interestingly, the sensitivity of these two cell lines varied, with MiaPaca-2 being more sensitive to LCL-161 than BxPC-3 and BxPC-3 being more sensitive to P-LCL161$_{HYD}$ than MiaPaca-2. This difference may be attributed to various characteristics of these two cancer cell lines, such as different endocytic activity, and variations in the intracellular environment, including pH in the endolysosomal pathway.

Conversely, HPMA copolymer-based micelle with entrapped AZD5582 (Micelle AZD5582) showed no difference in cytostatic activity compared to the free drug (**Fig. 20, p. 67**). This could be explained by the rapid release of the drug from the micelles, with almost 60 % of the drug being released within the first hour (data to be published).

IAP inhibitors as single agents exhibited also cytotoxic effects in the Annexin V-binding assay. LCL-161 and AZD5582 induced apoptosis in four out of five cancer cell lines, except PC-3, in a concentration-dependent manner (**Fig. 22, p. 68, Fig. 23, p. 69**).

Similarly to the [^{3}H]-thymidine incorporation assay, P-LCL161$_{HYD}$ exhibited minimal activity compared to the free drug when tested for cytotoxic activity (**Fig. 24, p. 70**). A slight cytotoxic effect (~ 25 % of cells in the late apoptosis phase) was observed at a concentration of 50 000 nM, which was comparable to the effect of the free drug at a concentration of 50 nM. The low *in vitro* activity of P-LCL161$_{HYD}$ may be attributed to the high stability of the bond between the DDS and LCL-161 and thus very slow LCL-161 release.

The potentiation of gemcitabine activity by IAP inhibitors was assessed using [^{3}H]-thymidine incorporation, Annexin V-binding, and caspase-3 activity assays. IAP inhibitors enhanced the cytostatic effect of gemcitabine in all tested cell lines, with the most significant effect observed in MiaPaca-2 and MDA-MB-231 cell lines (**Fig. 25, p. 72, Fig. 26, p. 73**). To further evaluate this combination effect, SynergyFinder 3.0 analysis was conducted, revealing a synergistic effect between LCL-161 or AZD5582 and gemcitabine in both MiaPaca-2 and MDA-MB-231 cell lines (**Fig. 27, p. 74**). This synergy was further supported by the determination of cytotoxic activity using Annexin V-binding and caspase-3 activity assays (**Fig. 28, 29, 30, 31, p. 76-82**). In both MiaPaca-2 and MDA-MB-231 cell lines, the combination treatment demonstrated a significantly higher cytotoxic effect, resulting in larger populations of cells in the late apoptosis phase. This was further confirmed by the caspase-3 activity assay, which showed significantly increased activity only in the combination-treated samples. The lack of caspase-3 activity increase in IAP inhibitors alone treated cells compared to the control group in the caspase-3 activity assay can be caused by the sensitivity of the assay, as these agents were capable of inducing apoptosis alone at the same concentration in the Annexin V-binding assay and are known to inhibit IAPs function, i.e. caspase inhibition.

The toxicity of HPMA copolymer conjugates bearing gemcitabine or SMAC mimetics was assessed in mice either alone or in combination. Micelle AZD5582 was administered at a dose of 5 mg/kg, based on literature that used 3 mg/kg (AZD5582) [145]. However, this dose of Micelle AZD5582 proved to be toxic, resulting in the death of one mouse in the experimental group and an average body weight drop to ~ 83 % of the original body weight (**Fig. 32, p. 84**). Further testing was not conducted due to technical issues. The toxicity of P-Gem and P-LCL161$_{HYD}$ was evaluated at two different doses (**Fig. 33, p. 85**). While P-Gem at 70 mg/kg (gemcitabine) resulted in the death of one mouse, 60 mg/kg showed minimal change in body weight. Both doses of P-LCL161$_{HYD}$, 10 and 20 mg/kg (LCL-161), were not toxic, with body weights dropping to 93 % (10 mg/kg) and 86 % (20 mg/kg) before rebounding. These results were unexpected, as we anticipated no weight change at these doses based on the literature and considering the high stability and almost lack of *in vitro* activity of the conjugate (P-LCL161$_{HYD}$) [190]. This might be caused by a faster release from the conjugate *in vivo* compared to *in vitro* conditions, however, further tests are needed to confirm this hypothesis.

The combination of 50 mg/kg P-Gem and 10 mg/kg P-LCL161$_{HYD}$ proved to be highly toxic, as the average body weight of the mice dropped to 80 % on day 3, and all 4 mice died by day 4. Therefore, further experiments will combine 50 mg/kg P-Gem with

lower doses of P-LCL161$_{HYD}$ to determine the optimal dosage before assessing the antitumor activity of these compounds in combination.

The data collectively indicates that IAP inhibitors alone possess cytostatic and cytotoxic activity and can enhance the effectiveness of gemcitabine in certain cancer cell lines. LCL-161 is currently in Phase 1 trials in combination with nab-paclitaxel and gemcitabine for metastatic pancreatic cancer and Phase 2 trials with paclitaxel for breast cancer. With its ability to target multiple IAP proteins, increase circulating cytokine levels (TNF-α, IL-8), and inhibit the multi-drug efflux activity of P-gp, LCL-161 shows promise as a drug to enhance the efficacy of other chemotherapeutic agents [144], [191], [192], [193]. AZD5582 exhibits potent binding to the BIR3 domain of cIAP1, cIAP2, and XIAP, thus inhibiting their function and inducing cIAP1 autoubiquitination. Additionally, it has demonstrated significant tumor regression as a single agent in mice bearing MDA-MB-231 cancer [146]. Our findings suggest that AZD5582 might be more potent than LCL-161, whether administered alone or in combination with gemcitabine. However, further research is needed to fully understand the effects and molecular mechanisms of AZD5582 before it progresses to clinical trials. Moreover, all three agents tested in this diploma thesis (gemcitabine, LCL-161, and AZD5582) could potentially benefit from the prolonged circulation time and tumor localization provided by HPMA copolymer-based delivery systems. However, optimizing these DDS, such as increased stability of the Micelle AZD5882 compound, and evaluating their antitumor activity are necessary steps for their further development as anticancer drugs.

6 Conclusion

The anticancer activity of two SMAC mimetics (LCL-161 and AZD5582) as single agents and their ability to potentiate the anticancer activity of gemcitabine across five different human cancer cell lines (pancreatic carcinomas: PANC1, BxPC-3, and MiaPaca-2, prostatic carcinoma: PC-3, breast carcinoma: MDA-MB-231) was investigated. Furthermore, HPMA copolymers bearing these compounds were characterised for their toxicity. The results of this diploma thesis can be summarized in the following points:

1) Both SMAC mimetics LCL-161 and AZD5582 demonstrated cytostatic and cytotoxic activities, as evidenced by [^{3}H]-thymidine incorporation and Annexin V-binding assays. Notably, MiaPaca-2 and BxPC-3 cell lines exhibited the highest sensitivity, with AZD5582 displaying much higher potency compared to LCL-161.

2) Evaluation of cIAP1, cIAP2, and XIAP across all cell lines revealed no correlation between sensitivity to IAP inhibitors and gene expression levels. However, consistent patterns of increased cIAP1 expression relative to cIAP2 were observed across almost all cell lines.

3) Both LCL-161 and AZD5582 potentiated the cytostatic and cytotoxic effects of gemcitabine in all cell lines, with the most pronounced synergism observed in MiaPaca-2 and MDA-MB-231 cell lines.

4) HPMA copolymer conjugates bearing LCL-161, AZD5582, and gemcitabine exhibited lower cytostatic and cytotoxic activities compared to free drugs. While P-Gem showed ~ 10 times higher IC_{50} values than gemcitabine, P-LCL161$_{HYD}$ displayed even lower activity compared to LCL-161, suggesting a very slow release of the drug. Interestingly, the activity of Micelle AZD5582 was comparable to free AZD5582, likely due to rapid release.

5) *In vivo* toxicity evaluation determined the optimal treatment dose for P-Gem as a single agent to be slightly below 70 mg/kg (gemcitabine), as 70 mg/kg proved toxic and 60 mg/kg resulted in minimal change in body weight. The maximal tolerated dose for P-LCL161$_{HYD}$ was found to be 20 mg/kg (LCL-161). However, the combination of P-Gem at 50 mg/kg (gemcitabine) and P-LCL161$_{HYD}$ at 10 mg/kg (LCL-161) was toxic. Notably, Micelle AZD5582 exhibited significant toxicity at a dose of 5 mg/kg (AZD5582), highlighting the

need for further investigation into the safety profile of these compounds before evaluating their anticancer activity.

7 References

[1] L. Pecorino: *Molecular biology of cancer: mechanisms, targets, and therapeutics*, Third edition. Oxford: Oxford University Press, 2012. ISBN 978-0199577170.

[2] H. Sung *et al.*: Global Cancer Statistics 2020: GLOBOCAN Estimates of Incidence and Mortality Worldwide for 36 Cancers in 185 Countries, *CA. Cancer J. Clin.*, **vol. 71**, no. 3, p. 209–249 (2021).

[3] J.-J. Wang *et al.*: Tumor microenvironment: recent advances in various cancer treatments, *Eur. Rev. Med. Pharmacol. Sci.*, **vol. 22**, no. 12, p. 3855–3864 (2018).

[4] Q. Song *et al.*: Cancer classification in the genomic era: five contemporary problems, *Hum. Genomics*, **vol. 9** (2015).

[5] R. A. Weinberg: *The Biology of Cancer*, 2nd ed. New York: W.W. Norton & Company (2013). ISBN 978-0815342205.

[6] J. Huang *et al.*: Disease Burden, Risk Factors, and Trends of Leukaemia: A Global Analysis, *Front. Oncol.*, **vol. 12** (2022).

[7] D. Hanahan and R. A. Weinberg: The hallmarks of cancer, *Cell*, **vol. 100**, no. 1, p. 57–70 (2000).

[8] D. Hanahan and R. A. Weinberg: Hallmarks of cancer: the next generation, *Cell*, **vol. 144**, no. 5, p. 646–674 (2011).

[9] D. Hanahan: Hallmarks of Cancer: New Dimensions, *Cancer Discov.*, **vol. 12**, no. 1, p. 31–46 (2022).

[10] S. Kumari *et al.*: Unboxing the molecular modalities of mutagens in cancer, *Environ. Sci. Pollut. Res. Int.*, vol. 29, **no. 41**, p. 62111–62159 (2022).

[11] S. Hodgson: Mechanisms of inherited cancer susceptibility, *J. Zhejiang Univ. Sci. B*, **vol. 9**, no. 1, p. 1–4 (2008).

[12] A. M. Lewandowska *et al.*: Environmental risk factors for cancer - review paper, *Ann. Agric. Environ. Med. AAEM*, **vol. 26**, no. 1, p. 1–7 (2019).

[13] A. Vincent *et al.*: Pancreatic cancer, *Lancet Lond. Engl.*, **vol. 378**, no. 9791, p. 607–620 (2011).

[14] A. P. Klein: Pancreatic cancer epidemiology: understanding the role of lifestyle and inherited risk factors, *Nat. Rev. Gastroenterol. Hepatol.*, **vol. 18**, no. 7, p. 493–502 (2021).

[15] Z. Zhao and W. Liu: Pancreatic Cancer: A Review of Risk Factors, Diagnosis, and Treatment, *Technol. Cancer Res. Treat.*, **vol. 19** (2020).

[16] V. Goral: Pancreatic Cancer: Pathogenesis and Diagnosis, *Asian Pac. J. Cancer Prev. APJCP*, **vol. 16**, no. 14, p. 5619–5624 (2015).

[17] Pancreatic Cancer Types. Accessed: Apr. 15, 2024. [Online]. Available: https://www.hopkinsmedicine.org/health/conditions-and-diseases/pancreatic-cancer/pancreatic-cancer-types

[18] Conroy Thierry *et al.*: FOLFIRINOX or Gemcitabine as Adjuvant Therapy for Pancreatic Cancer, *N. Engl. J. Med.*, **vol. 379**, no. 25, p. 2395–2406 (2018).

[19] P. A. Philip *et al.*: Nab-paclitaxel plus gemcitabine in patients with locally advanced pancreatic cancer (LAPACT): a multicentre, open-label phase 2 study, *Lancet Gastroenterol. Hepatol.*, **vol. 5**, no. 3, p. 285–294 (2020).

[20] N. Harbeck and M. Gnant: Breast cancer, *Lancet Lond. Engl.*, **vol. 389**, no. 10074, p. 1134–1150 (2017).

[21] M. Arnold *et al.*: Current and future burden of breast cancer: Global statistics for 2020 and 2040, *Breast Off. J. Eur. Soc. Mastology*, **vol. 66**, p. 15–23 (2022).

[22] K. Barzaman *et al.*: Breast cancer: Biology, biomarkers, and treatments, *Int. Immunopharmacol.*, **vol. 84** (2020).

[23] L. Bian *et al.*: Survival benefit of platinum-based regimen in early stage triple negative breast cancer: A meta-analysis of randomized controlled trials, *Npj Breast Cancer*, **vol. 7**, no. 1, p. 1–8 (2021).

[24] S. Wasim *et al.*: Complexities of Prostate Cancer, *Int. J. Mol. Sci.*, **vol. 23**, no. 22, p. 14257 (2022).
[25] L. Wang *et al.*: Prostate Cancer Incidence and Mortality: Global Status and Temporal Trends in 89 Countries From 2000 to 2019, *Front. Public Health*, **vol. 10** (2022).
[26] G. Wang *et al.*: Genetics and biology of prostate cancer, *Genes Dev.*, **vol. 32**, no. 17–18, p. 1105–1140 (2018).
[27] C. E. Barbieri *et al.*: The Mutational Landscape of Prostate Cancer, *Eur. Urol.*, **vol. 64**, no. 4, p. 567–576 (2013).
[28] M. Sekhoacha *et al.*: Prostate Cancer Review: Genetics, Diagnosis, Treatment Options, and Alternative Approaches, *Mol. Basel Switz.*, **vol. 27**, no. 17 (2022).
[29] G. P. Murphy *et al.*: Measurement of serum prostate-specific membrane antigen, a new prognostic marker for prostate cancer, *Urology*, **vol. 51**, p. 89–97 (1998).
[30] U. Hennrich and M. Eder: [68Ga]Ga-PSMA-11: The First FDA-Approved 68Ga-Radiopharmaceutical for PET Imaging of Prostate Cancer, *Pharmaceuticals*, **vol. 14**, no. 8 (2021).
[31] Z.-K. Qin *et al.*: Short-term efficacy of combined chemotherapy of gemcitabine and cisplatin on advanced hormone refractory prostate cancer, *Ai Zheng Aizheng Chin. J. Cancer*, **vol. 23**, no. 12, p. 1700–1703 (2004).
[32] R. Kaur *et al.*: Cancer treatment therapies: traditional to modern approaches to combat cancers, *Mol. Biol. Rep.*, **vol. 50**, no. 11, p. 9663–9676 (2023).
[33] D. T. Debela *et al.*: New approaches and procedures for cancer treatment: Current perspectives, *SAGE Open Med.*, **vol. 9** (2021).
[34] L. Wyld *et al.*: The evolution of cancer surgery and future perspectives, *Nat. Rev. Clin. Oncol.*, **vol. 12**, no. 2, p. 115–124 (2015).
[35] Z. Abbas *et al.*: An Overview of Cancer Treatment Modalities, *Neoplasm*, IntechOpen (2018).
[36] L. H. Sobin: TNM: evolution and relation to other prognostic factors, *Semin. Surg. Oncol.*, **vol. 21**, no. 1, p. 3–7 (2003).
[37] J. Brierley *et al.*: Global Consultation on Cancer Staging: promoting consistent understanding and use, *Nat. Rev. Clin. Oncol.*, **vol. 16**, no. 12, p. 763–771 (2019).
[38] R. Baskar *et al.*, Cancer and radiation therapy: current advances and future directions, *Int. J. Med. Sci.*, **vol. 9**, no. 3, p. 193–199 (2012).
[39] D. Abshire and M. K. Lang, The Evolution of Radiation Therapy in Treating Cancer, *Semin. Oncol. Nurs.*, **vol. 34**, no. 2, p. 151–157 (2018).
[40] R. Baskar and K. Itahana: Radiation therapy and cancer control in developing countries: Can we save more lives?, *Int. J. Med. Sci.*, **vol. 14**, no. 1, p. 13–17 (2017).
[41] M. Donya *et al.*: Radiation in medicine: Origins, risks and aspirations, *Glob. Cardiol. Sci. Pract.*, **vol. 2014**, no. 4, p. 437–448 (2014).
[42] Y. Zhang and Z. Zhang: The history and advances in cancer immunotherapy: understanding the characteristics of tumor-infiltrating immune cells and their therapeutic implications, *Cell. Mol. Immunol.*, **vol. 17**, no. 8, p. 807–821 (2020).
[43] M. Abbott and Y. Ustoyev: Cancer and the Immune System: The History and Background of Immunotherapy, *Semin. Oncol. Nurs.*, **vol. 35**, no. 5 (2019).
[44] R. S. Riley *et al.*: Delivery technologies for cancer immunotherapy, *Nat. Rev. Drug Discov.*, **vol. 18**, no. 3, p. 175–196 (2019).
[45] G. Barchiesi *et al.*: Neoadjuvant Endocrine Therapy in Breast Cancer: Current Knowledge and Future Perspectives, *Int. J. Mol. Sci.*, **vol. 21**, no. 10 (2020).
[46] K. Desai *et al.*: Hormonal Therapy for Prostate Cancer, *Endocr. Rev.*, **vol. 42**, no. 3, p. 354–373 (2021).
[47] G. Emons and C. Gründker: The Role of Gonadotropin-Releasing Hormone (GnRH) in Endometrial Cancer, *Cells*, **vol. 10**, no. 2 (2021).
[48] J. Yuan *et al.*: The role of the tumor microenvironment in endocrine therapy resistance in hormone receptor-positive breast cancer, *Front. Endocrinol.*, **vol. 14** (2023).

[49] W.-L. Lee *et al.*: Hormone therapy for patients with advanced or recurrent endometrial cancer, *J. Chin. Med. Assoc. JCMA*, **vol. 77**, no. 5, p. 221–226 (2014).
[50] U. Anand *et al.*: Cancer chemotherapy and beyond: Current status, drug candidates, associated risks and progress in targeted therapeutics, *Genes Dis.*, **vol. 10**, no. 4, p. 1367–1401 (2022).
[51] M. Shields: Chapter 14 - Chemotherapeutics, *Pharmacognosy*, S. Badal and R. Delgoda, Eds., Boston: Academic Press, p. 295–313 (2017). ISBN 9780128021040.
[52] M. T. Amjad *et al.*: Cancer Chemotherapy, in *StatPearls*, Treasure Island (FL): StatPearls Publishing, 2024. Accessed: Feb. 21, 2024. [Online]. Available: http://www.ncbi.nlm.nih.gov/books/NBK564367/
[53] H. K. Chew: Adjuvant therapy for breast cancer, *West. J. Med.*, **vol. 174**, no. 4, p. 284–287 (2001).
[54] E. N. Imyanitov and G. A. Yanus: Neoadjuvant therapy: theoretical, biological and medical consideration, *Chin. Clin. Oncol.*, **vol. 7**, no. 6 (2018).
[55] C. M. Tilsed *et al.*: Cancer chemotherapy: insights into cellular and tumor microenvironmental mechanisms of action, *Front. Oncol.*, **vol. 12** (2022).
[56] R. Ralhan and J. Kaur: Alkylating agents and cancer therapy, *Expert Opin. Ther. Pat.*, **vol. 17**, no. 9, p. 1061–1075 (2007).
[57] B. Biersack: Alkylating anticancer agents and their relations to microRNAs, *Cancer Drug Resist.*, **vol. 2**, no. 1, p. 1–17 (2019).
[58] S. Agnihotri *et al.*: ATM regulates 3-Methylpurine-DNA glycosylase and promotes therapeutic resistance to alkylating agents, *Cancer Discov.*, **vol. 4**, no. 10, p. 1198–1213 (2014).
[59] E. Scholar: Alkylating Agents, *xPharm: The Comprehensive Pharmacology Reference*, S. J. Enna and D. B. Bylund, Eds., New York: Elsevier, p. 1–4 (2007).
[60] J. Egea *et al.*: Alkylating Agent-Induced Toxicity and Melatonin-Based Therapies, *Front. Pharmacol.*, **vol. 13** (2022).
[61] A. C. Bharti *et al.*: Chapter 1 - Pathways Linked to Cancer Chemoresistance and Their Targeting by Nutraceuticals, *Role of Nutraceuticals in Cancer Chemosensitization*, **vol. 2**, Academic Press, p. 1–30 (2018).
[62] Y. Gao *et al.*: Antibiotics for cancer treatment: A double-edged sword, *J. Cancer*, **vol. 11**, no. 17, p. 5135–5149 (2020).
[63] S. Venugopal *et al.*: DNA intercalators as anticancer agents, *Chem. Biol. Drug Des.*, **vol. 100**, no. 4, p. 580–598 (2022).
[64] R. Mattioli *et al.*: Doxorubicin and other anthracyclines in cancers: Activity, chemoresistance and its overcoming, *Mol. Aspects Med.*, **vol. 93** (2023).
[65] K. Studzian *et al.*: Subcellular localization of anthracyclines in cultured rat cardiomyoblasts as possible predictors of cardiotoxicity, *Invest. New Drugs*, **vol. 33**, p. 1032–1039 (2015).
[66] R. T. Dorr: Bleomycin pharmacology: mechanism of action and resistance, and clinical pharmacokinetics, *Semin. Oncol.*, **vol. 19**, no. 2, p. 3–8 (1992).
[67] M. Tomasz: Mitomycin C: small, fast and deadly (but very selective), *Chem. Biol.*, **vol. 2**, no. 9, p. 575–579 (1995).
[68] D.-F. Lu *et al.*: Actinomycin D inhibits cell proliferations and promotes apoptosis in osteosarcoma cells, *Int. J. Clin. Exp. Med.*, **vol. 8**, no. 2, p. 1904–1911 (2015).
[69] J. Tischer and F. Gergely: Anti-mitotic therapies in cancer, *J. Cell Biol.*, **vol. 218**, no. 1, p. 10–11 (2019).
[70] G. J. Brouhard and L. M. Rice: Microtubule Dynamics: an interplay of biochemistry and mechanics, *Nat. Rev. Mol. Cell Biol.*, **vol. 19**, no. 7, p. 451–463 (2018).
[71] L. Mosca *et al.*: Taxanes in cancer treatment: Activity, chemoresistance and its overcoming, *Drug Resist. Updat.*, **vol. 54** (2021).
[72] J. Škubník *et al.*: Current Perspectives on Taxanes: Focus on Their Bioactivity, Delivery and Combination Therapy, *Plants*, **vol. 10**, no. 3 (2021).

[73] Y. Li, H. Zhang *et al.*: Toll-like receptor 4 signaling contributes to paclitaxel-induced peripheral neuropathy, *J. Pain Off. J. Am. Pain Soc.*, **vol. 15**, no. 7, p. 712–725 (2014).
[74] M. Moudi *et al.*: Vinca Alkaloids, *Int. J. Prev. Med.*, **vol. 4**, no. 11, p. 1231–1235 (2013).
[75] A. Banyal *et al.*: Vinca alkaloids as a potential cancer therapeutics: recent update and future challenges, *3 Biotech*, **vol. 13**, no. 6, p. 211 (2023).
[76] A. Talukdar *et al.*: Topoisomerase I inhibitors: Challenges, progress and the road ahead, *Eur. J. Med. Chem.*, **vol. 236** (2022).
[77] S. A. Martin: Chapter 6 - The DNA mismatch repair pathway, in *DNA Repair in Cancer Therapy (Second Edition)*, M. R. Kelley and M. L. Fishel, Eds., Boston: Academic Press, p. 151–177 (2016). ISBN 9780128035825.
[78] J. L. Delgado *et al.*: Topoisomerases as Anticancer Targets, *Biochem. J.*, **vol. 475**, no. 2, p. 373–398 (2018).
[79] A. Dehshahri *et al.:* Topoisomerase inhibitors: Pharmacology and emerging nanoscale delivery systems, *Pharmacol. Res.*, **vol. 151**, p. 104551 (2020).
[80] Topoisomerase I Inhibitors | DrugBank Online. Accessed: Apr. 17, 2024. [Online]. Available: https://go.drugbank.com/categories/DBCAT001116
[81] K. R. Hande: Topoisomerase II inhibitors, *Update Cancer Ther.*, vol. 3, no. 1, p. 13–26 (2008).
[82] S. Farber and L. K. Diamond: Temporary remissions in acute leukemia in children produced by folic acid antagonist, 4-aminopteroyl-glutamic acid, *N. Engl. J. Med.*, **vol. 238**, no. 23, p. 787–793 (1948).
[83] S. B. Kaye: New antimetabolites in cancer chemotherapy and their clinical impact., *Br. J. Cancer*, **vol. 78**, no. Suppl 3, p. 1–7 (1998).
[84] C. Avendaño and J. C. Menéndez: Chapter 2 - Antimetabolites, in *Medicinal Chemistry of Anticancer Drugs*, C. Avendaño and J. C. Menéndez, Eds., Amsterdam: Elsevier, p. 9–52 (2008). ISBN 9780444528247.
[85] I. S. Kovalev *et al.*: Folic Acid Antimetabolites (Antifolates): A Brief Review on Synthetic Strategies and Application Opportunities, *Molecules*, **vol. 27**, no. 19, p. 6229 (2022).
[86] W. B. Parker: Enzymology of purine and pyrimidine antimetabolites used in the treatment of cancer, *Chem. Rev.*, **vol. 109**, no. 7, p. 2880–2893 (2009).
[87] F. De Castro *et al.*: Platinum-Nucleos(t)ide Compounds as Possible Antimetabolites for Antitumor/Antiviral Therapy: Properties and Perspectives, *Pharmaceutics*, **vol. 15**, no. 3, p. 941 (2023).
[88] What Are Antimetabolites?, Cleveland Clinic. Accessed: Feb. 26, 2024. [Online]. Available: https://my.clevelandclinic.org/health/drugs/24790-antimetabolites
[89] D. Rushworth *et al.*: Dihydrofolate Reductase and Thymidylate Synthase Transgenes Resistant to Methotrexate Interact to Permit Novel Transgene Regulation, *J. Biol. Chem.*, **vol. 290**, no. 38 (2015).
[90] J. Ciccolini *et al.*: Pharmacokinetics and pharmacogenetics of Gemcitabine as a mainstay in adult and pediatric oncology: an EORTC-PAMM perspective, *Cancer Chemother. Pharmacol.*, **vol. 78**, p. 1–12 (2016).
[91] S. Paroha *et al.*: Recent advances and prospects in gemcitabine drug delivery systems, *Int. J. Pharm.*, **vol. 592** (2021).
[92] L. Toschi *et al.*: Role of gemcitabine in cancer therapy, *Future Oncol.*, **vol. 1**, no. 1, p. 7–17 (2005).
[93] A. K. Beutel and C. J. Halbrook: Barriers and opportunities for gemcitabine in pancreatic cancer therapy, *Am. J. Physiol. - Cell Physiol.*, **vol. 324**, no. 2, p. 540–552 (2023).
[94] L. de Sousa Cavalcante and G. Monteiro: Gemcitabine: Metabolism and molecular mechanisms of action, sensitivity and chemoresistance in pancreatic cancer, *Eur. J. Pharmacol.*, **vol. 741**, p. 8–16 (2014).
[95] P. Bilalis *et al.*: Self-Healing pH- and Enzyme Stimuli-Responsive Hydrogels for Targeted Delivery of Gemcitabine To Treat Pancreatic Cancer, *Biomacromolecules*, **vol. 19**, no. 9, p. 3840–3852 (2018).

[96] K. O. Alfarouk *et al.*: Resistance to cancer chemotherapy: failure in drug response from ADME to P-gp, *Cancer Cell Int.*, **vol. 15**, p. 71 (2015).
[97] K. Bukowski *et al.*: Mechanisms of Multidrug Resistance in Cancer Chemotherapy, *Int. J. Mol. Sci.*, **vol. 21**, no. 9 (2020).
[98] J. Shanu-Wilson *et al.*: Biotransformation: Impact and Application of Metabolism in Drug Discovery, *ACS Med. Chem. Lett.*, **vol. 11**, no. 11, p. 2087–2107 (2020).
[99] I. El-Serafi *et al.*: Cytochrome P450 Oxidoreductase Influences CYP2B6 Activity in Cyclophosphamide Bioactivation, *PLoS ONE*, **vol. 10**, no. 11 (2015).
[100] M. S. Singh *et al.*: Tamoxifen, cytochrome P450 genes and breast cancer clinical outcomes, *Breast Edinb. Scotl.*, **vol. 20**, no. 2, p. 111–118 (2011).
[101] E. Buck *et al.*: Tumor response to irinotecan is associated with CYP3A5 expression in colorectal cancer, *Oncol. Lett.*, **vol. 17**, no. 4, p. 3890 (2019).
[102] B. Mansoori, *et al.*: The Different Mechanisms of Cancer Drug Resistance: A Brief Review, *Adv. Pharm. Bull.*, **vol. 7**, no. 3, p. 339–348 (2017).
[103] R. Jan and G.-S. Chaudhry: Understanding Apoptosis and Apoptotic Pathways Targeted Cancer Therapeutics, *Adv. Pharm. Bull.*, **vol. 9**, no. 2, p. 205–218 (2019).
[104] J. Spetz *et al.*: T Cells and Regulated Cell Death: Kill or Be Killed, *Int. Rev. Cell Mol. Biol.*, **vol. 342**, p. 27–71 (2019).
[105] X. Xu *et al.*: Apoptosis and apoptotic body: disease message and therapeutic target potentials, *Biosci. Rep.*, **vol. 39**, no. 1 (2019).
[106] Y. Abuetabh *et al.*: DNA damage response revisited: the p53 family and its regulators provide endless cancer therapy opportunities, *Exp. Mol. Med.*, **vol. 54**, no. 10, p. 1658–1669 (2022).
[107] G. C. Cavalcante *et al.*: A Cell's Fate: An Overview of the Molecular Biology and Genetics of Apoptosis, *Int. J. Mol. Sci.*, **vol. 20**, no. 17 (2019).
[108] R. M. Mohammad *et al.*: Broad targeting of resistance to apoptosis in cancer, *Semin. Cancer Biol.*, **vol. 35**, p. 78–103 (2015).
[109] B. A. Carneiro and W. S. El-Deiry: Targeting apoptosis in cancer therapy, *Nat. Rev. Clin. Oncol.*, **vol. 17**, no. 7, p. 395–417 (2020).
[110] N. E. Crook *et al.*: An apoptosis-inhibiting baculovirus gene with a zinc finger-like motif, *J. Virol.*, **vol. 67**, no. 4, p. 2168–2174 (1993).
[111] J. Silke and P. Meier: Inhibitor of Apoptosis (IAP) Proteins–Modulators of Cell Death and Inflammation, *Cold Spring Harb. Perspect. Biol.*, **vol. 5**, no. 2 (2013).
[112] P. Cetraro *et al.*: A Review of the Current Impact of Inhibitors of Apoptosis Proteins and Their Repression in Cancer, *Cancers*, **vol. 14**, no. 7, p. 1671 (2022).
[113] N. Roy *et al.*: The gene for neuronal apoptosis inhibitory protein is partially deleted in individuals with spinal muscular atrophy, *Cell*, **vol. 80**, no. 1, p. 167–178 (1995).
[114] P. Liston *et al.*: Suppression of apoptosis in mammalian cells by NAIP and a related family of IAP genes, *Nature*, **vol. 379**, no. 6563, p. 349–353 (1996).
[115] H.-P. Hauser *et al.*: A Giant Ubiquitin-conjugating Enzyme Related to IAP Apoptosis Inhibitors, *J. Cell Biol.*, **vol. 141**, no. 6, p. 1415–1422 (1998).
[116] E. Morrish *et al.*: Future Therapeutic Directions for Smac-Mimetics, *Cells*, vol. 9, no. 2 (2020).
[117] B. P. Eckelman *et al.*: Human inhibitor of apoptosis proteins: why XIAP is the black sheep of the family, *EMBO Rep.*, **vol. 7**, no. 10, p. 988–994 (2006).
[118] G. Wu *et al.*: Structural basis of IAP recognition by Smac/DIABLO, *Nature*, **vol. 408**, no. 6815, p. 1008–1012 (2000).
[119] T. Samuel *et al.*: Distinct BIR domains of cIAP1 mediate binding to and ubiquitination of tumor necrosis factor receptor-associated factor 2 and second mitochondrial activator of caspases, *J. Biol. Chem.*, **vol. 281**, no. 2, p. 1080–1090 (2006).
[120] E. Varfolomeev *et al.*: The inhibitor of apoptosis protein fusion c-IAP2.MALT1 stimulates NF-kappaB activation independently of TRAF1 AND TRAF2, *J. Biol. Chem.*, **vol. 281**, no. 39, p. 29022–29029 (2006).

[121] J. E. Vince *et al.*: IAP antagonists target cIAP1 to induce TNFalpha-dependent apoptosis, *Cell*, **vol. 131**, no. 4, p. 682–693 (2007).
[122] T. Kirisako *et al.*: A ubiquitin ligase complex assembles linear polyubiquitin chains, *EMBO J.*, **vol. 25**, no. 20, p. 4877–4887 (2006).
[123] A. J. McClellan *et al.*: Cellular functions and molecular mechanisms of non-lysine ubiquitination, *Open Biol.*, **vol. 9**, no. 9 (2019).
[124] D. Komander and M. Rape: The ubiquitin code, *Annu. Rev. Biochem.*, **vol. 81**, p. 203–229 (2012).
[125] J. Lopez *et al.*: CARD-mediated autoinhibition of cIAP1's E3 ligase activity suppresses cell proliferation and migration, *Mol. Cell*, **vol. 42**, no. 5, p. 569–583 (2011).
[126] J. D. Webster and D. Vucic: The Balance of TNF Mediated Pathways Regulates Inflammatory Cell Death Signaling in Healthy and Diseased Tissues, *Front. Cell Dev. Biol.*, **vol. 8** (2020).
[127] P. D. Mace *et al.*: Structures of the cIAP2 RING domain reveal conformational changes associated with ubiquitin-conjugating enzyme (E2) recruitment, *J. Biol. Chem.*, **vol. 283**, no. 46, p. 31633–31640 (2008).
[128] R. Feltham *et al.*: Smac Mimetics Activate the E3 Ligase Activity of cIAP1 Protein by Promoting RING Domain Dimerization, *J. Biol. Chem.*, **vol. 286**, no. 19, p. 17015–17028 (2011).
[129] Q.-H. Yang and C. Du: Smac/DIABLO selectively reduces the levels of c-IAP1 and c-IAP2 but not that of XIAP and livin in HeLa cells, *J. Biol. Chem.*, **vol. 279**, no. 17, p. 16963–16970 (2004).
[130] D. J. Mahoney *et al.*: Both cIAP1 and cIAP2 regulate TNFα-mediated NF-κB activation, *Proc. Natl. Acad. Sci. U. S. A.*, **vol. 105**, no. 33, p. 11778–11783 (2008).
[131] P. D. Mace *et al.*: Asymmetric recruitment of cIAPs by TRAF2, *J. Mol. Biol.*, **vol. 400**, no. 1, p. 8–15 (2010).
[132] J. Silke: The regulation of TNF signaling: what a tangled web we weave, *Curr. Opin. Immunol.*, **vol. 23**, no. 5, p. 620–626 (2011).
[133] M. Feoktistova *et al.*: cIAPs block Ripoptosome formation, a RIP1/caspase-8 containing intracellular cell death complex differentially regulated by cFLIP isoforms, *Mol. Cell*, **vol. 43**, no. 3, p. 449–463 (2011).
[134] T. Tenev *et al.*: The Ripoptosome, a signaling platform that assembles in response to genotoxic stress and loss of IAPs, *Mol. Cell*, **vol. 43**, no. 3, p. 432–448 (2011).
[135] T. W. Mak and W.-C. Yeh: Signaling for survival and apoptosis in the immune system, *Arthritis Res.*, **vol. 4**, p. 243–252 (2002).
[136] P. Pluta *et al.*: Expression of IAP family proteins and its clinical importance in breast cancer patients, *Neoplasma*, **vol. 62**, no. 4, p. 666–673 (2015).
[137] R. B. Lopes *et al.*: Expression of the IAP protein family is dysregulated in pancreatic cancer cells and is important for resistance to chemotherapy, *Int. J. Cancer*, **vol. 120**, no. 11, p. 2344–2352 (2007).
[138] M. Krajewska *et al.*: Elevated expression of inhibitor of apoptosis proteins in prostate cancer, *Clin. Cancer Res. Off. J. Am. Assoc. Cancer Res.*, **vol. 9**, no. 13, p. 4914–4925 (2003).
[139] A. M. Verhagen *et al.*: Identification of DIABLO, a mammalian protein that promotes apoptosis by binding to and antagonizing IAP proteins, *Cell*, **vol. 102**, no. 1, p. 43–53 (2000).
[140] J. Chai *et al.:* Structural and biochemical basis of apoptotic activation by Smac/DIABLO, *Nature*, **vol. 406**, no. 6798, p. 855–862 (2000).
[141] C. Baggio *et al.*: Design of Potent pan-IAP and Lys-Covalent XIAP selective Inhibitors Using a Thermodynamics Driven Approach, *J. Med. Chem.*, **vol. 61**, no. 14, p. 6350–6363 (2018).
[142] K.-F. Chen *et al.*: Inhibition of Bcl-2 improves effect of LCL161, a SMAC mimetic, in hepatocellular carcinoma cells, *Biochem. Pharmacol.*, **vol. 84**, no. 3, p. 268–277 (2012).
[143] E. Weisberg *et al.*: Smac mimetics: implications for enhancement of targeted therapies in leukemia, *Leukemia*, **vol. 24**, no. 12, p. 2100–2109 (2010).

[144] J. R. Infante *et al.*: Phase I dose-escalation study of LCL161, an oral inhibitor of apoptosis proteins inhibitor, in patients with advanced solid tumors, *J. Clin. Oncol. Off. J. Am. Soc. Clin. Oncol.*, **vol. 32**, no. 28, p. 3103–3110 (2014).
[145] J.-H. Moon *et al.*: A novel small-molecule IAP antagonist, AZD5582, draws Mcl-1 down-regulation for induction of apoptosis through targeting of cIAP1 and XIAP in human pancreatic cancer, *Oncotarget*, **vol. 6**, no. 29, p. 26895–26908 (2015).
[146] E. J. Hennessy *et al.*: Discovery of a novel class of dimeric Smac mimetics as potent IAP antagonists resulting in a clinical candidate for the treatment of cancer (AZD5582), *J. Med. Chem.*, **vol. 56**, no. 24, p. 9897–9919 (2013).
[147] C. C. Nixon *et al.*: Systemic HIV and SIV latency reversal via non-canonical NF-κB signaling in vivo, *Nature*, **vol. 578**, no. 7793, p. 160–165 (2020).
[148] V. V. Veselov *et al.*: Targeted Delivery Methods for Anticancer Drugs, *Cancers*, **vol. 14**, no. 3, p. 622 (2022).
[149] G. Tiwari *et al.*: Drug delivery systems: An updated review, *Int. J. Pharm. Investig.*, **vol. 2**, no. 1, p. 2–11 (2012).
[150] A. M. Vargason *et al.*: The evolution of commercial drug delivery technologies, *Nat. Biomed. Eng.*, **vol. 5**, no. 9, p. 951–967 (2021).
[151] G. Liu *et al.*: A Review on Drug Delivery System for Tumor Therapy, *Front. Pharmacol.*, **vol. 12** (2021).
[152] S. Jain *et al.*: Gold nanoparticles as novel agents for cancer therapy, *Br. J. Radiol.*, **vol. 85**, no. 1010, p. 101 (2012).
[153] D. Kovács *et al.*: Cancer Therapy by Silver Nanoparticles: Fiction or Reality?, *Int. J. Mol. Sci.*, **vol. 23**, no. 2, p. 839 (2022).
[154] S. Anjum *et al.*: Recent Advances in Zinc Oxide Nanoparticles (ZnO NPs) for Cancer Diagnosis, Target Drug Delivery, and Treatment, *Cancers*, **vol. 13**, no. 18, p. 4570 (2021).
[155] Y. Pan *et al.*: Gold nanoparticles of diameter 1.4 nm trigger necrosis by oxidative stress and mitochondrial damage, *Small Weinh. Bergstr. Ger.*, **vol. 5**, no. 18, p. 2067–2076 (2009).
[156] F. Zhou *et al.*: A multifunctional core-shell nanoplatform for enhanced cancer cell apoptosis and targeted chemotherapy, *J. Mater. Chem. B*, **vol. 4**, no. 17, p. 2887–2894 (2016).
[157] V. Chandrakala *et al.*: Review on metal nanoparticles as nanocarriers: current challenges and perspectives in drug delivery systems, *Emergent Mater.*, **vol. 5**, no. 6, p. 1593–1615 (2022).
[158] S. Senapati *et al.*: Controlled drug delivery vehicles for cancer treatment and their performance, *Signal Transduct. Target. Ther.*, **vol. 3**, no. 1, p. 1–19 (2018).
[159] M. D. Fulton and W. Najahi-Missaoui: Liposomes in Cancer Therapy: How Did We Start and Where Are We Now, *Int. J. Mol. Sci.*, **vol. 24**, no. 7 (2023).
[160] P. Liu *et al.*: A Review of Liposomes as a Drug Delivery System: Current Status of Approved Products, Regulatory Environments, and Future Perspectives, *Molecules*, **vol. 27**, no. 4 (2022).
[161] H. M. Patel and S. M. Moghimi: Serum-mediated recognition of liposomes by phagocytic cells of the reticuloendothelial system - The concept of tissue specificity, *Adv. Drug Deliv. Rev.*, **vol. 32**, no. 1–2, p. 45–60 (1998).
[162] J. Li *et al.*: Recent Advances in Targeted Drug Delivery Strategy for Enhancing Oncotherapy, *Pharmaceutics*, **vol. 15**, no. 9 (2023).
[163] J. Dai *et al.*: Exosomes: key players in cancer and potential therapeutic strategy, *Signal Transduct. Target. Ther.*, **vol. 5**, no. 1, p. 1–10 (2020).
[164] R. Kar *et al.*: Exosome-Based Smart Drug Delivery Tool for Cancer Theranostics, *ACS Biomater. Sci. Eng.*, **vol. 9**, no. 2, p. 577–594 (2023).
[165] A. Anitha *et al.*: Synthesis, characterization, cytotoxicity and antibacterial studies of chitosan, *O*-carboxymethyl and *N*,*O*-carboxymethyl chitosan nanoparticles, *Carbohydr. Polym.*, **vol. 78**, no. 4, p. 672–677 (2009).
[166] J. Li *et al.*: Chitosan-Based Nanomaterials for Drug Delivery, *Mol. J. Synth. Chem. Nat. Prod. Chem.*, **vol. 23**, no. 10, p. 2661 (2018).

[167] M. A. Mohammed *et al.*: An Overview of Chitosan Nanoparticles and Its Application in Non-Parenteral Drug Delivery, *Pharmaceutics*, vol. 9, no. 4, p. 53 (2017).
[168] M. Prabaharan: Chitosan-based nanoparticles for tumor-targeted drug delivery, *Int. J. Biol. Macromol.*, **vol. 72**, p. 1313–1322 (2015).
[169] P. Chytil *et al.*: HPMA Copolymer-Based Nanomedicines in Controlled Drug Delivery, *J. Pers. Med.*, **vol. 11**, no. 2 (2021).
[170] H. Maeda *et al.*: The EPR effect for macromolecular drug delivery to solid tumors: Improvement of tumor uptake, lowering of systemic toxicity, and distinct tumor imaging in vivo, *Adv. Drug Deliv. Rev.*, **vol. 65**, no. 1, p. 71–79 (2013).
[171] H. Maeda: The enhanced permeability and retention (EPR) effect in tumor vasculature: the key role of tumor-selective macromolecular drug targeting, *Adv. Enzyme Regul.*, **vol. 41**, no. 1, p. 189–207 (2001).
[172] A. M. Jhaveri and V. P. Torchilin: Multifunctional polymeric micelles for delivery of drugs and siRNA, *Front. Pharmacol.*, **vol. 5** (2014).
[173] A. Ruggiero *et al.*: Paradoxical glomerular filtration of carbon nanotubes, *Proc. Natl. Acad. Sci. U. S. A.*, **vol. 107**, no. 27, p. 12369–12374 (2010).
[174] T. Etrych *et al.*: Polymer conjugates of doxorubicin bound through an amide and hydrazone bond: Impact of the carrier structure onto synergistic action in the treatment of solid tumours, *Eur. J. Pharm. Sci. Off. J. Eur. Fed. Pharm. Sci.*, **vol. 58**, p. 1–12 (2014).
[175] R. Zhang *et al.*: Synthesis and Evaluation of a Backbone Biodegradable Multiblock HPMA Copolymer Nanocarrier for the Systemic Delivery of Paclitaxel, *J. Control. Release Off. J. Control. Release Soc.*, **vol. 166**, no. 1, p. 66–74 (2013).
[176] T. Etrych *et al.*: Conjugates of doxorubicin with graft HPMA copolymers for passive tumor targeting, *J. Control. Release Off. J. Control. Release Soc.*, **vol. 132**, no. 3, p. 184–192 (2008).
[177] T. Etrych *et al.*: Biodegradable star HPMA polymer conjugates of doxorubicin for passive tumor targeting, *Eur. J. Pharm. Sci. Off. J. Eur. Fed. Pharm. Sci.*, **vol. 42**, no. 5, p. 527–539 (2011).
[178] L. Kostka and T. Etrych: High-molecular-weight HPMA-based polymer drug carriers for delivery to tumor, *Physiol. Res.*, **vol. 65**, p. 179–190 (2016).
[179] M. Talelli *et al.*: Micelles based on HPMA copolymers, *Adv. Drug Deliv. Rev.*, **vol. 62**, no. 2, p. 231–239 (2010).
[180] Y. Kato *et al.*: Acidic extracellular microenvironment and cancer, *Cancer Cell Int.*, **vol. 13**, no. 1, p. 89 (2013).
[181] K. D. Jensen *et al.*: Cytoplasmic delivery and nuclear targeting of synthetic macromolecules, *J. Controlled Release*, **vol. 87**, no. 1, p. 89–105 (2003).
[182] T. Etrych *et al.*: HPMA Copolymer Conjugates of Paclitaxel and Docetaxel with pH-Controlled Drug Release, *Mol. Pharm.*, **vol. 7**, no. 4, p. 1015–1026 (2010).
[183] T. Etrych *et al.*: HPMA copolymer-doxorubicin conjugates: The effects of molecular weight and architecture on biodistribution and in vivo activity, *J. Control. Release Off. J. Control. Release Soc.*, **vol. 164**, no. 3, p. 346–354 (2012).
[184] A. Ianevski *et al.*: SynergyFinder 3.0: an interactive analysis and consensus interpretation of multi-drug synergies across multiple samples, *Nucleic Acids Res.*, **vol. 50**, no. W1, p. 739–743 (2022).
[185] R. B. Mokhtari *et al.*: Combination therapy in combating cancer, *Oncotarget*, **vol. 8**, no. 23, p. 38022–38043 (2017).
[186] M. A. Khan *et al.*: Gemcitabine triggers angiogenesis-promoting molecular signals in pancreatic cancer cells: Therapeutic implications, *Oncotarget*, **vol. 6**, no. 36, p. 39140–39150 (2015).
[187] S. Liu *et al.*: Inhibition of ATR potentiates the cytotoxic effect of gemcitabine on pancreatic cancer cells through enhancement of DNA damage and abrogation of ribonucleotide reductase induction by gemcitabine, *Oncol. Rep.*, **vol. 37**, no. 6, p. 3377–3386 (2017).
[188] H. Zhu *et al.*: Bivalent SMAC Mimetics for Treating Cancer by Antagonizing Inhibitor of Apoptosis Proteins, *ChemMedChem*, **vol. 14**, no. 23, p. 1951–1962 (2019).

[189] A. Dashti *et al.*: AZD5582 plus SIV-specific antibodies reduce lymph node viral reservoirs in antiretroviral therapy-suppressed macaques, *Nat. Med.*, **vol. 29**, no. 10, p. 2535–2546 (2023).
[190] C. Yang *et al.*: LCL161 increases paclitaxel-induced apoptosis by degrading cIAP1 and cIAP2 in NSCLC, *J. Exp. Clin. Cancer Res. CR*, **vol. 35**, p. 158 (2016).
[191] Y.-C. Chang and C. H. A. Cheung: An Updated Review of Smac Mimetics, LCL161, Birinapant, and GDC-0152 in Cancer Treatment, *Appl. Sci.*, **vol. 11**, no. 1 (2021).
[192] Y.-C. Chang *et al.*: The SMAC mimetic LCL161 is a direct ABCB1/MDR1-ATPase activity modulator and BIRC5/Survivin expression down-regulator in cancer cells, *Toxicol. Appl. Pharmacol.*, **vol. 401** (2020).
[193] L. Yang *et al.:* LCL161, a SMAC mimetic, Preferentially Radiosensitizes Human Papillomavirus Negative Head and Neck Squamous Cell Carcinoma, *Mol. Cancer Ther.*, **vol. 18**, no. 6, p. 1025–1035 (2019).